X-RAY CRYSTALLOGRAPHY OF RECOMBINANT LACTOCCOCUS LACTIS PROLIDASE

A Thesis Submitted to the College of

Graduate Studies and Research

in Partial Fulfillment of the Requirements

for the Degree of Master of Science

in the Department of Food and Bioproduct Sciences

University of Saskatchewan

Saskatoon

By

OARABILE MICHAEL KGOSISEJO

PERMISSION TO USE

In presenting this thesis in partial fulfilment of the requirements for a Postgraduate degree from the University of Saskatchewan, I agree that the Libraries of this University may make it freely available for inspection. I further agree that permission for copying of this thesis in any manner, in whole or in part, for scholarly purposes may be granted by the professor who supervised my thesis work or, in their absence, by the Head of the Department or the Dean of the College in which my thesis work was done. It is understood that any copying, publication, or use of this thesis or parts thereof for financial gain shall not be allowed without my written permission. It is also understood that due recognition shall be given to me or to the University of Saskatchewan in any scholarly use which may be made of any material in my thesis.

Request for permission to copy or to make use of material in this thesis is whole or in part should be addressed to:

Head

Department of Food and Bioproduct Sciences

University of Saskatchewan

51 Campus Drive

Saskatoon, Saskatchewan

Canada S7N 5A8

ABSTRACT

Prolidase has potential applications in cheese debittering, organophosphate detoxification and as an enzyme replacement therapy in prolidase-deficient patients. Recombinant *Lactococcus lactis* prolidases and their catalytic properties have previously been characterized in Dr. Tanaka's research group. Unlike other prolidases, *L. lactis* prolidase shows allosteric behaviour, metal-dependent substrate specificity and substrate inhibition. The current project focuses on elucidating the three-dimensional structure of *L. lactis* prolidase using X-ray crystallography. Hexagonal plate-like crystals of wild-type *L. lactis* prolidase were grown by the hanging drop vapour diffusion method, allowing the crystals to grow to about 50 μm in their longest dimension. The crystallization cocktail in which they grew contained 0.08 M sodium cacodylate (pH 6.5), 0.16 M calcium acetate, 14 % PEG 8000 and 18 % glycerol. Crystal diffraction data was collected at a wavelength of 0.9795 Å on beamline 08ID-1 of the Canadian Macromolecular Crystallography Facility at the Canadian Light Source and was processed using X-ray Detector Software. The crystals belonged to space group C2 and estimated to contain three molecules in an asymmetric unit. The electron density map of this structure was solved by the molecular replacement method and the structure model was refined against 2.25 Å resolution data. Molecule A forms a dimer with molecule B, while molecule C forms a dimer with molecule C', which is located in the neighbouring crystal asymmetric unit. The electron density of molecule A was well-defined and complete. Therefore, all the 362 amino acid residues of *L. lactis* prolidase were fitted. The other two molecules were incomplete and less defined. Only 360 and 352 residues could be fitted in molecules B and C, respectively. Molecule C, the worst of the three, compromised the overall quality of the refined structure. However, the functional interpretation of the structure was not compromised since the well-defined molecules form a dimer with each other and the biologically-functional form of *L. lactis* prolidase is a homodimer. The final R_{work} and R_{free} are 22.39 and 27.77, respectively. Comparison with other known prolidases revealed that Asp 36 and His 38 are unique to *L. lactis* prolidase. These residues have been shown to be involved in the allosteric behaviour and substrate inhibition of this enzyme, respectively. Therefore, this crystal structure further supports their suggested contribution in *L. lactis* prolidase's unique catalytic properties.

TABLE OF CONTENTS

LIST OF TABLES

LIST OF FIGURES

LIST OF ABBREVIATIONS

ACh	acetylcholine
AChE	acetylcholinesterase
AChR	acetylcholine receptor
APP	aminopeptidase P
CCD	charge-coupled device
CMCF	Canadian macromolecular crystallography facility
CNS	central nervous system
DEAE	diethylaminoethyl
IPTG	isopropyl β-D-1-thiogalactopyranoside
LAB	lactic acid bacteria
LB	Luria-Bertani
LIMS	laboratory information management system
L. lactis	*Lactococcus lactis*
*Ll*prol	*Lactococcus lactis* prolidase
MAD	multiple-wavelength anomalous dispersion
MetAP	methionine aminopeptidase
MIR	multiple isomorphous replacement
MxLIVE	*macromolecular crystallography laboratory information virtual environment*
OP	organophosphorus
OPAA	organophosphorus acid anhydrolase
PDB	protein data bank
PEG	polyethylene glycol
P. furiosus	*Pyrococcus furiosus*
P. horikoshii	*Pyrococcus horikoshii*
*Pf*prol	*Pyrococcus furiosus* prolidase
*Ph*prol	*Pyrococcus horikoshii* prolidase
pK_a	acid dissociation constant
R-factor	residual factor, a measure of the agreement between observed and calculated structure factor amplitudes

R_{free}	residual factor computed using reflections not used in refinement
R_{merge}	measure of the agreement between equivalent reflections
R_{work}	residual factor computed using reflections used in refinement
RMSD	root mean square deviation
SAD	single-wavelength anomalous dispersion
SDS-PAGE	sodium dodecyl sulfate polyacrylamide gel electrophoresis
SIR	single isomorphous replacement
T. sibricus	*Thermococcus sibricus*
XDS	X-ray Detector Software

1   INTRODUCTION

The structure of proline is unique from the structures of the other 19 standard amino acids. Its side chain is connected to its nitrogen atom forming a cyclic structure (Figure 1.1). *Trans* conformation is preferred in most peptide bonds; however, a proline residue exists quite frequently in the *cis* conformation in peptides (Cunningham & O'Connor, 1997; Exarchos et al., 2009; Yaron & Naider, 1993). Due to the unique features of proline, proline-containing peptides are less susceptible to hydrolysis by general peptidases. Therefore, they tend to be preferrably hydrolyzed by proline-specific peptidases. The hydrolysis of proline-containing dipeptides is performed by prolinase (EC 3.4.13.8) and prolidase (EC 3.4.13.9), which hydrolyze proline-containing dipeptides with proline in the N- and C-terminal ends of the peptide bond, respectively.
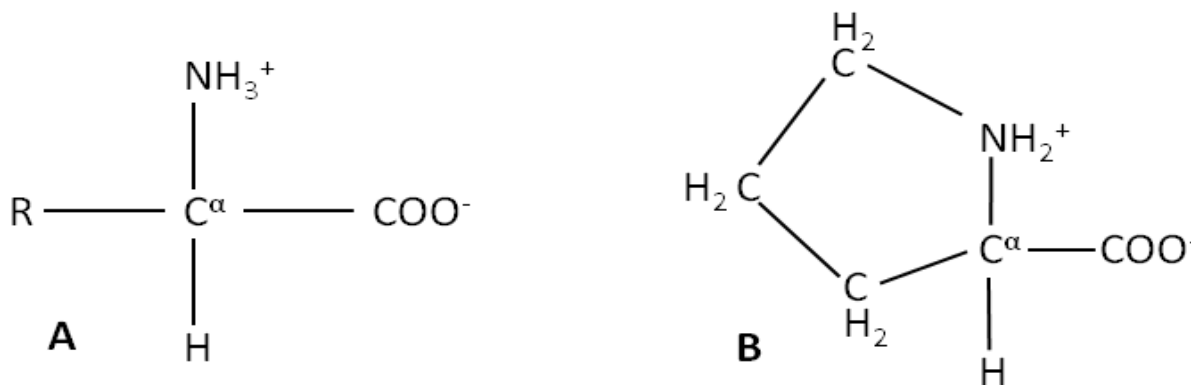
Figure 1.1 General structure of amino acids and the structure of proline.
A: Side chain (R), amine group, carboxylic group and hydrogen are attached to an α-carbon. **B:** In proline, the side chain is connected to the amine group forming a cyclic structure.

Prolidase has been isolated from mammalian tissues; including human liver, human kidney, human skin fibroblasts and human erythrocytes, and from microorganisms where it is involved in peptide metabolism (Fernandez-Espla et al., 1997; Ghosh et al., 1998; Wang et al., 2004). In humans, it is involved in the final stages of degradation of dietary proteins and in extracellular matrix collagen remodelling. Not only is this enzyme important in human physiology, but also it is involved in the liberation of amino acids in microbes needed for their growth. A typical

example of such importance in microbial activities is found in milk fermentation. Caseins, or milk proteins, are very rich in proline and therefore their degradation involves the action of proline-specific proteases and peptidases, including prolidase. Lactic acid bacteria (LAB) are often major strains used in milk fermentation, and they have a proteolytic system that is responsible for the liberation of free amino acids from casein and its hydrolytic products, including several proline-specific peptidases. Several other microbial species have been shown to require proline for their growth, such as *Pyrococcus furiosus*, of which growth declined when proline was removed from its growth media (Raven & Sharp, 1997). Prolidase has been isolated from *P. furiosus* (Ghosh et al., 1998). These findings suggest that prolidase plays a very critical role in the release of proline needed for growth by this bacterial species.

Prolidase generally prefers substrates in which the N-terminal residue is non-polar, such as leucine, methionine, valine, phenylalanine and alanine (Ghosh et al., 1998; Yang & Tanaka, 2008). It belongs to a class of enzymes called the "pita-bread" enzymes, due to the pita-bread-like fold of the C-terminal domains of enzymes in this class. These enzymes are metalloenzymes and the amino acid residues coordinating the metal centers are conserved (Lowther & Matthews, 2002). Other members of this class of enzymes include methionine aminopeptidase (MetAP: EC 3.4.11.18) and aminopeptidase P (APP: EC 3.4.11.9). MetAP removes methionine from the N-terminus of peptides in which the second residue is small and uncharged, while APP removes the N-terminal residue from peptides in which the second residue is proline. MetAP and APP prefer peptides with longer chains (at least three amino acid residues), unlike prolidase whose substrates are primarily dipeptides.

Lactococcus lactis prolidase has been previously characterized in Dr. Tanaka's research group (Yang & Tanaka, 2008). This enzyme is a homodimer and each subunit is approximately 40 kDa in size. Like other studied prolidases, it is a metalloenzyme and has specific activity towards Xaa-Pro peptides. Unlike other prolidases; it demonstrates allosteric behavior, substrate inhibition and metal-dependent substrate specificity. The most preferred substrate was Leu-Pro in the presence of Zn^{2+} and it changed to Arg-Pro when Zn^{2+} was replaced with Mn^{2+}. The allosteric nature of this enzyme was indicated by sigmoidal curves for plots of enzyme catalytic rate against substrate concentration for both Leu-Pro and Arg-Pro (Yang & Tanaka, 2008). The sigmoidal curves suggest that the binding of one substrate or ligand molecule to the enzyme affects its affinity for other substrate or ligand molecules. Dr. Tanaka's research group has conducted some

studuies to reveal the influence of specific residues on the functionality of this enzyme based on a amino acid sequence-based predicted model. However, the predicted model has its own limitations, and therefore the three-dimensional structure, i.e., X-ray crystallographic model is required to support their findings.

2 LITERATURE SURVEY

2.1 Potential applications of prolidase

2.1.1 Cheese ripening

There are three major catabolic processes that are involved in flavor development during cheese ripening. These are lactose fermentation, lipolysis, and hydrolysis of milk caseins (van Kranenburg et al., 2002). The enzymes responsible for these processes are indigenously present in milk, present in LAB (starter and non-starter culture) and/or exogenously supplied during manufacturing (Wilkinson & Kilcawley, 2005). Among these, the most important flavor development process in hard-type and semi-hard-type cheeses is the degradation of milk caseins, which comprises protein degradation into polypeptides (proteolysis) and polypeptide hydrolysis into small peptides and free amino acids by peptidases (peptidolysis). During the degradation by LAB these hydrolytic processes are catalyzed by a cell wall-bound proteinase and several intracellular peptidases, respectively. The intracellular peptidases comprise endopeptidases, aminopeptidases, di-/tri-peptidases and proline-specific peptidases, including prolidase (Bockelmann, 1995). Another important step in LAB casein metabolism is the transport of peptides into the cell where the peptidases are located. This is done via di-/tripeptide transport system and/or the oligopeptide transport system depending on the bacterial strain (Kunji et al., 1996; Liu et al., 2010). The proteolytic system of LAB is illustrated in Figure 2.1. Peptides from casein hydrolysis impart flavor to the fermented products, some of which may be undesirable, such as bitterness (Paul et al., 2014; Fallico et al., 2005). Also reported in the literature is the reduction in bitterness of cheese after further hydrolysis of the bitter peptides. In a study by Bockelmann (1995), a LAB starter strain with a high proteinase activity but low peptidase activity produced bitter-tasting milk, while the milk treated with strains with higher peptidase activity was not bitter. This suggests that a good balance between proteolysis and peptidolysis is critical for the development of flavor and the control of bitterness in fermented dairy products. The peptidase profile of a LAB strain used in cheese production influences its flavor and texture (Liu et al., 2010; Paul et al., 2014; van Kranenburg et al., 2002). Milk proteins (caseins) are rich in proline, leading to a higher occurrence of proline-containing peptides that are hard to hydrolyze. Proline-containing peptides have been shown to have a bitter taste (Ishibashi et al.,

4

1988). Therefore, cheese can show the bitterness in the process and the importance of proline-specific peptidases in this process cannot be overstated. Prolidase is one of such proline-specific peptidases and it is responsible for hydrolyzing the smallest proline-containing peptides (Xaa-Pro). In addition to hydrolyzing proline dipeptides, prolidases generally prefer hydrophobic dipeptides. These prolidase substrates have been shown to exhibit higher levels of bitterness compared to the amino acid constituting them, that is, Xaa-Pro peptides are more bitter than Xaa and Pro alone (Ishibashi et al., 1988). Therefore, prolidase could be used to reduce bitterness of fermented dairy products.
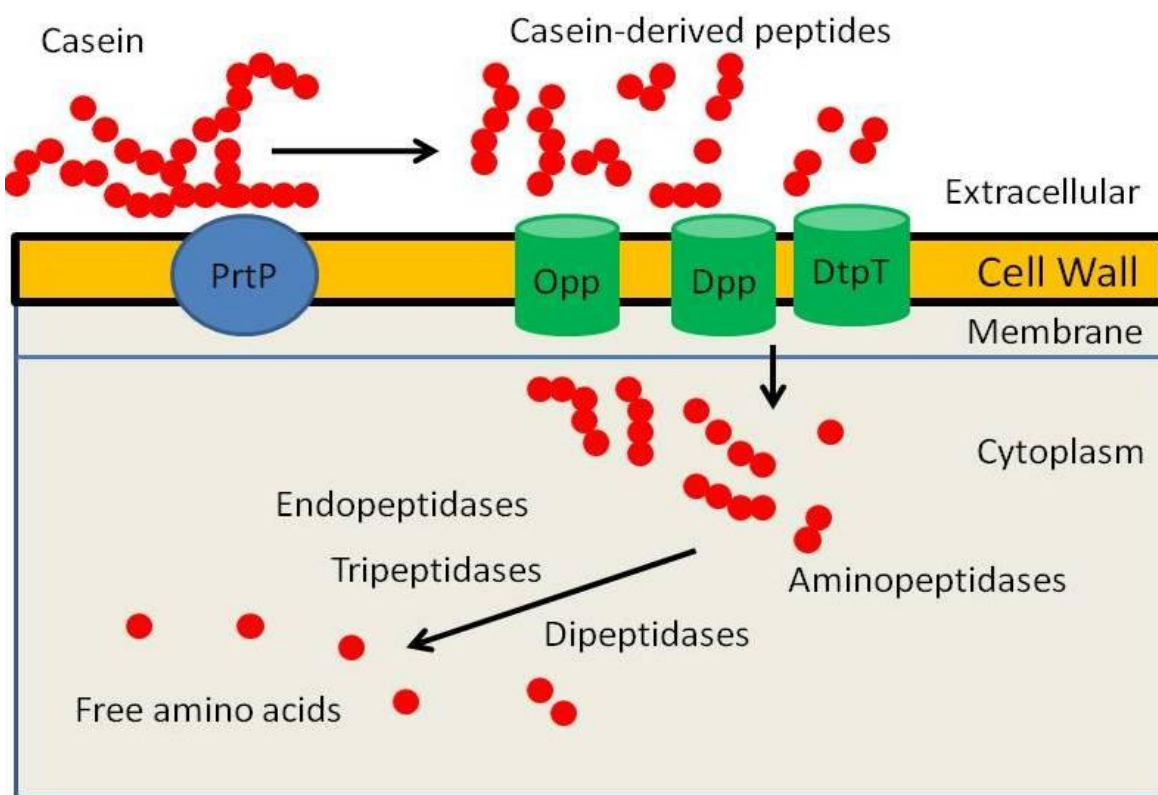
Figure 2.1 Illustration of the proteolytic system of *Lactococcus lactis.*
Casein molecules are hydrolyzed by cell wall proteinase (PrtP). The oligopeptide (Opp) and the di-/tripeptide transport (DtpT) systems carry the resulting peptides into the cell where they are further hydrolyzed into smaller peptides and free amino acids by several intracellular peptidases. Dpp = peptide-binding proteins (Adapted from Pinto et al., 2012).

2.1.2   Treatment of prolidase deficiency

The extracellular matrix comprises different families of protein, and collagens are the most abundant among them. Their functions include providing structural support to the cells, regulating cell-to-cell communication and acting as storage for growth factors for the cells (Gelse et al., 2003). Collagens are rich in proline and hydroxyproline, with these residues making up to 25 % of the amino acid residues in collagens (Phang et al., 2008). Hydroxyproline is formed by post-translational hydroxylation of proline and the added hydroxyl group is involved in intramolecular hydrogen bonding to provide mechanical strength to these proteins. Like other proline-rich proteins, collagens are resistant to hydrolysis by general proteases, such as pepsin, trypsin and chymotrypsin (Bruckner & Prockop, 1981). Therefore, they can only be hydrolyzed by specific collagenases and the resulting proline-rich peptides are hydrolyzed by several proline-specific peptidases. Prolinase and prolidase are involved in the final steps of collagen breakdown for the release of free proline and other amino acids, which are then used for various functions such as protein synthesis and matrix remodelling (Figure 2.2). Lack of prolinase activity has not been associated with any disorder. On the other hand, lack of or reduced prolidase activity has been associated with a rare autosomal recessive disorder known as prolidase deficiency (Powell et al., 1974) caused by mutations in the prolidase gene. All of the reported mutations involve the residues in the C-terminal domain, which harbors the enzyme active site (Lupi et al., 2008). Its characteristic symptoms are skin ulcerations, recurrent skin infections, mental retardation and iminopeptiduria (Kikuchi et al., 2000; Klar et al., 2010; Lupi et al., 2004, 2006). The relationship between the clinical manifestations and the genotype is still poorly understood, probably due to the rarity of this disorder. Some of the adapted methods of treatment include oral supplementation with manganese, which is needed for prolidase activity, and topical treatment of the ulcers with proline and antioxidants. Although these have been reported to improve the skin lesions in some patients, they do not mitigate the molecular defects (i.e., they do not restore prolidase activity). It is not clear whether or not blood transfusion could treat prolidase deficiency. In one study, repeated apheresis erythroexchanges were performed in two prolidase-deficient patients (Lupi et al., 2002). Although this did not improve their prolidase activity, it led to improvement of skin ulcerations and reduction of imidodipeptides in the patients' urine (Lupi et al., 2002). On the other hand, prolidase activity was detected when cultured fibroblasts from prolidase-deficient patients were incubated with liposomes loaded with prolidase from porcine

kidney (Perugini et al., 2005). This suggests that purified prolidase could potentially be used to treat prolidase deficiency. Gene therapy has also shown to be a viable option in treating prolidase deficiency (Ikeda et al., 1997).
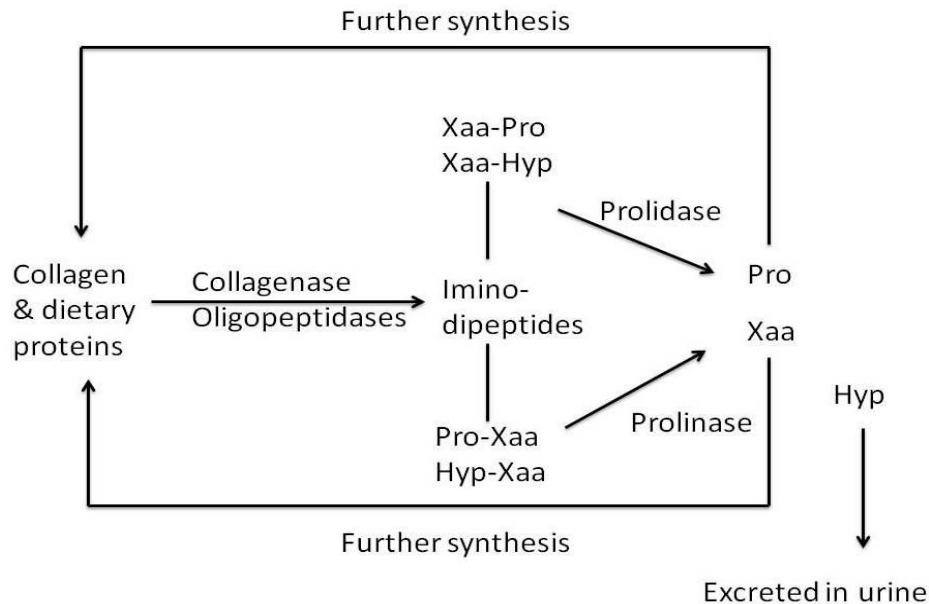
Figure 2.2 A schematic illustration showing prolinase and prolidase at the final stages of collagen breakdown.
Xaa is any amino acid, while Pro and Hyp are proline and hydroxyproline, respectively (Adapted from Kurien et al., 2006 and Myara et al., 1984).

2.1.3   Organophosphorus (OP) compounds detoxification

2.1.3.1 What are organophosphorus compounds?

The general structure of toxic organophosphorus compounds comprises a central phosphorus atom bonded to an oxygen or sulphur atom by a double bond and three other chemical constituents by single bonds (Figure 2.3). They are used as insecticides, pesticides and herbicides. Another group of organophosphorus compounds known as nerve agents finds use as chemical weapons and these have been used to attack humans during military conflicts and terrorist attacks. Nerve agents are considered the most lethal chemical warfare agents known. They belong to two main groups, G-agents and V-agents. The G-agents were first discovered by a

German scientist, Dr. Gerhard Schrader during his work on OP pesticides in the 1930's. This was followed by large-scale production of these compounds due to their importance in military. Some of the well-known nerve agents of the G-type include tabun (GA, ethyl-*N,N*-dimethyl phosphoramidocyanide), sarin (GB, isopropyl methyl phosphonofluoridate), cyclosarin (GF, cyclohexyl methyl phosphonofluoridate) and soman (GD, pinacolyl methyl phosphonofluoridare). The V-agents were synthesized after World War II through combined investigational efforts by US and British laboratories. Full scale production of VX (o-ethyl-S-(2-diisopropylamino-ethyl)-methyl phosphonothiolate) started in 1961 (Szinicz, 2005).
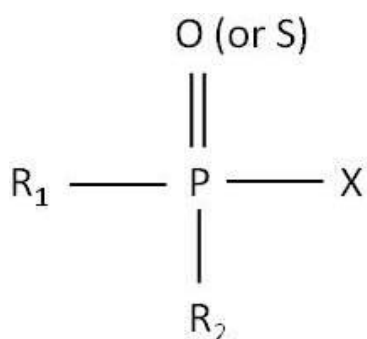
Figure 2.3 General structure of organophosphorus (OP) compounds.
R1 and R2 can be alkyl, alkoxy or amine groups. X is a leaving group and may be attached to a phosphorus atom by oxygen or sulphur atom (Manco, 2008).

Nerve agents were first used in warfare in the 1980's, including during the Iraq-Iran war during which sarin was used by the Iraqi armed forces (Macilwain, 1993). They were later used during terrorist attacks, including the two sarin attacks in Japan in 1994 and 1995. In 1994 this toxin was released in Matsumoto, a city of 200,000 residents. This led to 600 poisonings, 56 hospitalizations and seven deaths (Suzuki et al., 1997 and Yanagisawa et al., 1995). The second sarin attack, which happened in 1995, was in Tokyo subway lines, after which more than 5,000 victims required emergency medical attention. This attack led to twelve deaths, two of which happened on the day of the attack (Okumura et al., 1996, 2003).

2.1.3.2 Mechanism of OP toxicity

Acetylcholine (ACh) is a neurotransmitter responsible for the transmission of nerve impulses at cholinergic, synaptic and neuromuscular junctions. It is released by the presynaptic neuron into the synaptic gap and interacts with acetylcholine receptor (AChR) on the postsynaptic membrane causing stimulation of the neuron. Neurotransmission is regulated by acetylcholinesterase (AChE, EC 3.1.1.7), which hydrolyzes acetylcholine into acetic acid and choline (Engelhard et al., 1967) and terminates neurotransmission. Organophosphorus compounds (OP pesticides and nerve agents) inhibit AChE by binding to the serine hydroxyl group in the enzyme active site. This phosphylation (inhibition) of AChE is similar to the acetylation of this enzyme by acetylcholine during its normal function. However, the breakdown of the acetylated acetylcholinesterase to release the free enzyme is more rapid than the breakdown of the inhibited acetylcholinesterase (Aldridge, 1950). Depending on the organophosphorus agent attached to AChE, a non-enzymatic time-dependent intramolecular rearrangement may result in the loss of an alkyl group from the phosphoryl group, known as "aging". This leads to the formation of an enzyme-organophosphorus moiety that is resistant to reactivation (Figure 2.4B), thus permanently inhibiting the AChE. OPs that undergo this rearrangement include soman, sarin, tabun and VX (Jokanović, 2009). Inhibition of AChE leads to accumulation of acetylcholine at nerve synapses and overstimulation of nerves, thereby paralyzing the functions of the human body.

2.1.3.3 Current detoxification methods and their limitations

Standard treatment of organophosphorus poisoning comprises antimuscarinic agents, cholinesterase reactivators and anticonvulsants. Antimuscarinic drugs, such as atropine, antagonize the effects of excess acetylcholine at end organs having muscarinic receptors. However, OPs do not only affect organs with muscarinic receptors, but also organs that have nicotinic receptors, such as muscles and respiratory organs. Therefore, these drugs do not address muscle weakness, twitching and respiratory depression that are caused by overstimulation of nicotinic receptors. Cholinesterase reactivators normally used are pralidoxime and obidoxime. They reactivate OP-inhibited AChE by binding to the phosphorus of the OP then liberating the enzyme. Although they have been used effectively to treat OP poisoning, their effectiveness depends on the structure of the OP involved (Worek et al., 2004).
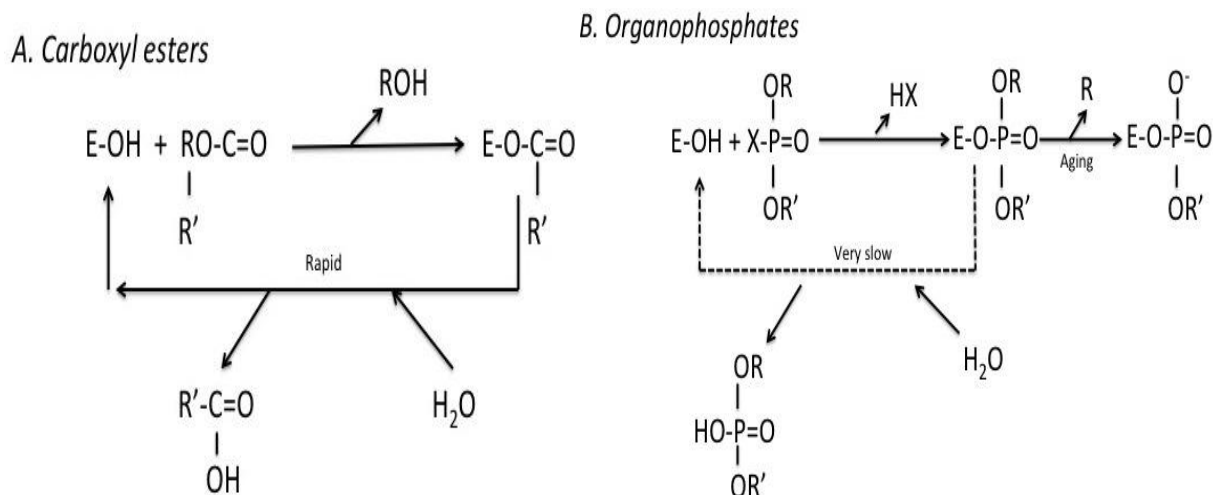
Figure 2.4 Interaction of acetylcholinesterase (AChE) with its substrates and inhibitors.
A: Hydrolysis of carboxyl esters (e.g. acetylcholine) by AChE (E-OH). The liberation of the enzyme is rapid. **B:** Inhibition of AChE (E-OH) by OPs. Spontaneous reactivation of the enzyme is very slow. Depending on the chemical nature of the OP the AChE-OP complex may undergo an irreversible loss of one of their alkyl groups, therefore, permanently inhibiting the enzyme (Adapted from Glynn, 1999).

These two cholinesterase reactivators are ineffective against some nerve agents, including soman, tabun and cyclosarin. Also, some OPs age very rapidly and reactivation of AChE inhibited with these OPs using oximes is ineffective (Worek et al., 2004 and Worek et al., 2004). In addition to aging, some OPs, such as fenthion, are highly lipophilic and are stored in the adipose tissue and subsequently delivered into circulation even after administration of treatment drugs. Others have very low volatility and these are absorbed very slowly by human tissues. This absorption may continue several hours after exposure (Dalton et al., 2006). On the other hand, the currently used oximes (pralidoxime and obidoxime) are highly polar and are therefore short-lived in circulation (Eyer et al., 2007). Therefore, the treatment drugs are outlasted by these persistent OPs. Another limitation of oximes is that most of them are quaternary drugs with limited central nervous system (CNS) penetration and therefore, do not alleviate the central effects of poisoning (Yanagisawa et al., 2006).

2.1.3.4 Prolidase as a method of OP detoxification

Currently there are stockpiles of nerve agents that need to be destroyed. The traditional methods of destruction of chemical weapons, including nerve agents, involve the use of chemicals (Chauhan, 2008 and Yang, 1999). Large volumes of chemicals are required for this, therefore the chemical method is not economical. Also, the chemical treatment leaves behind byproducts that may be harmful to the environment (water, soil, air and animals exposed to them). While enzymes may not be applicable in treating OP-poisoned patients due to immunogenicity and limitations in delivery, they are a good potential in destructing stockpiles of OPs. Enzymatic methods are more efficient and more environmental-friendly than chemical methods.

Organophosphorus acid anhydrolase (OPAA: EC 3.1.8.2) were originally isolated from *Alteromonas* species (Defrank & Cheng, 1991 and Cheng et al., 1993). Although their natural function in bacteria is unknown, these enzymes are capable of hydrolyzing toxic organophosphorus compounds. The sources of these enzymes do not have cholinesterases, that is acetylcholinesterase and butyrylcholinesterase, like insects and mammals. Therefore, it is unlikely that their natural function is to protect these organisms from organophosphorus poisoning. Comparison of the amino acid sequence of OPAA with the protein database has revealed a high level of similarity with prolidase. In addition to the structural similarity between these two enzymes, OPAA had prolidase activity (cleavage of dipeptides with proline in the C-terminus position) (Cheng & Calomiris, 1996). Prolidase from different organisms have also demonstrated hydrolytic activity towards toxic organophosphorus compounds (Park et al., 2004). These findings suggest that OPAA is a prolidase whose natural role is peptide metabolism, but is also capable of detoxifying organophosphorus compounds. Therefore, several researches have focused on the structural and functional studies of prolidase as a potential enzyme for organophosphorus detoxification. This does not only include treating organophosphate poisoning, but also the destruction of stockpiles available worldwide (Kim & Lee, 2001). The prolidases of different origins have varying substrate and stereochemical specificities. Consequently, further studies are required to optimize their catalytic activity, which would require knowledge of their three-dimensional structures.

2.2   Protein X-ray crystallography

X-ray crystallography finds application in rational drug design, genetic engineering of proteins and the study of biological systems, such as enzyme catalysis (Blundell et al., 2002; Kuhn et al., 2002; Minor, 2007). The flow diagram illustrating the experimental procedures undertaken during structure determination by X-ray crystallography is shown in Figure 2.5. The success of structure determination by X-ray crystallography depends on the ability to grow crystals of sufficient size and quality for X-ray diffraction. Therefore, crystallization is considered the rate-limiting step in X-ray crystallographic studies of macromolecules.
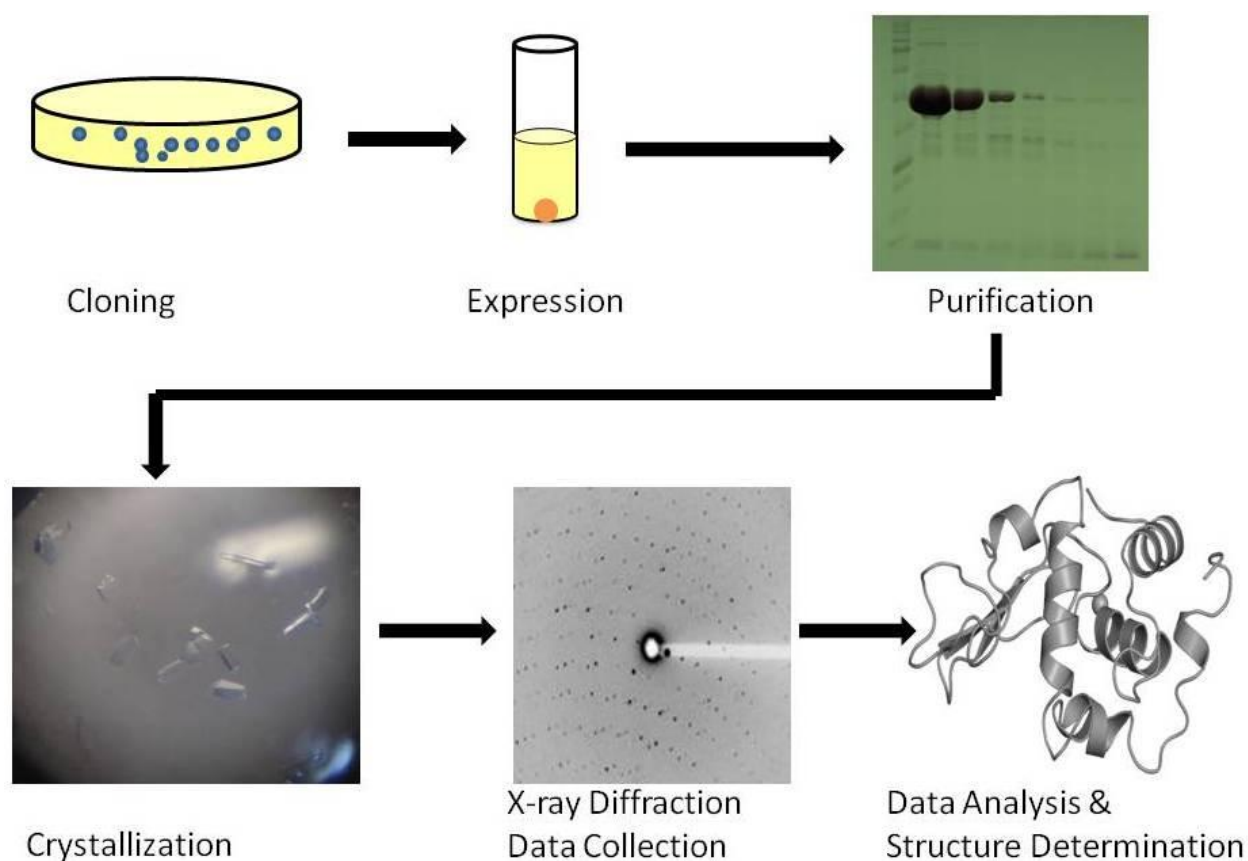
Figure 2.5 Overview of the experimental procedures undertaken during protein X-ray crystallography (Adapted from Chayen & Saridakis, 2008 and Minor, 2007).

2.2.1 Purification

The purity of a protein sample is very important not only in determining the success of crystallization, but also in the quality of the resulting crystal. This is because a crystal is a periodic arrangement of molecules into a three-dimensional lattice. Therefore, if the protein solution is not homogeneous, the foreign material may interfere with the packing of protein molecules into a crystal lattice. The more ordered the crystal lattice, higher the diffracting power of the crystal and hence the better the quality of the solved crystal structure (McPherson, 2004).

2.2.2 Crystallization

In a crystallization study the objective is to supersaturate the protein and initiate nucleation and crystal growth. When a protein is undersaturated it is fully-dissolved and will never crystallize. However, when it is supersaturated, nucleation or crystal growth may occur depending on the level of supersaturation. This can be explained by a crystallization phase diagram (Figure 2.6). Precipitating agents decrease the solubility of protein by interacting with water molecules making them unavailable to the protein molecules. When supersaturation is very high the protein precipitates and no crystal growth occurs. Moderate supersaturation is considered labile and in this supersaturation phase nucleation is favored. The level of supersaturation just below labile saturation is considered metastable and this is where crystal growth occurs.

The two major steps during crystallization are screening and optimization. The former involves the identification of physical, chemical and biochemical conditions that may aid the growth of crystals, which may not necessarily be of sufficient quality for X-ray diffraction. These conditions include temperature, pH, precipitant type and protein concentration. There are commercial screen kits that have been formulated based on the conditions that have led to successful crystallization in the past. These screens are called sparse-matrix screens (Jancarik & Kim, 1991). The other kind of screens is called systematic screens (Brzozowski & Walton, 2001). Systematic screens sample the crystallization parameters in a rational way based on the properties of the protein sample under investigation. During optimization the conditions that give leads during the screening phase are further explored or fine-tuned to enhance the quality of the crystals for X-ray diffraction. These leads could be crystals of any quality, precipitates or any sign of phase separation. The conditions are screened and optimized using some of the available

crystallization techniques. These include dialysis, free-interface, microbatch and vapour diffusion. These explore the crystallization phase diagram differently as illustrated in Figure 2.6.

Dialysis and free-interface diffusion methods are the least commonly used. In dialysis method, the protein solution and the crystallization solution are separated by a semi-permeable membrane, which allows the small molecules to move across down their concentration gradient. The large molecules, on the other hand, are trapped on one side of the membrane. In free-interface diffusion method, the protein solution and the crystallization are layered on top of each other in a capillary tube along which they gradually diffuse into each other (Salemme, 1972).

Microbatch method involves simply mixing the protein solution with crystallization reagents. This is usually conducted in 72- or 96-well plates. Modification of the microbatch method involves covering the crystallization reagents-protein drop with low-density paraffin oil (0.87 g/ml) and this is known as microbatch-under-oil method (Chayen, 1997). The denser crystallization drop remains under the oil and the oil acts as a barrier to control or prevent evaporation and contamination of the drop by foreign material (Figure 2.7). However, the use of oil may limit the choice of reagents used since some of them may dissolve in it (Chayen, 1998). Supersaturation is achieved immediately since the initial protein concentration is the same as its final concentration. If the conditions are ideal nucleation occurs and is followed by a decrease in supersaturation, and hopefully crystal growth.

In vapour diffusion method, 0.5 - 1 ml of the crystallization cocktail is pipetted into a well of a 24-well plate. Then, 1 - 10 µl is drawn from this reservoir and is mixed with the same volume of a protein solution and this drop is allowed to equilibrate against the crystallization cocktail in the reservoir through vapour exchange between them. This method is divided into the hanging drop and sitting drop vapour diffusion methods. In the hanging drop method, the crystallization drop is prepared on a siliconized cover glass. Grease is applied on the circumference of the well and the cover glass containing the crystallization drop is inverted over the well allowing the drop to hang over the sealed reservoir (Figure 2.8A). In the sitting drop method, the crystallization drop is prepared on a raised platform inside the well (Figure 2.8B). The well is also sealed to prevent evaporation. During vapour diffusion, the protein is fully dissolved or undersaturated at the beginning. Because the concentration of the precipitating agent in the drop is half the concentration in the well, there is evaporation of water molecules from the drop to the well (down their concentration gradient).

14
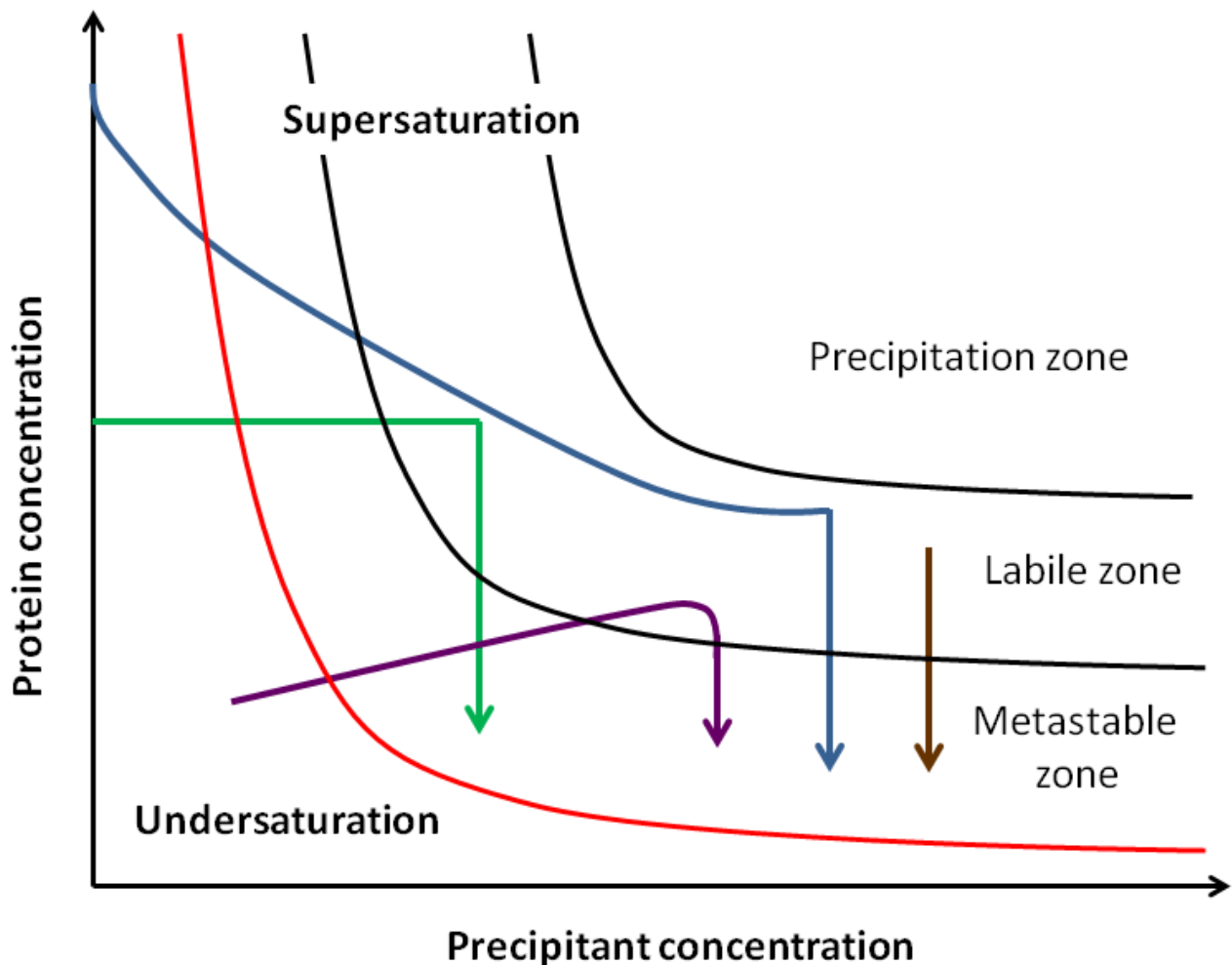
Figure 2.6 Protein crystallization phase diagram.

The solubility curve is coloured red and the regions below and above this curve are undersaturation and supersaturation, respectively. The three levels of supersaturation are illustrated. The precipitation zone is the zone of high supersaturation where solutes (proteins) precipitate. The labile zone is the zone of moderate supersaturation where nucleation occurs. The metastable zone is the zone of slight supersaturation and this is where crystals grow. Green line represents dialysis method, blue line represents free-interface diffusion, brown line represents batch method and purple line represents vapour diffusion methods (Adapted from McPherson & Gavira, 2014; Chayen, 2004).
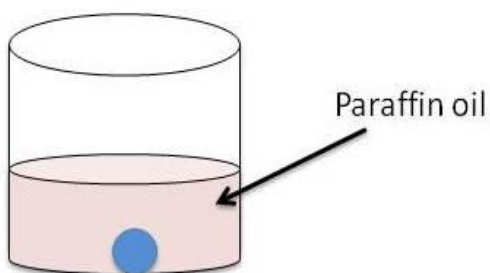
Figure 2.7 Illustration of microbatch-under-oil crystallization method.
The crystallization drop consists of the crystallization cocktail and the protein solution and is covered with paraffin oil, which is less dense that the crystallization drop.

This does not only lead to an increase in the concentration of the precipitant, but also that of the protein in the drop. This increase in protein concentration drives it to supersaturation. Ideally, if it is moderately supersaturated there will be formation of nuclei. When the protein molecules are used in nucleation there is less of them in solution, therefore, a drop in protein concentration. This will move the system from a labile nucleation zone towards a metastable zone where the crystals will grow.
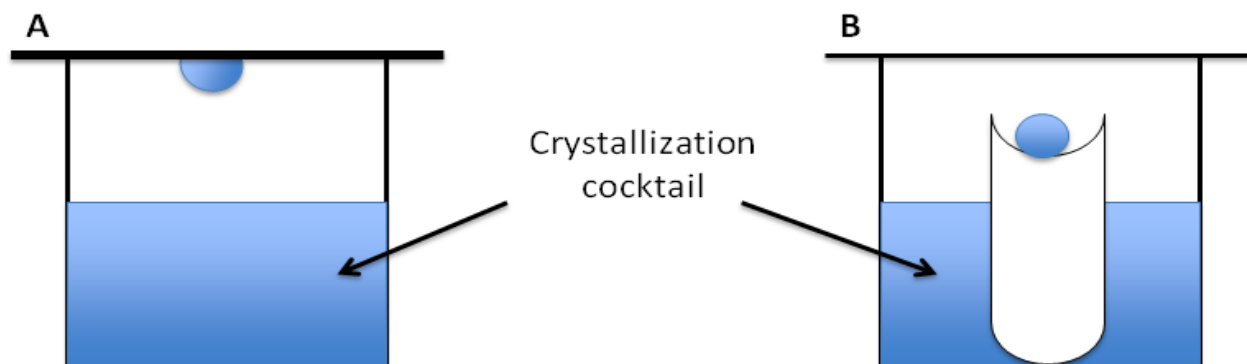
Figure 2.8 Illustration of vapour diffusion methods of crystallization.
The crystallization drops consists of the crystallization cocktail and the same volume of the protein solution. **A:** The crystallization drop hangs over the reservoir on a siliconized cover glass. **B:** The crystallization drop "sits" on a platform.

One of the major advantages of vapour diffusion over microbatch method is the fact that the crystallization conditions can be changed without disturbing the crystallization drop. The cover glass can be easily transferred to a well of different composition (Chayen, 2005) or the crystallization cocktail in the reservoir may be changed without touching the crystallization drop. On the other hand, the crystallization conditions remain constant during microbatch crystallization. This allows the experimenter to have control over the experimental conditions, which is not the case with diffusion-based methods during which diffusion leads to changes in crystallization parameters.

High-throughput crystallization methods have been developed in order to speed up the crystallization step of X-ray crystallography. These methods allow for the screening of a wider range of conditions within a short period of time. They also allow for miniaturization of the reagents and the protein sample needed for crystallization (Bard et al., 2004; DeLucas et al., 2003; Luft et al., 2003; Walter et al., 2005). At Oxford Protein Production Facility, the sitting drop vapour diffusion is conducted in 96-well plates using 100 nl of the reagents and of the protein solution (Walter et al., 2005). At Hauptman Woodward Research Institute, they use 200 nl of each of the protein solution and the crystallization reagent under 5 µl of paraffin oil. A set up of 1536 wells is completed within 10 minutes (Luft et al., 2003). Technologies capable of employing as low as 20 nl of the reagents have also been developed (DeLucas et al., 2003, 2005). In addition to liquid handling and dispensing, image capturing, storing and analysis are automated at the high-throughput crystallization facilities (Bard et al., 2004; DeLucas et al., 2003, 2005; Luft et al., 2003; Walter et al., 2005), which further reduces human intervention. The drawbacks of miniaturization include the growth of crystals that cannot be scaled up and the false negatives from conditions that would have otherwise produced crystals at larger cocktail volumes (Chayen & Saridakis, 2008).

Sometimes only nucleation occurs, suggesting that the decrease in protein concentration was not adequate to drive the protein to metastable zone, where nuclei grow into large crystals. One may use these tiny crystals as seeds from which large crystals grow. The seeds are used in a system of lower supersaturation (metastable zone) since the aim is crystal growth rather than nucleation. This could be a lower protein concentration, lower precipitant concentration or even a lower temperature (Bergfors, 2003; D'Arcy et al., 2007; Gavira et al., 2011; McPherson & Gavira, 2014). An alternative to using the protein crystal as seeds is using different material, such

as minerals, glass charged or charged molecules (Fermani et al., 2001; Rong et al., 2002; Saridakis & Chayen, 2009; Tsekova et al., 1999). Too much nucleation may be due to the presence of dust or denatured protein particles in the protein solution. In order to address this, one may have to centrifuge or filter the protein sample through a 0.22 µm filter. On the other hand, this foreign material may be needed for nucleation and subsequent crystal growth. Therefore, it is recommended that filtering be done at the optimization stage to mitigate over nucleation rather than during the screening stage. Applying it during screening may result in passing out on the conditions suitable for crystal growth (Chayen & Saridakis, 2008). Another approach to address the issue of too much nucleation is intervening when nucleation has occurred and introducing the conditions suitable for enlargement of crystals, which are different from those required for nucleation. Some of the ways of achieving that include diluting the crystallization drop with protein-free buffer, transferring the crystallization drop to a reservoir of lower crystallization reagent concentration, and varying the incubation temperature. The latter finds application particularly in diffusion-based crystallization methods during which temperature determines the rate of diffusion and hence the rate of supersaturation of the protein sample. Another way of controlling the rate of supersaturation is by applying a layer of paraffin/silicon oil over a crystallization reservoir in vapour diffusion methods. This has been shown to slow down the crystallization process and lead to growth of larger crystals when compared to crystallization without an oil layer (Chayen, 1997).

In addition to manipulating the crystallization conditions, one may need to modify the protein sample itself to enhance its crystallizability. This may involve removal of heterogeneous groups such as carbohydrates in glycoproteins, site-directed mutations and removal of flexible loop regions for which mobility may be responsible for lack of, or poor molecule packing during crystallization (Dale et al., 2003), and the use of affinity tags.

2.2.3   X-ray data collection and processing

Synchrotron radiation is the most common source of radiation for protein crystallography (http://biosync.sbkb.org/; accessed on April 5, 2015). A typical synchrotron beamline consists of three main components: a source of radiation, optical elements, and a detector (Dauter, 1996). The source may be a bending magnet or an insertion device. Both source types are available at the Canadian Light Source (08B1-1 and 08ID-1) and they constitute the Canadian

Macromolecular Crystallography Facility (Grochulski et al., 2011, 2012). Optical elements may include monochromators for selection of wavelengths, focusing mirrors and collimating slits. Most synchrotron beamlines are equipped with CCD-based detectors (Gruner & Ealick, 1995; Walter et al., 1995). These are very sensitive and fast, and therefore allow for collection and recording of both weak and strong reflections within a short period of time (Walter et al., 1995). Modern synchrotrons are superior to conventional laboratory X-ray sources due to primarily their high intensity and tunability. The latter finds application in collection of anomalous data, during which different wavelengths / energies are selected for optimization of the anomalous signal.

One of the major drawbacks of the intense synchrotron radiation in X-ray crystallography is the radiation damage crystals undergo when collection diffraction data at room temperature. There are two types of radiation damage that crystals undergo during X-ray diffraction: primary and secondary damage. Primary radiation involves the interaction of the beam with the molecules, which generates heat and results in breakage of bonds and generation of free radicals. Secondary damage, on the other hand, is due to the diffusion of the free radicals and other reactive products through the crystal which cause damage at different areas of the crystal, including those which are not in direct contact with the beam. Primary radiation damage is dose-dependent, while secondary radiation damage is time- and temperature-dependent (Garman, 1999). Disulfide bonds, sulfur-containing residues and acidic residues, including aspartates and glutamates, have been shown to be more susceptible to radiation damage than other protein elements, suggesting that radiation damage is specific (Weik et al., 2000, 2001). Radiation damage to glutamates and aspartates may lead to decarboxylation of these residues (Weik et al., 2001). Another factor that has been shown to influence the radiation sensitivity of proteins is the location of the residues in the structure: active site residues and the residues with more solvent accessibility tend to be more radiation sensitive that their buried counterparts (Burmeister, 2000; Weik et al., 2000, 2001). The latter are more exposed to radiolytic products of water, hydroxyl and hydrogen radicals, than the residues buried within the protein structure.

Radiation damage is mitigated by collecting diffraction data at cryogenic temperatures (near 100 K), which minimizes secondary damage by the diffusion of reactive products. Prior to cooling the crystal with a cryogen it is treated with a cryoprotectant, which prevents the formation of ice in the crystal during cryogenic cooling. It does this by forming a vitreous glass layer around the crystal (Garman, 1999; Garman & Schneider, 1997). Just like crystallization

19

conditions, adequate cryoprotectant has to be determined and optimized. In some cases there may be ligands in the crystal and one may have to maintain the concentration of the ligand in the crystal during cryoprotection in order to make sure that the protein/crystal does not lose the ligand (Leif et al., 2003). The ligand may be needed for protein stability, structure solution and the interpretation of the protein function once the structure has been solved. Also, the method of cryoprotection has to be determined. One of them is soaking the crystal with a solution, usually the mother liquor, containing a cryoptotectant. Ideally, the cryoprotectant is included in the crystallization solution, which helps minimize crystal handling (Garman, 1999). With reduced radiation damage at cryo-temperatures usually a single crystal suffices for the collection of the entire data set. This is particularly important during multiple-wavelength anomalous dispersion (MAD) data collection during which a single crystal may be exposed to radiation dose for longer periods of time at multiple wavelengths. Collection of diffraction data from multiple crystals could mean more likelihood to introduce systematic errors, including non-isomorphism, and reduction of the chances to solve the crystal structure. Cryocrystallography also allows for safe storage and transport of crystals without them losing their diffraction quality. This allows efficient use of synchrotron beam lines whereby the crystals can be retrieved when beam time becomes available or when it is convenient for the crystallographer to do so (Garman & Schneider, 1997). However, cryocooling the crystals may lead to crystal lattice disorder, increased mosaicity (due to rapid temperature change), poor resolution, high B-factors and ice ring diffraction (Garman, 1999; Kriminski et al., 2002). This can be mitigated by crystal annealing, which involves warming the frozen crystal for a short period of time and then cooling it again (Kriminski et al., 2002; Hanson et al., 2003). This promotes crystal lattice relaxation.

Advances in synchrotron radiation continue to make X-ray crystallography more robust. This includes the capability of some beamlines to be accessed remotely. Both beamlines of the CMCF, 08B1-1 and 08ID-1, at the Canadian Light Source are equipped with this technology (Grochulski et al., 2012). A laboratory information management system [*MX Laboratory Information Virtual Environment* (*MxLIVE*)] at the CMCF (Fodje et al., 2012) and other LIMS at other synchrotron facilities (Beteva et al., 2006; Delagenière et al., 2011; Gabadinho et al., 2010) allow for efficient management of data both on-site and off-site.

The process of X-ray diffraction data collection involves: 1) mounting the crystal on the goniometer and aligning it along the X-ray beam, 2) characterization of the crystal to determine

the strategy for data collection, and 3) implementing the optimum strategy for collection of the data (Winter & McAuley, 2011). The first step may be done manually, semi-automatically or automatically (Cipriani et al., 2006; Fodje et al., 2012; Pothineni et al., 2006; Ravelli et al, 2006). The second step involves collecting a few diffraction images and determining the characteristics of the crystal from these preliminary images; such as lattice type, unit cell dimensions and the presence of any crystal defects that may influence how the rest of the data should be collected for optimum quality. If the crystal is expected to contain a heavy atom and the experimenter considers collecting anomalous data, the characterization of the crystal will involve performing an excitation or a fluorescence scan, which reports on the elemental composition of the crystal. The crystallographer then determines the possible strategies for the collection of complete dataset. For example, for a high symmetry crystal a narrow total range of rotation may be sufficient to collect a complete data set, for example 45° total sweep for tetragonal symmetry. On the other hand, for a low symmetry crystal one may want to choose a wider rotation range, for example 180° for triclinic symmetry (Dauter, 1999). This is because symmetry-equivalent reflections have identical intensities and there are more of these in higher symmetry crystals than there are in lower symmetry crystals. The preliminary image analysis also helps determine the optimum exposure time. Exposure time should be long enough for collection of weak reflections, but not too long that the crystal ends up being overexposed to radiation dose leading to radiation damage. This analysis also helps determine the optimum crystal-detector distance to record all the reflections, including high resolution reflections at the edge of the detector. In case of potential defects, the experimenter determines whether it is worth going ahead with collection of the entire data set or if a different crystal needs to be examined. Possible crystal defects include twining, presence of ice rings and excessive mosaicity. For anomalous data collection the strategy would involve optimized X-ray wavelength(s) for optimum anomalous signal.

The data is processed using some of the commonly used softwares, including *XDS* (Kabsch, 2010), *BEST* (Popov & Bourenkov, 2003), *HKL-2000* (Minor & Otwinowski, 1997), *xia2* (Winter, 2010). This involves indexing, during which the geometry of the crystal is determined. Diffraction data processing also involves integration, scaling and merging of the reflections. It is during the latter that symmetry-equivalent reflections are combined. Some of the parameters used to measure the quality of the diffraction data are resolution, signal-to-noise ratio, completeness, multiplicity and R_{merge}. Resolution is the minimum distance between diffracting planes of a

crystal with the crystal still yielding diffraction data (Wlodawer et al., 2008). The smaller the spacing the more the reflections recorded, which means more data for structure solution and refinement. A complete data set is a data set in which all the reflections have been recorded. This is not always the case as crystals are very susceptible to radiation damage. Multiplicity is the average number of measurements for equivalent reflections. R_{merge} is a measure of the agreement between equivalent reflections (Equation 2.1).

$$R_{merge} = \Sigma_h \Sigma_i \left| <I_h> - I_{h,i} \right| / \Sigma_h \Sigma_i I_{h,i} \qquad (2.1)$$

where h is the unique reflections and i is their symmetry-equivalent contributors.

2.2.4   Structure determination

Once the diffraction data has been collected, the next step is to calculate an electron density map from which the molecular model is built. The electron density map is a Fourier transform of structure factors, which are comprised of amplitudes and phases (Equations 2.2 and 2.3). The amplitudes are calculated from the intensities of reflections recorded during data collection. The phase information, on the other hand, is not recorded and has to be determined (Taylor, 2003). This is termed the "phase problem" in crystallography and structure determination is the determination of phase information needed to calculate the electron density map.

$$\mathbf{F}_{hkl} = \left| F_{hkl} \right| e^{i\alpha_{hkl}} \qquad (2.2)$$

$$\rho(xyz) = 1/V \Sigma \left| F_{hkl} \right| e^{i\alpha_{hkl}} e^{-2\pi i(hx + ky + lz)} \qquad (2.3)$$

where $\mathbf{F}_{hkl}$ are structure factors, $\left| F_{hkl} \right|$ are the amplitudes, α_{hkl} are the phase angles for the reflections hkl and $\rho(xyz)$ is electron density. The amplitudes, $\left| F_{hkl} \right|$, are derived from the intensities recorded during X-ray diffraction data collection ($I \propto \left| F_{hkl} \right|^2$, where I are intensities of reflections).

Small molecules contain fewer atoms and diffract to higher resolution compared to large molecules, such as proteins. Phases of reflections in small molecules can be calculated from their

diffraction data alone based on strong reflections at certain regions of the unit cell. These methods of phase determination are called direct methods and they rely on estimation of phases of some reflections and using them to deduce the phases of the rest of the reflections (Cowtan, 2001 and Taylor, 2003). For large molecules, on the other hand, this approach does not work. Additional experiments have to be conducted to determine the phases and these include molecular replacement, isomorphous replacement and anomalous dispersion.

2.2.4.1 Molecular replacement

This structure determination method requires the availability of a structure of a homologous model. Normally the minimum sequence identity required for a model to qualify to be used as a search probe is 25 % (Taylor, 2003). However, search models with varying sequence identities have been reported in the literature with varying successes (Scapin, 2013). This method of phase determination involves the rotation of the search model (homologous model) to determine its orientation with respect to that of the unknown in the crystal unit cell. The oriented model is then translated to determine its position relative to the position of the unknown in the crystal unit cell and if correctly rotated and translated it is placed in the crystal unit cell. Structure factors of the placed model are calculated and compared to those of the unknown structure. If they agree, the phases of the search model and amplitudes of the unknown (from the diffraction data) are used to calculate the electron density. There are several computer programs for searching molecular replacement solutions. These include *Phaser* (McCoy et al., 2007), *SOMoRe* (Jamrog et al., 2005), *AMoRe* (Navaza, 1994; Navaza, 2001), *MOLREP* (Vagin & Teplyakov, 1997; Vagin & Teplyakov, 2010). Depending on the complexity of the problem one program may be superior to the other due to the fact that they use different algorithms. Some of the factors that determine the success of a molecular replacement search are the quality of the search model (for example; completeness, resolution, final refinement statistics prior to depositing, and presence of flexible regions or loops which may adopt different conformations), the quality of the diffraction data (for example, the size of the unit cell and the number of molecule copies in it), the level of similarity between the search model and the target protein. In some situations the search model may have to be manipulated to increase the chances of success of molecular replacement. These modifications may include side chain mutations and deletion of gaps based on the amino acid sequence alignment of the search model and the provided sequence of the unknown structure. Some of

these molecular replacement programs have these model preparation features incorporated in them already (Lebedev et al., 2008; Vagin & Teplyakov, 2010).

2.2.4.2 Isomorphous replacement and anomalous dispersion

Isomorphous replacement and anomalous dispersion are similar in the sense that they rely on the presence of atoms other than carbon, nitrogen and oxygen in a crystal. Also, these two methods do not require the availability of a homologous model. When heavy atoms (such as mercury and silver) are present in a crystal, the reflections will be more intense than the reflections of a protein crystal in which there are only carbon, nitrogen and oxygen atoms normally found in proteins. This is because there are more electrons in heavy atoms than there are in light atoms. Isomorphous replacement involves collection of a native data set and a heavy atom derivative data set(s). The former is collected from crystals without heavy atom introduction and the latter is a data set from a crystal in which a heavy atom has been introduced. The two crystals must be isomorphous so that the only difference between them is the intensity of reflections due to the heavy atom, hence the name isomorphous replacement. The difference between the intensities of reflections of the heavy atom derivative and those of the native crystal gives the intensities of reflections of the heavy atom. Direct methods can then be used to derive the position of the heavy atom, which is subsequently used to calculate the phase information of the native crystal and hence its electron density map. When a single derivative is used the method is called single isomorphous replacement and when more than one heavy atom derivatives are used it is called multiple isomorphous replacement. In addition to contributing more intense reflections than light atoms, the intensities of reflections of the Friedel pairs of heavy atoms are not equal. This is due to the fact that their electrons are more tightly bound to their nuclei than it is the case with light atoms. Heavy atoms are therefore, considered anomalous scatterers and their presence in protein crystals give anomalous signal during X-ray diffraction (Drenth, 2007). Similar to isomorphous replacement, the anomalous signal is used to determine the position of the heavy atom by direct methods and subsequently, the electron density map of the protein is calculated. The anomalous signal contributed by heavy atoms is wavelenghth-dependent. The method is called single-wavelength anomalous dispersion or multi-wavelength anomalous dispersion when diffraction data is collected at a single wavelength or mutiple wavelengths, respectively.

2.2.5   Model building, refinement and validation

Model building involves fitting the polypeptide backbone and the side chains of the amino acid residues to the electron density map based on prior knowledge, such as amino acid sequence and the experimental data, that is the quality of the electron density map. In case of the electron density map calculated by molecular replacement, there will be some parts of the polypeptide backbone in the map already. Therefore, one may consider refinement before fitting the rest of the molecule in the map, and this may depend on the level of completeness of the model already built in the map. For the electron density map calculated by anomalous dispersion or isomorphous replacement, model fitting has to be started from the beginning. During refinement the aim is to find the closest agreement between the calculated and the observed structure factors by varying model parameters. The progress and the quality of the refinement strategy are normally monitored by the change in R-factors. These measure the deviation between the observed and calculated structure factor amplitudes (F_{obs} and F_{cal}; Equation 2.4) and a drop in these values indicate an improvement in the quality of the model. The two R-factors used are R_{work} and R_{free}. The former is calculated using the reflections used in refinement. During electron density map calculation and refinement a fraction of random reflections is set aside and is not used in these processes. These reflections are used to calculate R_{free} and this serves as a cross validation tool that is used to ensure that the diffraction data is not over-interpreted (Brunger 1992). In addition to the R-factors, geometrical parameters such as, bond lengths and angles are used to measure the quality of the refined model. Some of the programs used for this include *Molprobity* (Chen et al., 2010) and *PROCHECK* (Laskowski et al., 1993).

$$R\text{-factor} = \Sigma \left| F_{obs} - F_{cal} \right| / \Sigma F_{obs} \tag{2.4}$$

2.3   Crystal structures of prolidases

Prolidases whose crystal structures have been solved include the ones from *Pyrococcus furiosus* (1pv9), *Pyrococcus horikoshii* (1wy2)*,* and *Thermococcus sibricus* (4fkc). They are all homodimers with each subunit consisting of two domains, an N-terminal domain and a C-terminal domain, linked by a helical linker. Their C-terminal domains contain the enzyme active site with two metal ions coordinated by two aspartic acids, two glutamic acids and one histidine residue (Jeyakanthan et al., 2009; Maher et al., 2004; Trofimov et al., 2012). The metal ions are

needed for the enzymes' catalytic activity. Prolidases from *Pyrococcus* species are activated by Co^{2+} and to a lesser extent Mn^{2+}, whereas Zn^{2+} inactivates these enzymes (Ghosh et al., 1998; Jeyakanthan et al., 2009; Maher et al., 2004). The inhibitory effect of Zn^{2+} has been seen in prolidase from *Lactobacillus delbrueckii* and human liver as well (Stucky et al., 1995; Wang et al., 2005). Prolidases from *Escherichia coli* and humans prefer Mn^{2+} for full activity (Park et al., 2004; Wang et al., 2005). However, Zn^{2+} and Mn^{2+} have been shown to co-exist in the metal center of human prolidase with the enzyme retaining partial activity (Besio et al., 2010). Mutations of the residues coordinating the metal center in *P. furiosus* prolidase lead to reduced activity when the residues mutated are responsible for coordinating only one of the metal atoms. The mutant in which the residue mutated coordinates both metal atoms does not show activity (Du et al., 2005). These findings on two prolidases from different organisms, human and *P. furiosus*, suggest that at least one of the metal sites has to be occupied by a preferred metal for some activity and both of them have to be occupied for full activity by this enzyme.

The refined model of *P. furiosus* prolidase consists of a homodimer in the crystal asymmetric unit. However, its subunit A is more ordered than subunit B, which is missing some parts. The structure was solved with Zn in the metal center, which does not support enzyme activity (Ghosh et al., 1998 and Maher et al., 2004). This structure was solved at 2.0 Å resolution and the final R_{work} and R_{free} are 24 and 28, respectively (Maher et al., 2004). Like *P. furiosus* prolidase, the model of *P. horikoshii* prolidase consists of a homodimer in the crystal asymmetric unit (Jeyakanthan et al., 2009). Unlike *P. furiosus* prolidase, both subunits are well-defined and are of similar quality. In addition to the five amino acid residues coordinating the two Zn atoms in the metal center, a molecule of cacodylate is present next to the metal center and it is also involved in metal coordination. The structure was solved at 1.7 Å resolution and the final R_{work} and R_{free} are 18.7 and 21.0, respectively. The crystal structure of *T. sibricus* prolidase was solved at 2.6 Å resolution and the final R_{work} and R_{free} are 23.1 and 26.9, respectively (Trofimov et al., 2012). The structure was solved with two Cd atoms in the metal center.

The most studied prolidase among these is *P. furiosus* prolidase. Maher et al. (2004) revealed that in *P. furiosus* prolidase a segment of subunit B (residues 36B - 39B) was close to the active site in subunit A and proposed that these residues may be involved in enzyme function, including substrate selection (Maher et al., 2004). Residues 36 - 39 are part of a loop structure in *P. furiosus* prolidase. Structure prediction model revealed that the loop structure (residues 32 -

43) is also present in *L. lactis* prolidase (Chen & Tanaka, 2011). However, in *L. lactis* prolidase the loop is longer and it contains charged amino acid residues, which are not present in *P. furiosus* prolidase. These residues are Asp 36, His 38, Glu 39 and Arg 40. This led to the hypothesis that the charged loop residues of *L. lactis* prolidase could be responsible for its unique characteristics (allosteric behaviour, metal-dependent substrate specificity and substrate inhibition). A mutant without the charged residues, Δ36 - 40, does not show enzyme activity. Therefore, the mechanisms of involvement of the charged loop residues could not be elucidated from this mutant, while the crucial influence of the loop is confirmed (Zhang et al., 2009). The Δ36 - 40 mutant, however, maintained other properties of the wild-type enzyme, including its dimeric conformation as evidenced by native-PAGE and gel filtration. Recent research has focused on trying to reveal the structural elements responsible for the unique catalytic properties of *L. lactis* prolidase using site-directed mutagenesis and computational modeling. Substitution of Asp 36 (Chen & Tanaka, 2011) and Arg 293 (Zhang et al., 2009) with serine (D36S and R293S) led to disappearance of allosteric behavior, suggesting that the negative charge of Asp 36 and the positive charge of Arg 293 are involved in the allosteric nature of the enzyme. This hypothesis was proven when a double mutant with the charges at these positions kept, D36E/R293K, maintained allosteric behavior of the wild-type enzyme; whereas, R293S mutant lost its allosteric behaviour (Zhang et al., 2009). Although substitution of His 38 (H38S) maintained activity, this mutant exhibited reduced substrate inhibition, suggesting that His 38 was involved in substrate inhibition. On the other hand, substitutions of Glu 39 and Arg 40 (E39S, D36S/E39S, R40S, R40K, R40E and H38S/R40S) led to loss of activity, suggesting that these two loop residues are needed for enzyme catalysis (Chen & Tanaka, 2011). These results all indicate the involvement of the predicted loop structure of residues number 32 - 43. However, the arguments are based on the predicted models and may not reflect the true structure of prolidase.

3 HYPOTHESES AND OBJECTIVES

It is hypothesized that knowledge of the three-dimensional structure of *L. lactis* prolidase will help elucidate the mechanism of its catalysis and thus contribute knowledge towards some of its potential applications. Structure determination will be aided by the availability of crystal structures of homologous models, which will be used as search models in molecular replacement. It is generally known that more stable macromolecules crystallize better than flexible macromolecules. Therefore, it was hypothesized the mutant in which some of the residues have been deleted (Δ36-40) may crystallize better than the wild-type prolidase, due to the presence of the longer flexible loop in the former. Also, since the dimeric conformation of wild-type prolidase were preserved in the Δ36-40 mutant, it was hypothesized that its crystal structure could also be used to interpret the functional properties of wild-type prolidase. Since *L. lactis* prolidase shows unique characteristics from other known prolidases, the three-dimensional structure should show the structural differences that result in the functional differences. The objectives of the current study were, therefore, 1) to grow crystals of wild-type and Δ36-40 mutant *L. lactis* prolidase and to solve their crystal structures by molecular replacement method; and 2) to interpret the functions of *L. lactis* prolidase based on the solved crystal structure.

4 MATERIALS AND METHODS

4.1 *L. lactis* prolidase expression and purification

Prolidase gene-containing *Escherichia coli* TOP10F' (Yang & Tanaka 2008) was cultured in 2 x 1.5 L Luria-Bertani (LB) broth (pH 7.0) at 17 °C. Prolidase expression was induced by 1 mM isopropyl β-D-1-thiogalactopyranoside (IPTG) when an optical density of 600 nm was 0.5. The culture was allowed to grow at 17 °C for another 48 hours and the biomass was recovered by centrifugation (Sorvall Instruments Centrifuge; DuPont, Wilmington, DE, USA; Sorvall GSA rotor, 6000 rpm, 20 minutes, 4 °C). Purification of recombinant *L. lactis* prolidase was further optimized from what was previously described (Yang & Tanaka, 2008). In this thesis research it involved suspending harvested cells in 10-fold volume of 20 mM sodium citrate (pH 6.0)/ 1 mM manganese chloride. The cells were disrupted with a French press cell disruptor at 35 kPsi. The lysates were centrifuged at 11,000 rpm for 20 minutes yielding crude extraction of soluble proteins. The targeted recombinant protein was recovered by 60 % saturated ammonium sulfate precipitation. The protein was then dissolved in 3 ml of 20 mM sodium citrate (pH 6.0)/ 1 mM manganese chloride and dialyzed against 1 L of the same buffer at least three times. This was then loaded on DEAE anion exchange column (GE Healthcare DEAE Sephacel; Little Chalfont, Buckinghamshire, UK; 5 cm diameter × 20 cm), which was pre-equilibrated with the above-mentioned buffer. Prolidase was eluted with a 0 to 0.6 M sodium chloride linear gradient. Prolidase-containing fractions, as determined by SDS-PAGE (Figure 4.1), were combined and concentrated using an Amicon filtration unit (YM30; 30 kDa cut-off; Millipore, Billerica, MA, USA). The protein sample was filtered through a 0.2 µm filter and further purified using gel filtration chromatography (GE Health Science Superdex 200 10/300 GL; Little Chalfont, Buckinghamshire, UK; 24 ml). Two hundred and fifty microlitres of concentrated protein sample was loaded on the column and eluted with 20 mM sodium citrate (pH 6.0), 1 mM manganese chloride, 0.15 M sodium chloride and 15 % glycerol at a flow rate of 0.25 ml/min. Prolidase-containing fractions from this step were identified on SDS-PAGE. The chromatogram and the SDS-PAGE diagram from this purification step are shown in Figures 4.2 and 4.3, respectively. The prolidase-containing fractions were combined and concentrated using centrifugal devices (Microsep Advance Centrifugal Devices; Pall Corporation, Ann Arbor, MI, USA; 10 kDa cut-off). The concentration and purity were determined by the Bradford method and by the presence

29

of a single band on SDS-PAGE, respectively. The same procedure was followed for both wild-type and Δ36-40 mutant *L. lactis* prolidase. Prior to crystallization the protein solution was diluted to the desired concentration using 2 mM sodium citrate (pH 6.0)/ 1 mM manganese chloride, which had been filtered through a 0.2 µm filter. The protein solution was also filtered and/or centrifuged at 14,000 rpm for 5 minutes to remove any foreign material and denatured proteins.
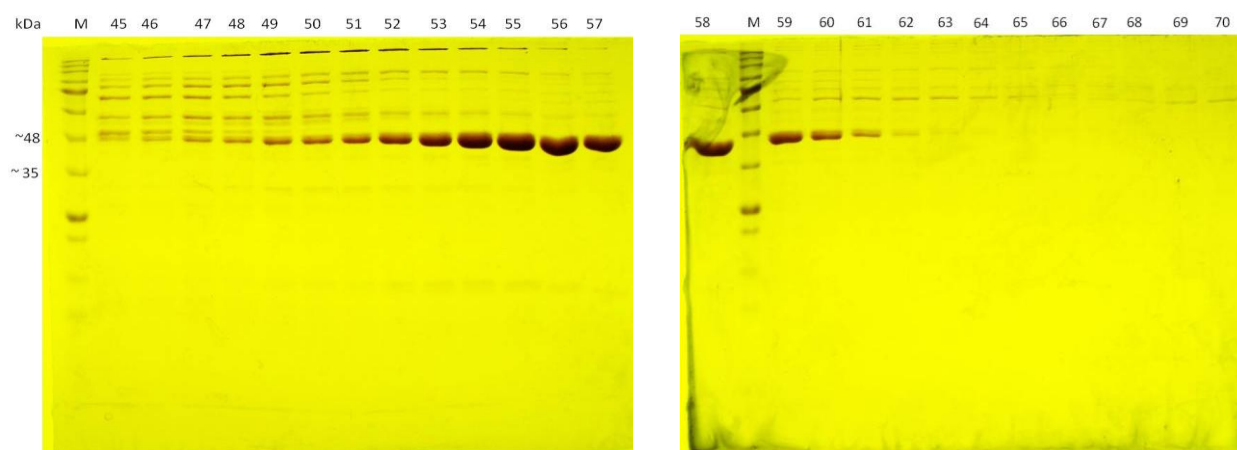
Figure 4.1 SDS-PAGE showing wild-type *L. lactis* prolidase fractions from DEAE anion exchange chromatography.

"M" is molecular weight marker and the numbers represent the fraction numbers. Fractions 53 - 59 are wild type prolidase-containing fractions that were chosen for further purification.
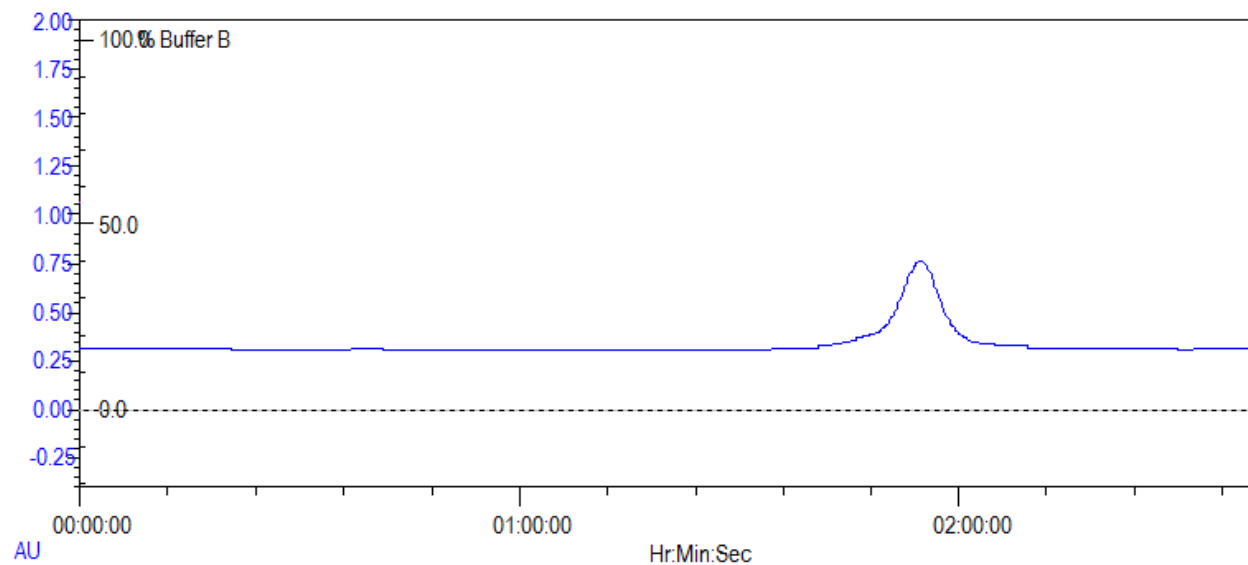
Figure 4.2 Size exclusion chromatogram of wild type *L. lactis* prolidase.

The eluent buffer comprised 20 mM sodium citrate (pH 6.0), 1 mM manganese chloride, 0.15 M sodium chloride and 15 % glycerol.
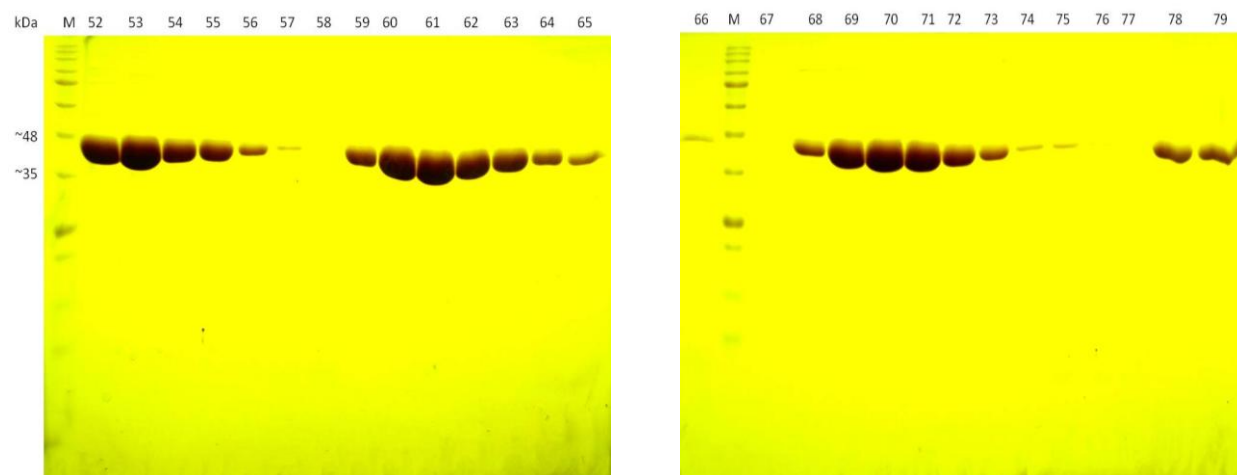
Figure 4.3 SDS-PAGE showing wild-type *L. lactis* prolidase fractions from size exclusion chromatography.

"M" is molecular weight marker and the numbers represent the fraction numbers. The fractions that were combined and concentrated are 52 - 55, 59 - 63 and 69 - 72.

4.2 Crystallization

4.2.1 Screening

Hampton Research screens HR2-110 and HR2-112 (Tables A1 and A2) were used as the initial screens for crystallization using the hanging drop vapour diffusion method. Reagents 25 and 27 of HR2-110 were not used since they are known for not producing crystals. Therefore, the total number of reagents used was 96. The starting concentration was 10 mg/ml for both wild type and Δ36-40 mutant *L. lactis* prolidase solutions. Two identical set ups were carried out in 24-well plates, one at room temperature and the other at 4 °C. The crystallization drops consisted of 2 µl of the reservoir solution and 2 µl of the protein solution during initial screening.

In order to investigate a wider range of conditions, a purified wild-type *L. lactis* prolidase solution was sent to Hauptman-Woodward Research Institute for automatic high-throughput screening. The method used was microbatch-under-oil and 1536 reagents were screened. This involved mixing 200 nl of the protein sample with the same volume of the crystallization screening reagent and covering the drop with paraffin oil. Image capturing and recording was done a day after setting up and weekly after for a total period of six weeks. The detailed procedure followed is explained in Luft et al. (2003)

4.2.2 Optimization

The conditions that produced any form of crystals, including microcrystals, needles and plates, from Hampton screens were optimized. Optimization involved varying temperature, protein concentration, concentrations of the screening reagents, the pH of the buffer, and substituting metal salts in screening reagents with different ones. The same crystallization method, hanging drop vapour diffusion, was used during optimization.

For high-throughput screening only conditions that produced three-dimensional and symmetrical crystals were selected for optimization. Both hanging drop vapour diffusion and microbatch under oil methods were used to set up these optimization experiments. The latter was performed in 72-well microbatch plates by mixing 1 µl of the protein solution with 1 µl of the protein solution and covering the drop with paraffin oil. This is illustrated in Figure 4.4.
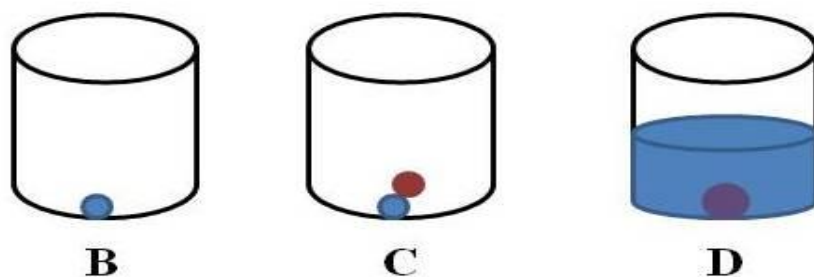
Figure 4.4 An illustration of the steps taken when setting up a microbatch-under oil crystallization experiment.

A: A 72-well microbatch plate used to prepare the setup. **B:** 1 µl of the crystallization cocktail was added to 5 replicate experiment wells. **C:** The same volume of a protein solution was by touching the pipette tip to the cocktail drop and dispensing the solution to each of the experiments. **D:** 20 µl of paraffin oil (PX0045-3; EMD Chemicals, Darmstadt, Germany) was added to each well. An additional 5 ml of paraffin oil was used to cover all the wells once all the drops had been set up.

Co-crystallization was done by including solutions of proline, proline + leucine, proline + arginine and proline + phenylalanine in the crystallization reagents and/or the crystallization drops. The criterion for co-crystallant selection was based on the preference of prolidase for Leu-Pro and Arg-Pro as substrates and its preference for substrates with hydrophobic residues at the N-terminal end of the dipeptide, such as Phe-Pro (Yang & Tanaka, 2008).

33

4.3   X-ray diffraction

Diffraction data was collected at a wavelength of 0.9795 Å on beamline 08ID-1 of the Canadian Macromolecular Crystallography Facility at the Canadian Light Source (CLS) (Grochulski et al., 2011). The crystals were individually scooped out of the crystallization cocktail using a loop and immediately immersed and cooled in liquid nitrogen. Additional cryoprotection was not considered since the crystallization solution contained 12 - 15 % PEG, which acts as a cryoprotectant. They were then rapidly transferred from the liquid nitrogen and mounted on a goniometer, under a stream of gaseous nitrogen, using a cryotong. Prior to collecting the entire data set, about 10 frames were collected and processed to characterize the crystal and determine the optimum strategy for the collection of diffraction data. In order to determine the elemental composition of the crystal and the surrounding mother liquor, X-ray fluorescence scanning was performed.

4.4   Structure determination

The amino acid sequence of *L. lactis* prolidase was used to search for the templates to be used in molecular replacement. The search models found in the Protein Data Bank with the highest amino acid sequence identities were prolidases from *P. furiosus* (1pv9) and *P. horikoshii* OT3 (1wy2). They both had 37 % amino acid sequence identity with *L. lactis* prolidase. Based on amino acid sequence alignments, the similarities at the N-terminal ends were lower compared to those at the C-terminal ends of the sequences (Figure 4.5). Therefore, a better match for the first 122 residues was searched for and was found to be *Streptococcus pneumoniae* proline dipeptidase (3pn9), which comprises 138 amino acid residues. It showed 43 % amino acid sequence identity with the N-terminal end (residues 1 - 122) of *L. lactis* prolidase. When using the remaining residues of *L. lactis* prolidase (residues 123 - 362), the sequence identity with *P. horikoshii* prolidase increased to 45 %. Therefore, *S. pneumoniae* prolidase and the C-terminal domain (residues 125 - 351) of *P. horikoshii* prolidase were selected as molecular replacement search templates. Model preparation involved removing the ligands they were solved with (including water molecules, metal atoms and crystallization solvents) and converting them to polyalanine peptides in *PHENIX* (Adams et al., 2010). Molecular replacement was performed using *Phaser* (McCoy et al., 2007), which is also in *PHENIX* suite.

```
Llprol:   2  SKIERISAFLNDKEVDMTFITNPTTLNYLTGLAIDPHERIAGLMIFRDSTPMLFTPALEV  61
             K+++I F++   +D  I    + Y++G          G ++    +  L+ P LE
Phprol:   6  EKVKKIIEFMDKNSIDAVLIAKNPNVYYISG----ASPLAGGYILITGESATLYVPELEY  61

Llprol:  62  EKAKEHTSGLDIFGYEDSQNPWEVVKNHVKSDVKSIAVEFSDIPLAKTEGLKAQFGDINF 121
             E AKE +  + ++  ++      ++ +      +KS+ +E S +P   E LK +     F
Phprol:  62  EMAKEES-NIPVEKFKKMDEFYKAL-----EGIKSLGIESS-LPYGFIEELKKKANIKEF 114

Llprol: 122  VNLTPLIERMRLIKSADEIEKMKVAGDFADKCFEIGFATAAERNGVTESDIVAKIEYEMK 181
                +  +I  MR+IKS  EI+ ++ A + ADK          G  E ++ AK+EY MK
Phprol: 115  KKVDDVIRDMRIIKSEKEIKIIEKACEIADKAVMAAIE--EITEGKKEREVAAKVEYLMK 172

Llprol: 182  RMGVPQMSFDTLVLSGARAANPHGAPENVEIQENKLLLFDLGVMSGGYASDATRTIAIGQ 241
             G  + +FDT++ SG R+A PHG   +  I+   L++ DLG +  Y SD TRTI +G
Phprol: 173  MNGAEKPAFDTIIASGYRSALPHGVASDKRIERGDLVVIDLGALYQHYNSDITRTIVVGS 232

Llprol: 242  PNDFDAEIHKIVKEAQQAAMDFIKPGVTAHEVDAVARDLITKAGYGEYFNHRLGHGIGMD 301
             PN+    EI++IV EAQ+ A++   KPG+TA E+D++AR++I + GYGEYFNH LGHG+G++
Phprol: 233  PNEKQKEIYEIVLEAQKKAVESAKPGITAKELDSIARNIIAEYGYGEYFNHSLGHGVGLE 292

Llprol: 302  VHEYPSIVAGNDLVIQEGMCFSNEPGIYIPGKVGVRIEDCLYVTENGCESFTHTDHDLL 360
             VHE+P +   ++ V++EGM + EPGIYIP   GVRIED + +T+NG +  T T+ +L+
Phprol: 293  VHEWPRVSQYDETVLREGMVITIEPGIYIPKIGGVRIEDTILITKNGSKRLIKTERELI 351
```

```
Llprol:   7  ISAFLNDKEVDMTFITNPTTLNYLTGLAIDPHERIAGLMIFRDSTPMLFTPALEVEKAKE  66
             +  F+++  +D  FI P + Y +G +          G +I      L+ P LE E AKE
Pfprol:   1  LVKFMDENSIDRVFIAKPVNVYYFSGTSPLGG----GYIILVDGDEATLYVPELEYEMAKE  56

Llprol:  67  HTSGLDIFGYEDSQNPWEVVKNHVKSDVKSIAVEFSDIPLAKTEGLKAQFGDINFVNLTP 126
             +  L + ++     +E++K      + +++ +E   +   E   K +     F   +
Pfprol:  57  ESK-LPVVKFKKFDEIYEILK-----NTETLGIEG-TLSYSMVENFKEKSXVKEFKKIDD 109

Llprol: 127  LIERMRLIKSADEIEKMKVAGDFADKCFEIGFATAAERNGVTESDIVAKIEYEMKRMGVP 186
             +I+ +R+IK+ +EIE ++ A + ADK          G  E ++ AK+EY MK   G
Pfprol: 110  VIKDLRIIKTKEEIEIIEKACEIADKAVMAAIE--EITEGKREREVAAKVEYLMKMNGAE 167

Llprol: 187  QMSFDTLVLSGARAANPHGAPENVEIQENKLLLFDLGVMSGGYASDATRTIAIGQPNDFD 246
             + +FDT++ SG R+A PHG   +  I+   L++ DLG +  Y SD TRTI +G PN+
Pfprol: 168  KPAFDTIIASGHRSALPHGVASDKRIERGDLVVIDLGALYNHYNSDITRTIVVGSPNEKQ 227

Llprol: 247  AEIHKIVKEAQQAAMDFIKPGVTAHEVDAVARDLITKAGYGEYFNHRLGHGIGMDVHEYP 306
             EI++IV EAQ+ A++   KPG+TA E+D++AR++I + GYG+YF H LGHG+G+++HE+P
Pfprol: 228  REIYEIVLEAQKRAVEAAKPGMTAKELDSIAREIIKEYGYGDYFIHSLGHGVGLEIHEWP 287

Llprol: 307  SIVAGNDLVIQEGMCFSNEPGIYIPGKVGVRIEDCLYVTENGCESFTHTDH 357
             I    ++ V++EGM + EPGIYIP   GVRIED + +TENG +  T T+
Pfprol: 288  RISQYDETVLKEGMVITIEPGIYIPKLGGVRIEDTVLITENGAKRLIKTER  33
```

Figure 4.5 Amino acid sequence alignments of _L. lactis_ prolidase (_Ll_prol) with _P. horikoshii_ (_Ph_prol, 1wy2) and _P. furiosus_ prolidase (_Pf_prol, 1pv9).

Identical and similar residues are highlighted green and marked with "+", respectively. The residues in the N-terminal ends of the prolidase sequences are less identical than the residues in the C-terminal ends. Alignments were performed using Basic Local Alignment Search Tool (Altschul et al., 1997).

4.5 Model building, refinement and validation

The molecular replacement solution was refined against the diffraction data in *PHENIX* (Adams et al., 2010). The protein residues were fitted in the electron density map using *Coot* (Emsley et al., 2010) for visual display, followed by real space refinement. Refinement strategies employed at the beginning included: rigid body, xyz, occupancies, individual *B*-factors, simulated annealing and NCS-restraints refinements. After fitting the polypeptide chains, the ligands were fitted from *Coot* library. Metal ion coordination and ligand restraints were generated using *ReadySet* implemented in *PHENIX*, which uses *electronic Ligand Builder and Optimization Workbench* (*eLBOW*) to generate ligand restraints (Moriarty et al., 2009). Water molecules were added automatically during refinement in *PHENIX*. The strategies employed towards the end of refinement included optimization of X-ray/stereochemistry and X-ray/ADP weights. Refinement was alternated with manual corrections of the model in *Coot*. The final refinement run was done using *REFMAC5* (Murshudov et al., 1997), incorporated in CCP4 program suite (Winn et al., 2011) and the refinement statistics table was compiled in *PHENIX*.

5   RESULTS

5.1   Crystallization

5.1.1   Screening

The crystallization screening results from both in-house hanging drop vapour diffusion setups are summarized in Table 5.1 and Figure 5.1. All successful conditions included PEG 8000 as the precipitant and sodium cacodylate as the buffer (Table 5.1). The crystallization screening results from high-throughput microbatch-under-oil are illustrated in Figure 5.2. In addition to the conditions consisting of PEG 8000 and sodium cacodylate producing crystalline material, more chemical reagents were successful at growing large three-dimensional and/or symmetrical crystals, including a variety of PEGs (Figure 5.2).

Table 5.1 Hampton Research reagents that were selected for optimization and the description of the crystalline material they produced.

Reagent formulation	Description of the crystals grown during screening
20 % (w/v) polyethylene glycol 8000, 0.1 M sodium cacodylate trihydrate (pH 6.5), 0.2 M magnesium acetate trihydrate	Rod clusters and single three-dimensional crystals
30% (w/v) polyethylene glycol 8,000, 0.1 M sodium cacodylate trihydrate (pH 6.5), 0.2 M sodium acetate trihydrate	Plate- and rod-like crystals, as well as three-dimensional crystals
18% (w/v) polyethylene glycol 8,000, 0.1 M sodium cacodylate trihydrate (pH 6.5), 0.2 M zinc acetate dihydrate	Plate-like (two-dimensional) crystals
18% (w/v) polyethylene glycol 8,000, 0.1 M sodium cacodylate trihydrate (pH 6.5), 0.2 M calcium acetate hydrate	Plate-like (two-dimensional) crystals
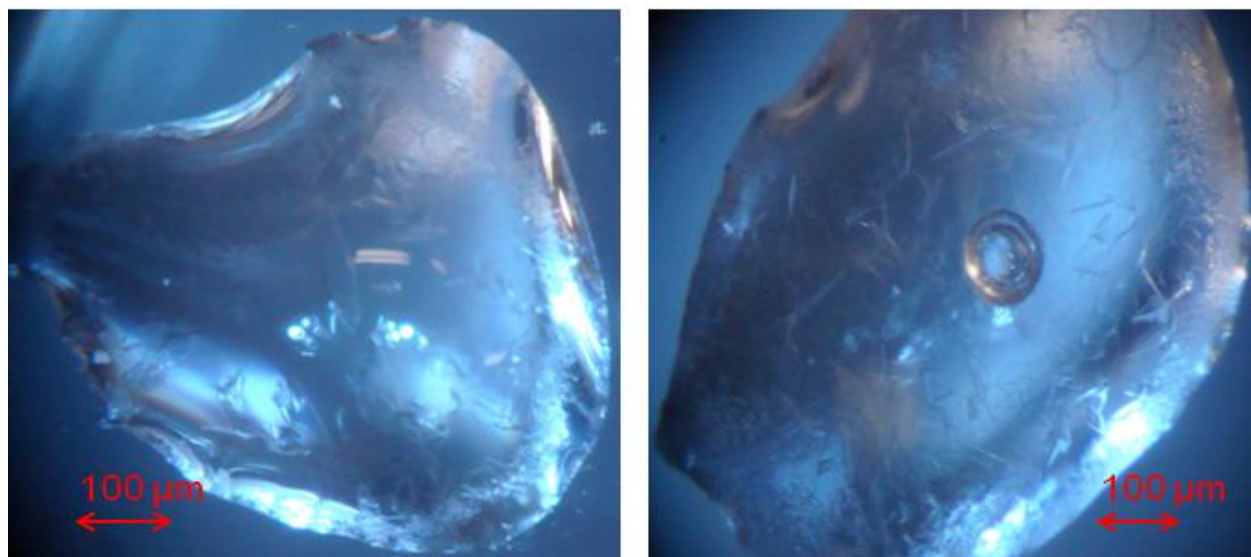
Figure 5.1 Needle-shaped and microcrystals obtained using Hampton Research crystallization reagents during in-house screening by the hanging drop vapour diffusion method.

These were obtained from crystallization solutions comprising PEG 8000, sodium cacodylate (pH 6.5) and 0.1 M manganese chloride.

5.1.2 Optimization

The conditions that produced crystals from optimizing Hampton Research screens were 0.1 M sodium cacodylate (pH 6.5), 12 - 16 % PEG 8000 and 0.1 M manganese chloride at 20 ℃ and room temperature (~25 ℃). Some of the crystals were bipyramidal in shape and about 250 µm in size (Figure 5.3). Others grew as long rods, rod clusters and twins. Optimization of the conditions from high-throughput screening using both the hanging drop vapour diffusion and microbatch under oil crystallization methods led to the growth of hexagonal plate-like crystals. However, the hanging drop method was preferred since the crystals floated in the crystallization drop and were easily scooped out during harvesting. On the other hand, crystals grown using the microbatch-under-oil method stuck to the bottom of the 72-well plate and were easily broken during harvesting. Thus, the diffraction data was only collected from the crystals from the hanging drop vapour diffusion method. Successful crystal growth was done in 0.08 M sodium cacodylate (pH 6.5), 0.16 M calcium acetate, 11 - 16 % PEG 8000, and 17 - 21 % glycerol.
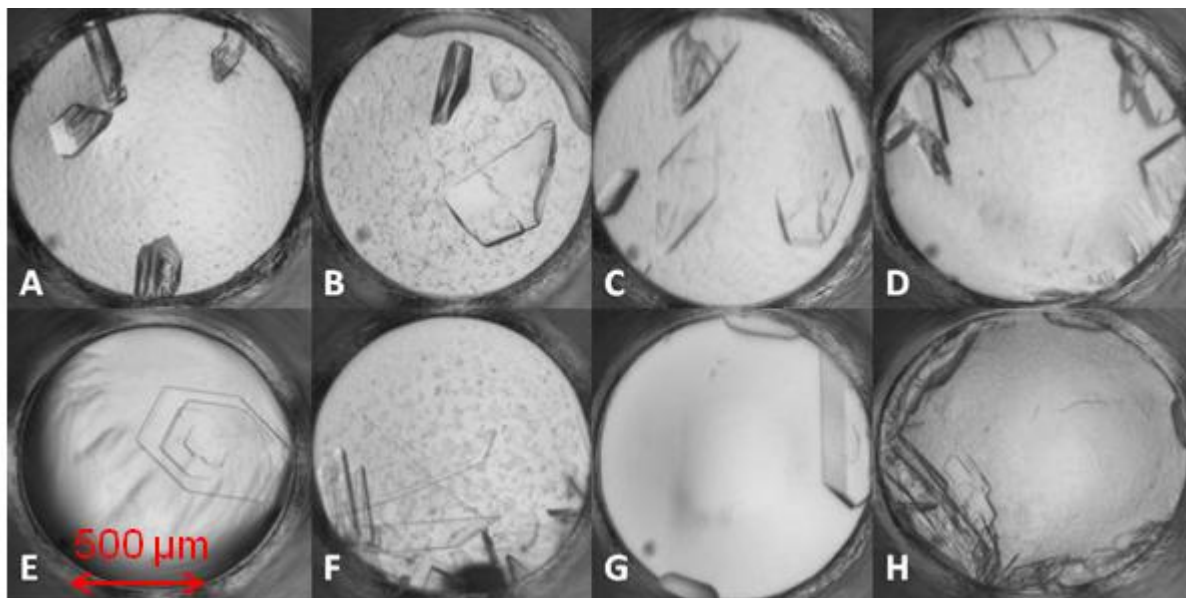
Figure 5.2 Three-dimensional and/or symmetrical crystals from high-throughput screening grown using microbatch-under-oil method.

Each crystallization drop consisted of 200 nl of 10 mg/ml wild-type *L. lactis* prolidase and 200 nl of the crystallization reagent. The reagents were **A:** 0.1 M ammonium nitrate, 0.1 M tris (pH 8), 24% PEG 20000; **B:** 0.1M lithium chloride, 0.1M tris (pH 8), 20% PEG 8000; **C:** 0.1M ammonium thiocyanate, 0.1M tris (pH 8), 20% PEG 8000; **D:** 0.1 M calcium acetate, 0.1 M bis-tris propane (pH 7), 20% PEG 4000; **E:** 0.16 M calcium acetate hydrate, 0.08M sodium cacodylate trihydrate (pH 6.5), 14.4% PEG 8000, 20% glycerol; **F:** 0.2M calcium chloride dihydrate (pH 5.1), 20% PEG 3350; **G:** 0.8M lithium sulfate monohydrate, 0.1M bis-tris propane (pH 7) and **H:** 1.5M lithium sulfate monohydrate, 0.1M tris (pH 8.5).

These conditions yielded plate-like hexagonal crystals (Figure 5.4), and interestingly, these conditions are very similar to the conditions that produced bipyramidal crystals (Figure 5.3). The same conditions that successfully yielded crystals of wild-type *L. lactis* prolidase also yielded large three-dimensional crystals of Δ36-40 mutant *L. lactis* prolidase. However, Δ36-40 crystals cracked and therefore, could not be used for X-ray diffraction. Representative crystals of Δ36-40 mutant *L. lactis* prolidase are illustrated in Figures 5.5. Co-crystallization with prolidase hydrolytic products, amino acids, was also successful. However, preliminary analysis of the diffraction data suggested that the crystals were not of sufficient quality for X-ray diffraction.
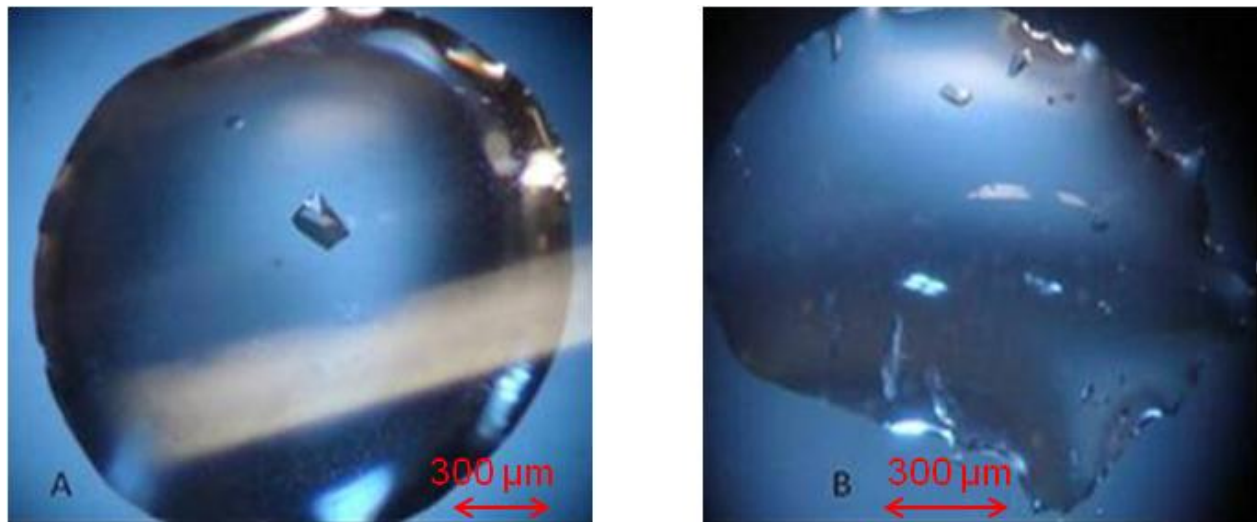
Figure 5.3 Crystals of wild type recombinant *L. lactis* prolidase grown using the hanging drop vapour diffusion method.

A: The drop consisted of 3 µl of the reservoir solution and 2 µl of 5 mg/ml wild type *L. lactis* prolidase. The reservoir solution comprised 15 % (w/v) PEG 8000, 0.1 M sodium cacodylate (pH 6.5) and 0.1 M manganese chloride. The set up was incubated at 20 ºC for 10 days. **B:** The drop consists of 2 µl of the reservoir solution and 2 µl of 5 mg/ml prolidase solution. The reservoir contained the same reagents as A, but the level of PEG 8000 was 12 % instead of 15 % (w/v). The set up was incubated at room temperature (~25 ºC) for 10 days.
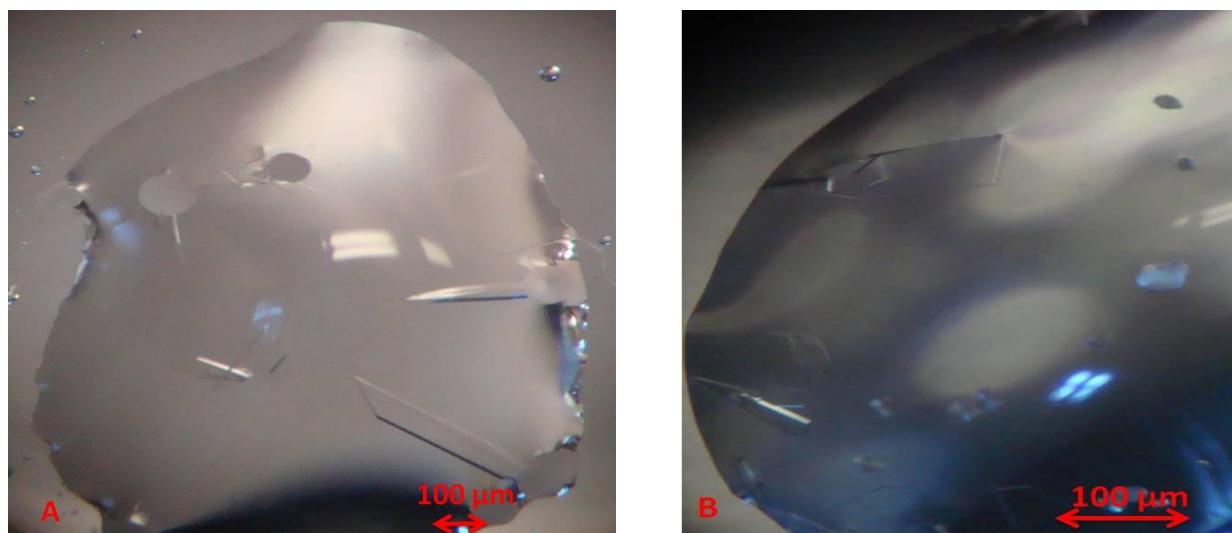
Figure 5.4 Crystals of wild type recombinant *L. lactis* prolidase grown in the presence and the absence of reaction products using the hanging drop vapour diffusion method.

A: The crystal drop comprised 2 µl of 5 mg/ml prolidase solution, 2 µl of the reservoir solution and 0.2 µl of 100 mM arginine. The reservoir comprised 0.16 M calcium acetate, 0.08 M sodium cacodylate (pH 6.5), 12 % PEG 8000, 20 % glycerol and 10 mM proline. The set up was incubated at 20 ℃ for 10 days. **B:** The crystallization drop comprised 2 µl of 5 mg/ml prolidase solution and 2 µl of the reservoir solution. The reservoir solution comprised 0.16 M calcium acetate, 0.08 M sodium cacodylate (pH 6.5), 14 % PEG 8000 and 18 % glycerol. The set up was incubated at room temperature (~25 ℃) for 10 days. These crystals were used for structure solution.
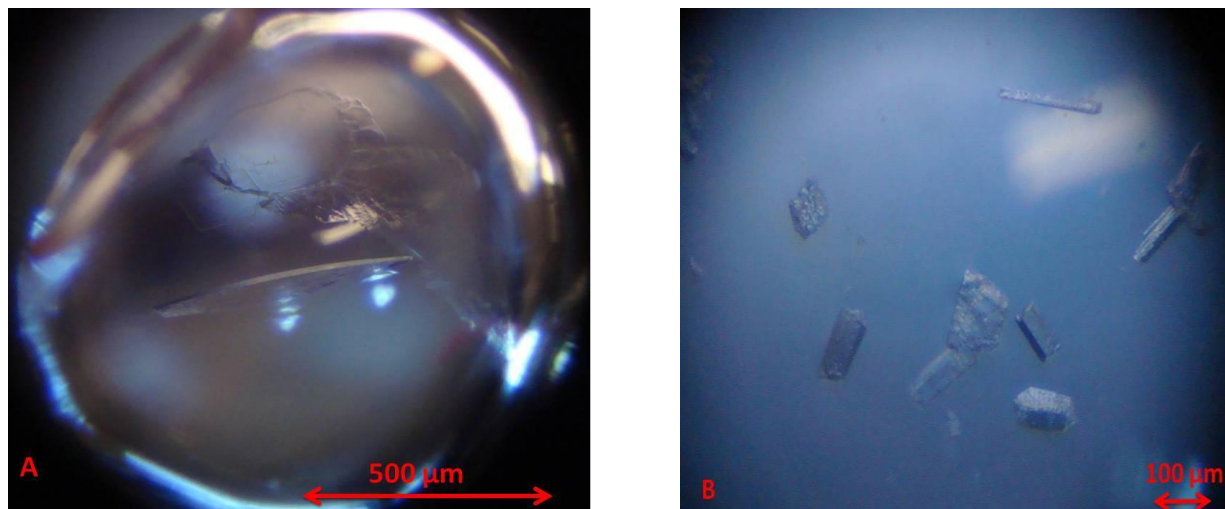
Figure 5.5 Crystals of Δ36-40 mutant recombinant *L. lactis* prolidase grown using the hanging drop vapour diffusion method.

A: The drop comprised 1 μl of 5 mg/ml prolidase solution, 1 μl of the reservoir solution and 0.2 μl of 100 mM leucine. The reservoir solution comprised 0.16 M calcium acetate, 0.08 M sodium cacodylate (pH 6.5), 15 % PEG 8000, 20 % glycerol and 10 mM proline. The set-up was incubated at 23 °C for 10 days. **B:** The drop comprised 2 μl of 5 mg/ml prolidase solution and 2 μl of the reservoir solution. The reservoir solution comprised 0.1 M calcium acetate, 0.1 M sodium cacodylate (pH 6.5) and 16 % PEG 8000. The set-up was incubated at 20 ºC for 10 days.

5.2   X-ray diffraction

The bipyramidal crystals produced from Hampton Research leads yielded 2.35 Å resolution and they belonged to space group *P*1. There was an estimate of six molecules in an asymmetric unit of the crystal. In addition to lack of symmetry and a high number of molecules in the crystal asymmetric unit, partial twinning was observed. This suggests that the large crystals grown were in fact multiple crystals that had grown on top of each other. Thus, the reflections recorded during X-ray diffraction data collection were from multiple crystals rather than a single crystal. The quality of the diffraction data was, therefore, low and determination of the three-dimensional structure of *L. lactis* prolidase using this data was not successful. On the other hand, the hexagonal crystals grown from high-throughput screening leads yielded 1.93 Å resolution data and they belonged to space group *C*2. There were three molecules in the crystal asymmetric unit. This data was of better quality than the former and was successfully used to determine the three-

dimensional structure of wild-type recombinant *L. lactis* prolidase. The data collection statistics from both crystal types are summarized in Table 5.2 for comparison.

Table 5.2 Data collection statistics from the first crystals of wild type *L. lactis* prolidase.

Crystal description	Bipyramidal	Hexagonal
Space group	$P1$	$C2$
Unit-cell parameters (Å, °)	$a = 81.27, b = 84.76,$	$a = 212.13, b = 76.99$
	$c = 100.47, \alpha = 73.68,$	$c = 88.92, \alpha = \gamma = 90,$
	$\beta = 69.01, \gamma = 89.91$	$\beta = 112.39$
Molecules per asymmetric unit	6	3
Resolution (Å)	2.35	1.93
$\{I/\sigma(I)\}$	10.96	6.28
Completeness (%)	97.80	99.8
Unique reflections	97414	99362
Multiplicity	3.9	3.8
R_{merge}	7.7	12.1

5.3 Structure determination and refinement

Molecular replacement program, *Phaser*, found a solution of three molecules in the crystal asymmetric unit. After fitting polypeptide residues and several rounds of refinement there were two blobs of positive electron density around Asp 221, Asp 232, His 296, Glu 325 and Glu 339, suggesting that some ligands were missing. In other prolidases the metal cluster is coordinated by the same amino acid residues, i.e. two aspartic acids, two glutamic acids and a histidine residue (Jeyakanthan et al., 2009; Maher et al., 2004; Trofimov et al., 2012). Accordingly, two manganese atoms were fitted per chain since manganese salt was used in the purification buffer. However, there was still positive electron density after fitting two manganese atoms, suggesting that another ligand present in the crystal was missing in the model (Figure 5.6). X-ray fluorescence scan suggested that there was arsenic in the sample (Figure 5.7). Since cacodylate used in the crystallization cocktail is an organic molecule of arsenic $((CH_3)_2AsO_2H)$, cacodylate

43

was fitted in the third site of the metal center. The crystal structure of *P. horikoshii* OT3 prolidase (1wy2) has also been solved with a cacodylate ion in the metal cluster of the structure.

The refined model of *L. lactis* prolidase consists of three molecules (chains A, B and C) in the asymmetric unit (Figure 5.8). In chain A, all the 362 molecules were fitted while in chains B and C the electron densities were disordered and broken, therefore only 360 and 352 amino acid residues could be fitted, respectively. Chain A forms a dimer with chain B both in the same aymmetric unit, while chain C forms a dimer with chain C' in the adjacent crystal asymmetric unit. Illustrations of the three refined molecules in an asymmetric unit and the dimeric form (chains A and B) of *L. lactis* prolidase are in Figure 5.8 and Figure 5.9, respectively.
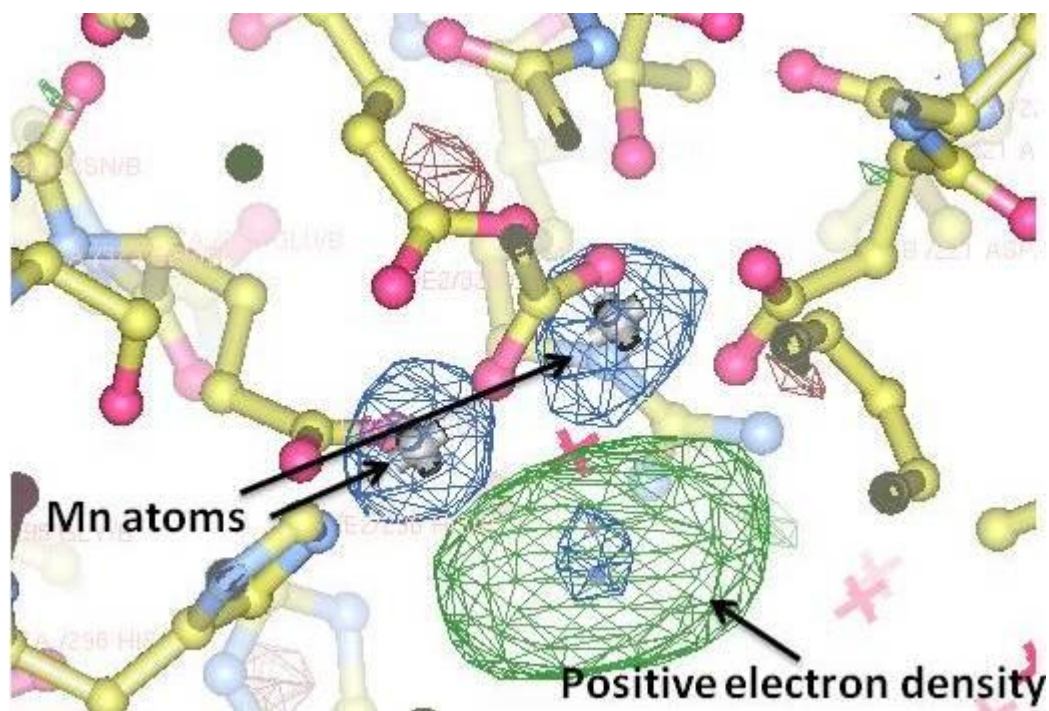
Figure 5.6 Ball and stick model of the metal center in the structure of *L. lactis* prolidase showing the additional positive electron density. Electron density (2Fo-Fc) was contoured at 6.62 rmsd.
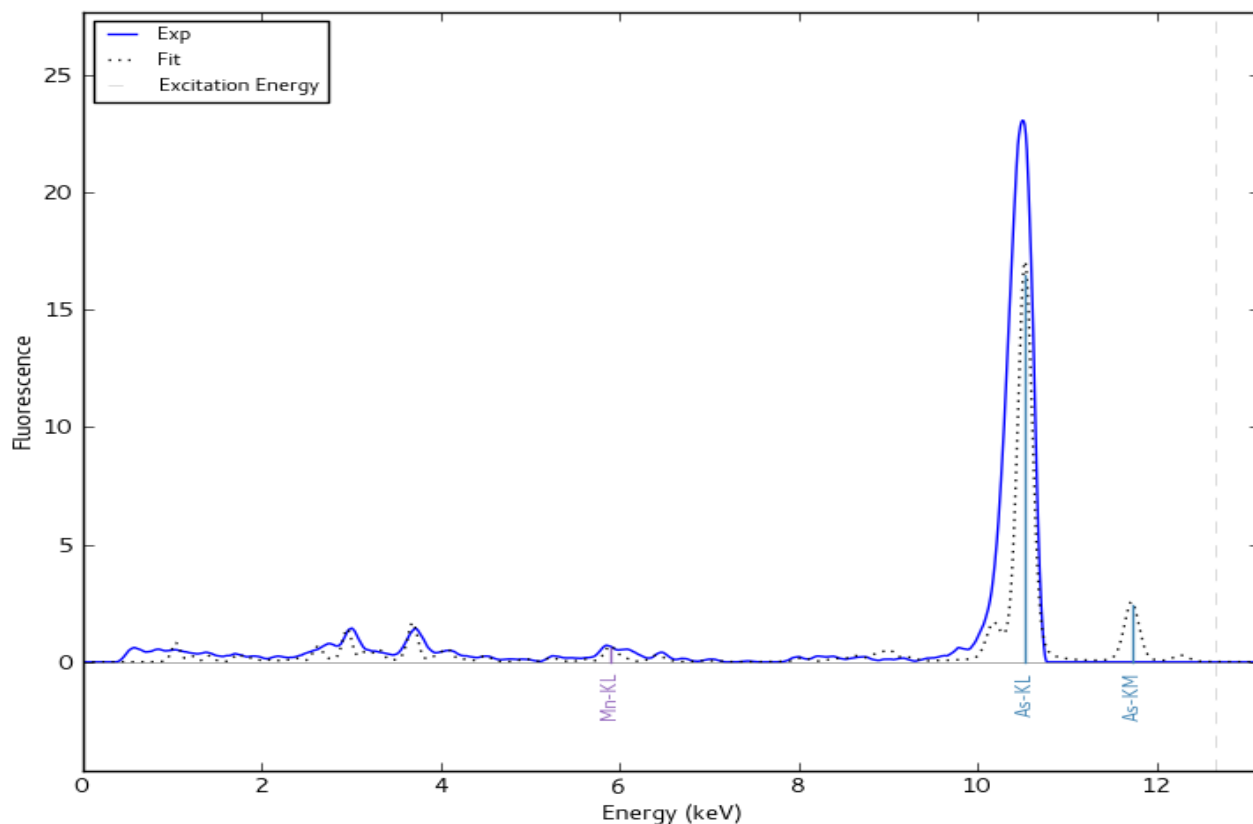
Figure 5.7 X-ray fluorescence of recombinant wild type *L. lactis* prolidase crystal showing a strong signal for arsenic.

The crystal was grown in a reservoir solution containing 0.16 M calcium acetate, 0.08 M sodium cacodylate (pH 6.5), 14 % PEG 8000 and 18 % glycerol.

Each chain/ subunit of *L. lactis* prolidase has an N-terminal domain and a C-terminal domain made up of residues 1-124 and 133 - 362, respectively. The two domains are linked by a helical linker made up of residues 125 - 132 (Figure 5.10). The C-terminal domain harbours the enzyme active site, which comprises the two manganese atoms coordinated by five amino acid residues. The first manganese is coordinated by both oxygen atoms of the carboxylic group of Asp 221 ($O^{\delta 1}$ and $O^{\delta 2}$), $O^{\varepsilon 1}$ of Glu 339, and $O^{\delta 1}$ of Asp 232. The second manganese atom is coordinated by $O^{\delta 2}$ of Asp 232, $O^{\varepsilon 2}$ of Glu 325, $O^{\varepsilon 2}$ of Glu 339, and $N^{\varepsilon 2}$ of His 296. The two manganese atoms are also coordinated by O^{1} of the cacodylate ion found in the metal center.
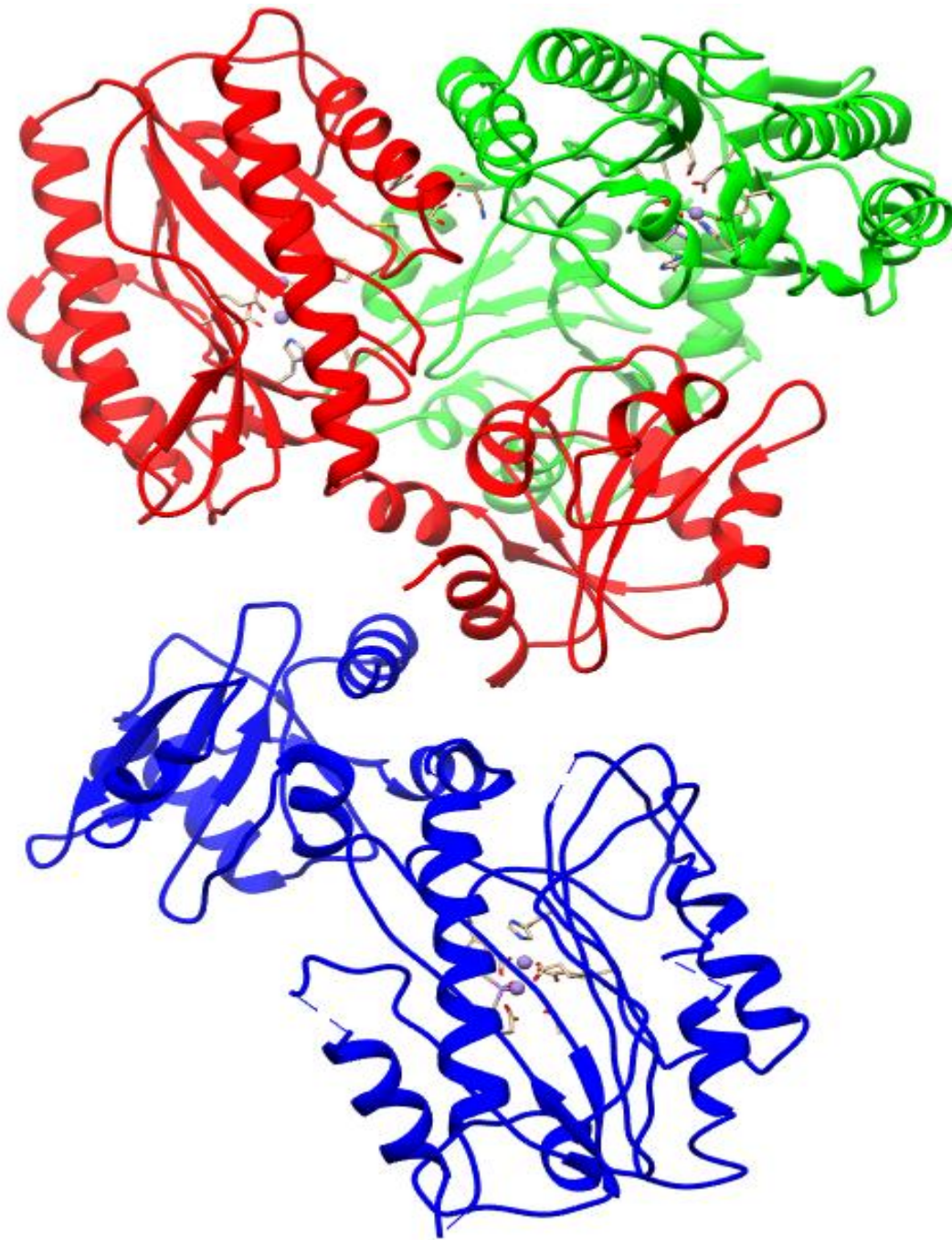
Figure 5.8 Cartoon representation of the three molecules of *L. lactis* prolidase.
Chains A, B and C are coloured red, green and blue; respectively. The purple balls buried in the
structure are manganese atoms. The pictures were drawn by Chimera (Pettersen et al., 2004).
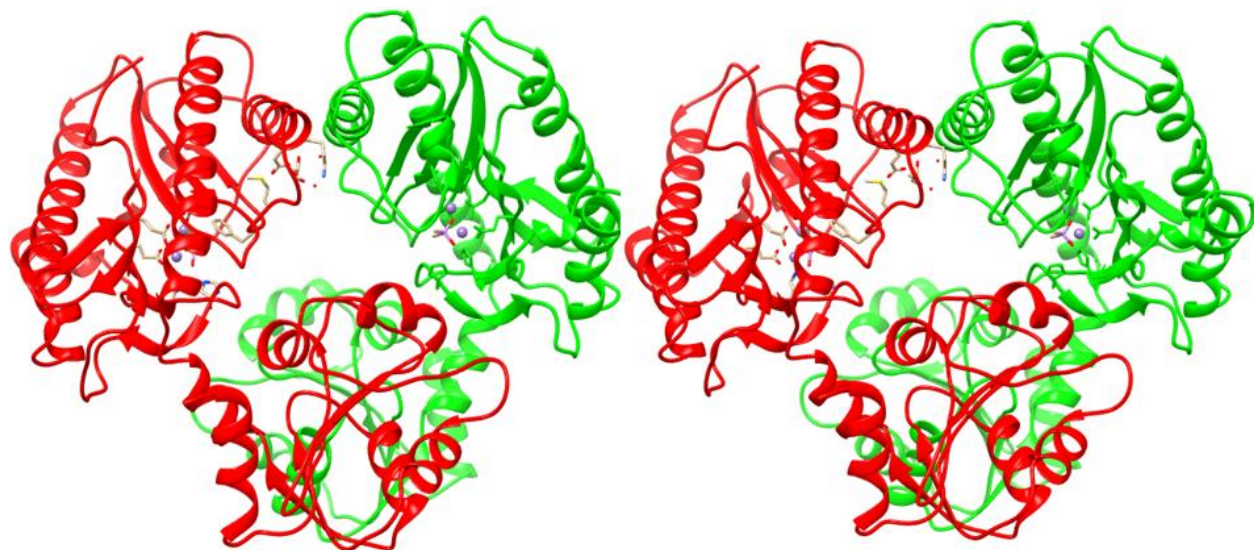
Figure 5.9 Stereodiagrams of the dimer of *L. lactis* prolidase.
Subunits A and B are coloured red and green, respectively.

Located over the active site of each subunit is a loop structure from the other subunit, which is the loop shown to influence enzyme activity and its unique properties, such as allosteric behaviour (Zhang et al., 2009 and Yang & Tanaka 2008). The loop comprises twelve amino acid residues: Gly 32, Leu 33, Ala 34, Ile 35, Asp 36, Pro 37, His 38, Glu 39, Arg 40, Ile 41, Ala 42 and Gly 43 (Figure 5.11). Among the 13 loop residues, Glu 39 of one subunit is the closest to the active site of the other subunit. The distances from the alpha carbon of Glu 39 in subunit A to the two manganese atoms in the active site of subunit B are 14.7 Å and 16.11 Å. The distances from the alpha carbon of Glu 39 in subunit B to the two manganese atoms in the active site of subunit A are 16.51 Å and 18.21 Å (Figure 5.12).
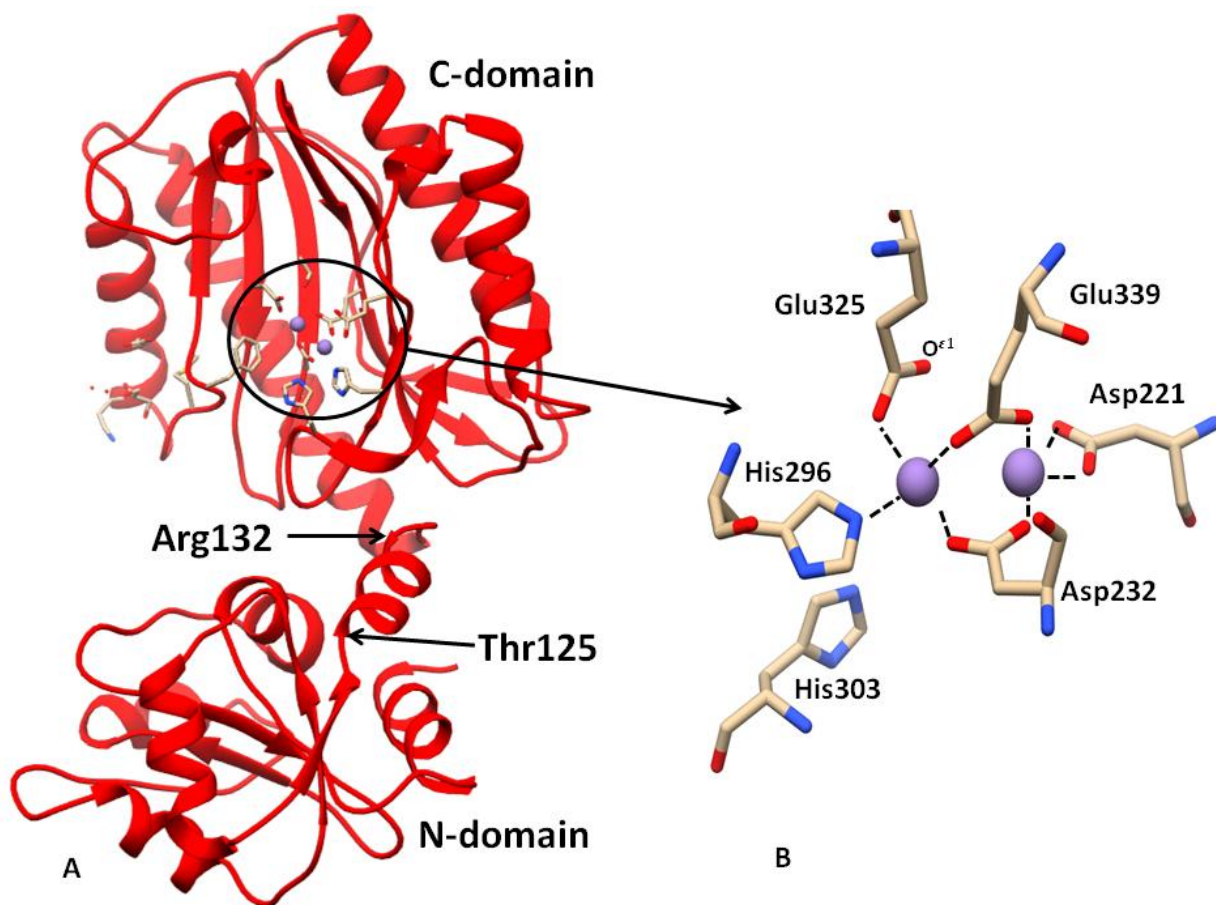
Figure 5.10 A monomeric representation of wild-type *L. lactis* prolidase with the enzyme active site highlighted.

A: The active site (metal center) is circled. The two domains are connected by a helical linker (residues 125 - 132). **B:** The five manganese-coordinating residues and the manganese atoms are shown, the latter are the purple balls. The coordination bonds are indicated by dashed lines. Not shown in this diagram is the cacodylate molecule, of which one of the oxygen atoms coordinates both the manganese atoms.
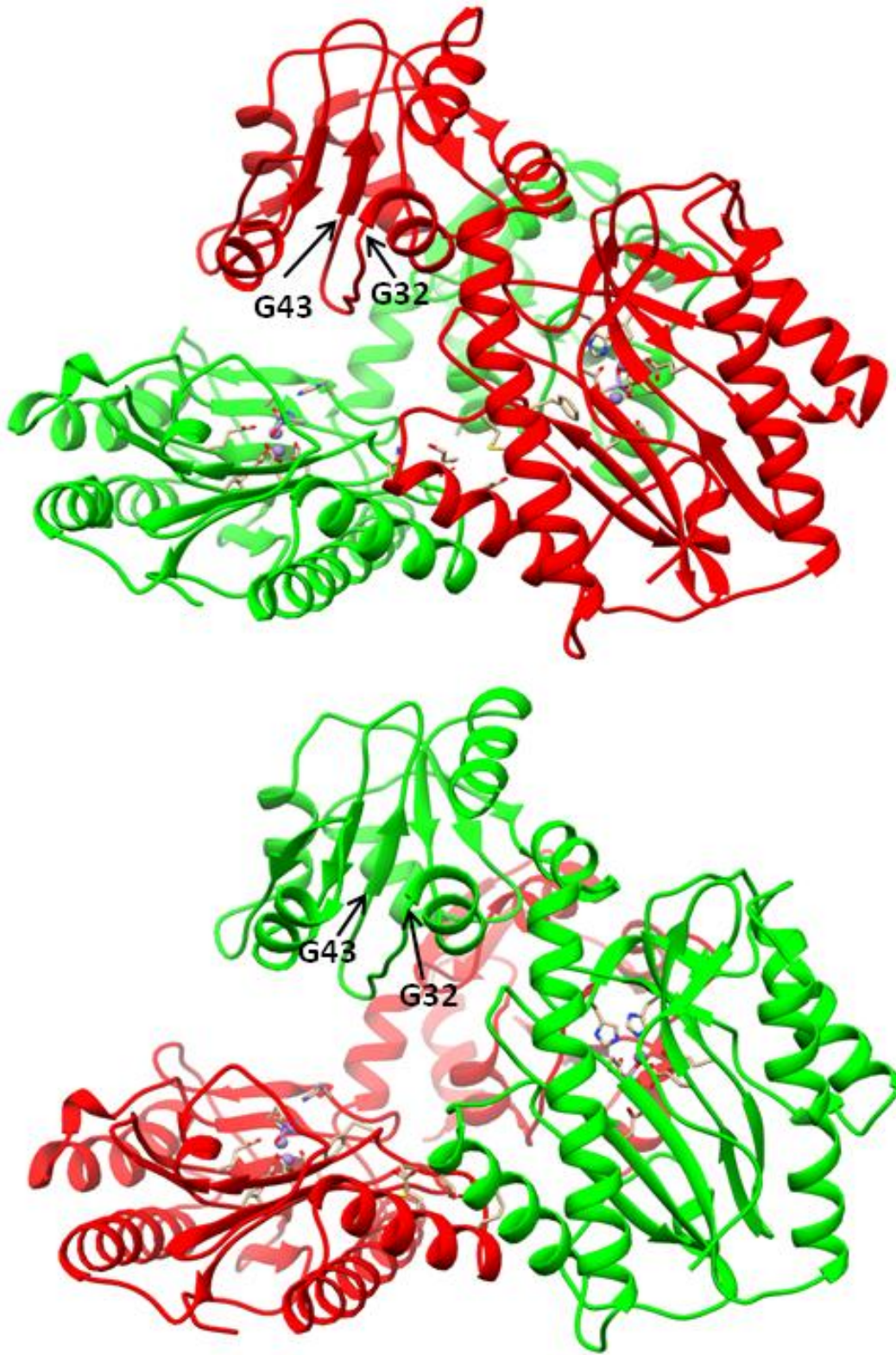
Figure 5.11 Structure of *L. lactis* prolidase showing the loop structure (residues 32 - 43) of one subunit over the active site of the other subunit.
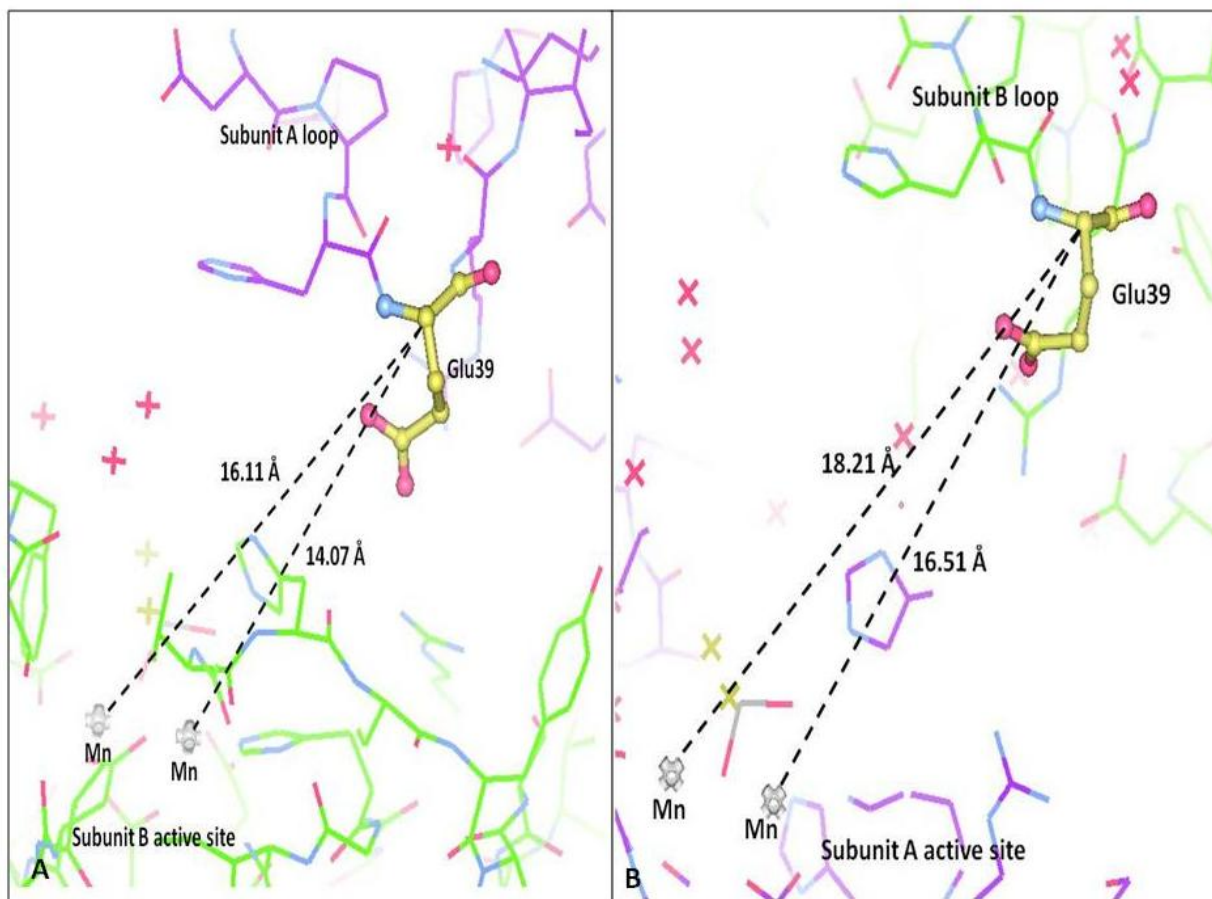
Figure 5.12 Illustration of the distance from the alpha carbon on Glu 39 located in the loop of one subunit to the manganese atoms located in the active site of the other subunit of *L. lactis* prolidase.

5.4   Structure quality

Most of the quality parameters of the refined model indicate that the quality is acceptable (Table 5.3). For example, the difference between R_{work} and R_{free} (22.39 and 27.77) is about 5 %. The difference in *R*-factors for a well-refined structure is expected to be between 4 % and 7 %. When the R_{work} is more than 7 % lower than the R_{free} value it indicates possible over-interpretation of the diffraction data, whereas a difference of these values smaller than 4 % may indicate that the R_{free} reflections were used during refinement leading to model bias (Wlodawer et al., 2008). About 90 % of the modeled residues are in the favoured region of the Ramachandran plot, while 7.4 % and 2.6 % are in the allowed and disallowed regions, respectively. Of the 2.6 %

50

in the disallowed regions 80 % are in chain C, while the remaining 20 % are in chains A and B (Figure 5.13).

Table 5.3 Refinement statistics of wild-type *L. lactis* prolidase.

Space group	C 1 2 1
Unit-cell parameters (Å, °)	$a = 212.13$, $b = 76.99$ $c = 88.92$, $\alpha = \gamma = 90$, $\beta = 112.39$
Resolution range (Å)	49.83 - 2.25 (2.33 - 2.25)
$\{I/\sigma (I)\}$	9.48 (1.74)
Completeness (%)	99.94 (99.90)
Total reflections	23,5259 (23,993)
Unique reflections	63,058 (6,269)
Multiplicity	3.7 (3.8)
R_{merge}	0.084 (0.80)
Wilson B factor (Å^2)	48.50
R_{work}/R_{free} (%)	22.39/ 27.77 (31.25/ 32.48)
No. of atoms	8646
Protein	8302
Ligands	27
Water	317
Mean B factor (Å^2)	62.60
R.m.s.d., bond lengths (Å)	0.023
R.m.s.d., bond angles (°)	1.73
Ramachandran favoured (%)	90
Ramachandran allowed (%)	7.4
Ramachandran outliers (%)	2.6

Statistics for the highest-resolution shell are shown in parentheses
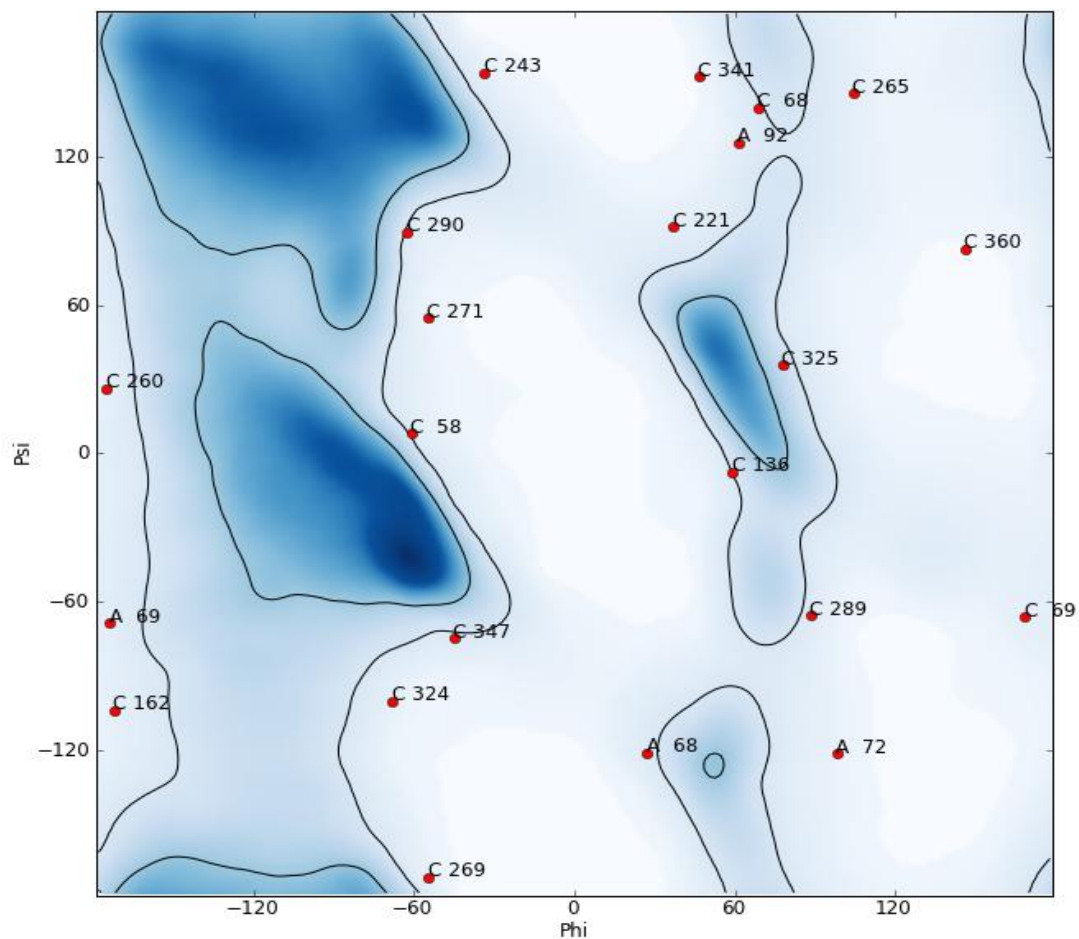
Figure 5.13 Ramachandran outliers in the refined model of *L. lactis* prolidase.

In addition to Ramachandran outliers, some residues fit poorly to the electron density. However, most of them are located in chain C. Sixty three residues fit poorly to the electron density, 55 of which are located in chain C. This is not surprising, since molecule C has the least defined electron density of all the three molecules in the crystal asymmetric unit. It is important to note that the electron density map for the loop structures (residues 32 - 43) of subunits A and B are also complete and well-defined, thus the residues in this region fit the map well (Figure 5.14). Comparison of the structure of *L. lactis* prolidase with structures solved at similar resolution revealed that most of its quality parameters are within the expected ranges (Table 5.4).
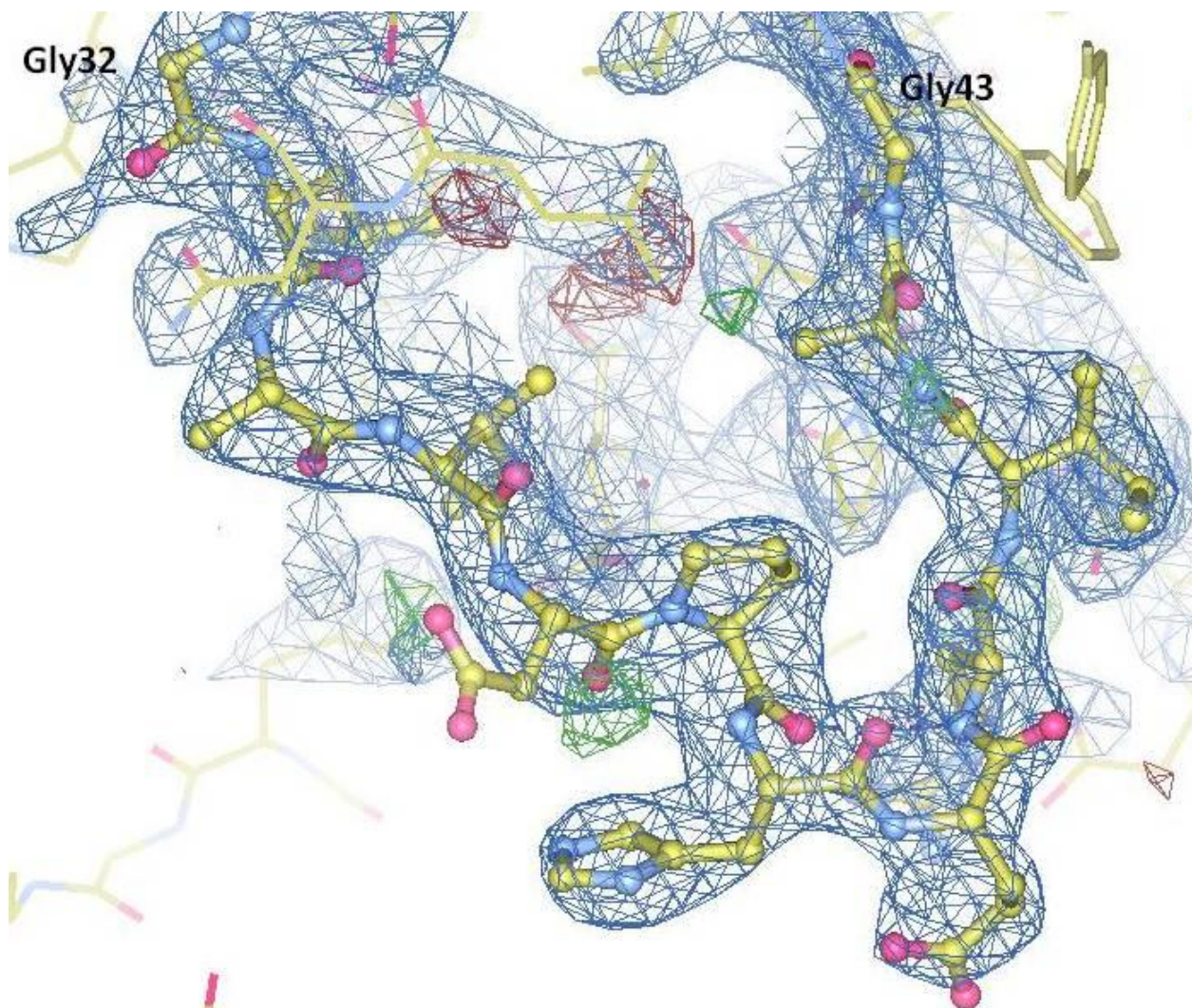
Figure 5.14 Electron density map (2Fo-Fc) of the loop structure (residues 32 - 43) of *L. lactis* prolidase at sigma level 1 rmsd.

Table 5.4 Comparison of the refinement statistics of the current structure with the range for structures solved at similar resolution.

	Range of other structures[a]	Statistic for the current structure
R_{work}	13.83 - 24.96	22.39
R_{free}	16.42 - 32.42	27.77
RMSD (bonds)	0.002 - 0.030	0.023
RMSD (angles)	0.42 - 2.05	1.73
Average *B*-factor	7.0 - 56.7	62.60

[a]The range is for 708 PDB structures solved at similar resolution (Urzhumtseva et al., 2009).

6 DISCUSSION

6.1 Crystallization

Successful growth of large three-dimensional crystals was achieved using both the hanging drop vapour diffusion and the microbatch-under-oil crystallization methods. The buffer, the precipitant and the ligand used were the same for both methods. This suggests that the chemical composition of the crystallization solution is more important than the crystallization method, at least in this study, in determining the success of a crystallization experiment. Manual screening of 96 commercial reagents identified several conditions, some of which grew X-ray-diffracting crystals upon optimization. Initially, bipyramidal-shaped crystals were grown, which tended to grow as twinned crystals rather than individual crystals. This compromised the quality of the diffraction data collected from these crystals. The crystals belonged to space group $P1$ and there was an estimate of six monomers of *L. lactis* prolidase in the crystal asymmetric unit. The low symmetry, high number of molecules in the crystal asymmetric unit, twinning and other errors in the crystal lowered the chance of solving the phase problem. Structure determination with this diffraction data was therefore, not successful. On the other hand, the high-throughput screening of 1536 conditions led to the identification of a diverse range of conditions that yielded crystals of different forms. Optimization of one of the lead conditions yielded crystals with a hexagonal shape. These crystals belonged to space group $C2$ with an estimate of three monomers in the crystal asymmetric unit. A smaller number of molecules in the crystal asymmetric unit and a higher symmetry of the crystal both make it suitable to solve the structure by X-ray crystallography. The shape of the crystal is determined by the internal arrangement of molecules in the crystal lattice, and the more symmetrical the internal arrangement the higher the number of equivalent reflections that can be collected with minimum radiation exposure. Thus, the more accurate the diffraction data from the higher symmetry crystals compared to the diffraction data from lower symmetry crystals. The conditions that produced the crystals from the two screening methods were very similar in the sense that they both comprised sodium cacodylate buffer (pH 6.5), a divalent metal salt (calcium or manganese salt) and PEG 8000 as the precipitant. The crystallization condition from high-throughput screening contained glycerol in addition to these three other components. This shows that not only is the choice of the chemical composition of the crystallization solution important in determining the success of a crystallization experiment, but

also in determining the quality of the crystals grown and thus, the success of structure determination by X-ray crystallography.

Co-crystallization of enzymes with their substrates, co-factors and other ligands has been reported to yield better crystallization results than crystallization of the enzyme alone. The co-crystallants stabilize the enzyme and the stable form tends to crystallize better than the free, non-stable form (McPherson, 2004). In this study, *L. lactis* prolidase was co-crystallized with its hydrolytic products, amino acids. Although this yielded three-dimensional crystals, preliminary analysis of diffraction data from one of the crystals suggested that the crystals were not of sufficient quality to collect a complete data set. However, this was not thoroughly investigated. Further experimentation would have to be performed, such as examining more crystals and different concentrations of the co-crystallants, before attempting to come up with a plausible explanation.

In previous studies in Dr. Tanaka's research group, computer-generated models of *L. lactis* prolidase have proposed that this enzyme has a loop structure from one subunit close to the active site of the other subunit. Deletion of five amino acid residues from the loop, residues 36 - 40, led to loss of activity. However, the physical properties of this enzyme, including its dimeric nature, were preserved (Zhang et al., 2009). Therefore, it was speculated that the crystal structure of Δ36 - 40 could still be used to elucidate the functional properties of *L. lactis* prolidase. Since the loop structure is flexible and crystallization involves packing of molecules in an ordered manner, it was hypothesized that Δ36 - 40 would have a higher success rate of crystallization than its wild-type counterpart. The same conditions that crystallized wild-type prolidase also crystallized Δ36 - 40. Surprisingly, crystals of Δ36 - 40 were not durable and did not diffract to high enough resolution for structure solution. The structural changes responsible for loss of activity in Δ36 - 40 could be responsible for loss of molecular order during crystallization of Δ36 - 40 and compromised diffraction quality in crystals of Δ36 - 40. It is speculated that different conditions are required to form good quality crystals of Δ36 - 40 mutant prolidase.

6.2 Model building and refinement

The crystal structure of wild-type *L. lactis* prolidase was successfully solved and refined at 2.25 Å resolution. The crystal asymmetric unit contained three molecules (chains A, B and C). The electron density of chain C was less ordered than the electron densities of chains A and B.

This explains why 90 % of the residues that fit poorly to the electron density are in chain C. Also, 80 % of the residues in the disallowed region of the Ramachandran plot are in chain C. Among all the refinement parameters investigated, the average *B*-factors were the only ones that fell out of the expected range based on PDB structures solved at similar resolution. The range of structures solved at similar resolution is 7.0 - 56.7 Å^2, whereas the average *B*-factor for the current model is 62.60 Å^2 (Table 5.3). This could be due to the high disorder and incompleteness of chain C. It is not uncommon to find one of the molecules in the crystal asymmetric unit disordered and incomplete. This is the case with the structure of *P. furiosus* prolidase (1pv9), of which the asymmetric unit contains two molecules (Maher et al., 2004). Chain A of this structure contains 337 of the 348 residues and only four of them fit poorly to the electron density. Chain B, on the other hand, has only 318 residues fitted to the electron density due to its incompleteness and 30 of these residues fit poorly to the electron density. This represents 90 % of the residues that fit poorly to the electron density of the refined model. The structure of *P. furiosus* prolidase is, therefore, described using only chain A, half of the dimer (Maher et al., 2004). *L. lactis* prolidase also exists as a dimer biologically (Yang & Tanaka, 2008). Unlike *P. furiosus* prolidase model, the two molecules that are more ordered (chains A and B) form a dimer with each other. This indicates that the structural interpretation of this enzyme (a homodimeric model consisting of chain A and B) is not compromised by the low quality of chain C.

6.3   Structure comparison with related proteins

Previous research has revealed *that L. lactis* prolidase, unlike other prolidases, shows allosteric behaviour, metal-dependent substrate specificity and substrate inhibition (Yang & Tanaka, 2008). Comparison of the sequence-based computer-generated model of *L. lactis* prolidase with the crystal structure of *P. furiosus* prolidase reveals that there is a loop structure in both models. Interestingly, the loop in *L. lactis* prolidase is longer by four amino acid residues. This number coincides with the number of charged residues found in the middle of the loop structure in *L. lactis* prolidase (Asp 36, His 38, Glu 39 and Arg 40), which are not present in the loop of *P. furiosus* prolidase (Maher et al., 2004; Yang & Tanaka, 2008). This led to the hypothesis that the charged residues on the loop structure could be responsible for the unique features of *L. lactis* prolidase. The deletion of these residues leads to loss of activity of this enzyme (Zhang et al., 2009). Therefore, their roles in the catalytic properties of the enzyme

cannot be elucidated using the catalytically inactive mutant, Δ36 - 40. On the other hand, the inactivity of Δ36 - 40 suggests that the loop is involved in enzyme activity. In the same study, they show that there is no evidence that the deletion of the loop residues (residues 36 - 40) influences the structural integrity of the dimer. The Δ36 - 40 mutant behaves similarly to the wild-type prolidase on gel filtration column. The loss of activity and little influence on the enzyme structure indicate that these loop residues are essential for activity, while their structural contribution to rigidity of the enzyme is minimum.

In this crystallographic study, it has been confirmed that the loop structure of *L. lactis* prolidase is longer than the loop structure of *P. furiosus* prolidase. However, it is three amino acids longer, which is different from the previously reported four residues. This is also the case with another homologous structure, *P. horikoshii* prolidase (1wy2), whose loop structure is three amino acids shorter than the loop structure of *L. lactis* prolidase. The residues in the loop of *L. lactis* prolidase in positions equivalent to gaps in these homologous structures are His 38, Glu 39 and Arg 40 (Figure 6.1). Two other homologous structures, prolidase from *Thermococcus sibricus* (4fkc) and a dipeptidase from *P. horikoshii* (2how), have loop structures the same length as the loop structure found in *L. lactis* prolidase (Figure 6.2). Glu 39 and Arg 40 (*L. lactis* prolidase numbering) are conserved among the structures with same length loop structure, while His 38 is not. Also structural comparisons revealed that Asp 36 is unique to *L. lactis* prolidase. Therefore, Asp 36 and His 38 are unique to *L. lactis* prolidase. This is summarized in Table 6.1. Previous mutation studies of these residues showed their importance in catalytic activity. Mutations of individual residues revealed that Asp 36 and His 38 are involved in allosteric behaviour and subtration inhibition, respectively. Glu 39 and Arg 40 were shown to be needed for catalytic activity (Zhang et al., 2011 and Chen & Tanaka, 2011). Allosteric behaviour, substrate inhibition and metal dependent substrate specificity have not been reported in any prolidase, including the ones with the same loop length as *L. lactis* prolidase. Therefore, this study supports the previously proposed involvement of Asp 36 and His 38 in allosteric behaviour and substrate inhibition of *L. lactis* prolidase, respectively.
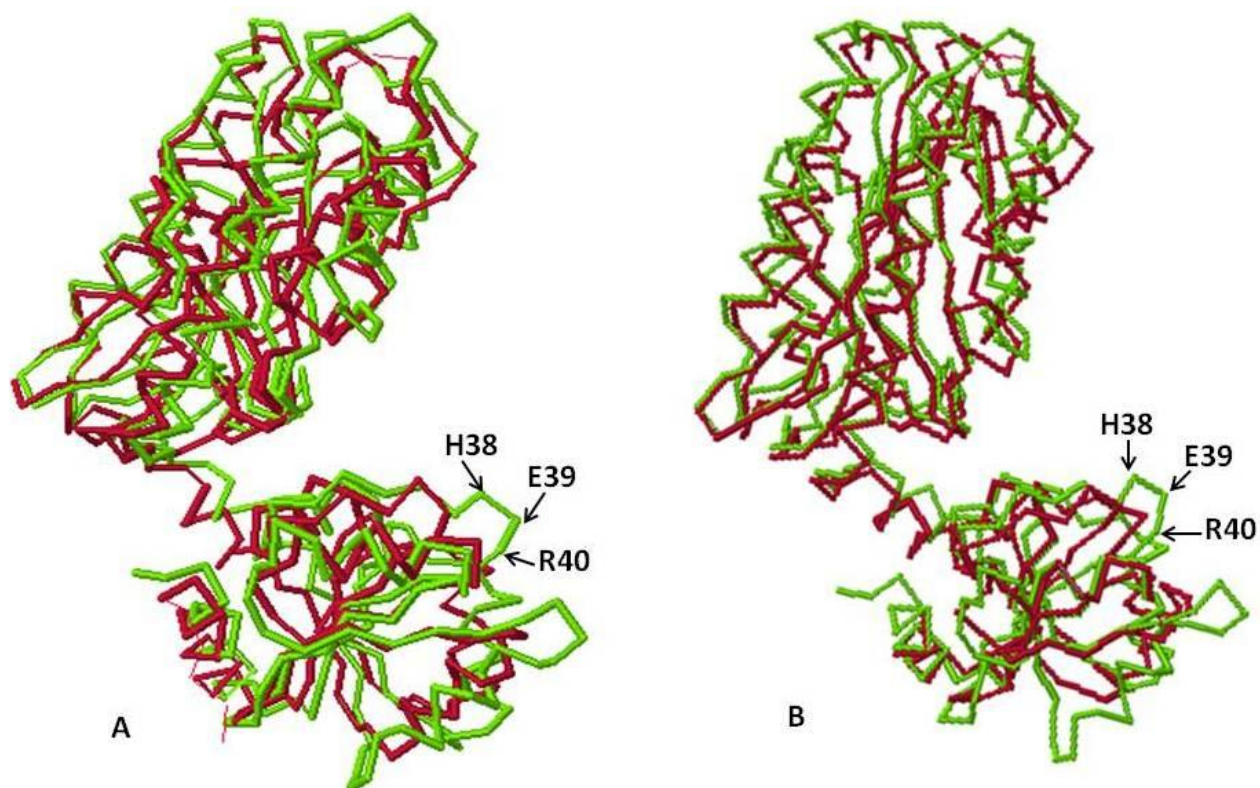
Figure 6.1 Superposition of *L. lactis* prolidase with A: *P. horikoshii* OT3 prolidase (1wy2) and B: *P. furiosus* prolidase (1pv9).

L. lactis prolidase is coloured green while *P. horikoshii* and *P. furiosus* prolidase structures are coloured red. The amino acid numbering is for *L. lactis* prolidase. His 38, Glu 39 and Arg 40 are found in *L. lactis* prolidase, but not in *P. horikoshii* and *P. furiosus* prolidase structures. Superposition of the structures was done using *Jmol* (Holm & Rosenström, 2010).
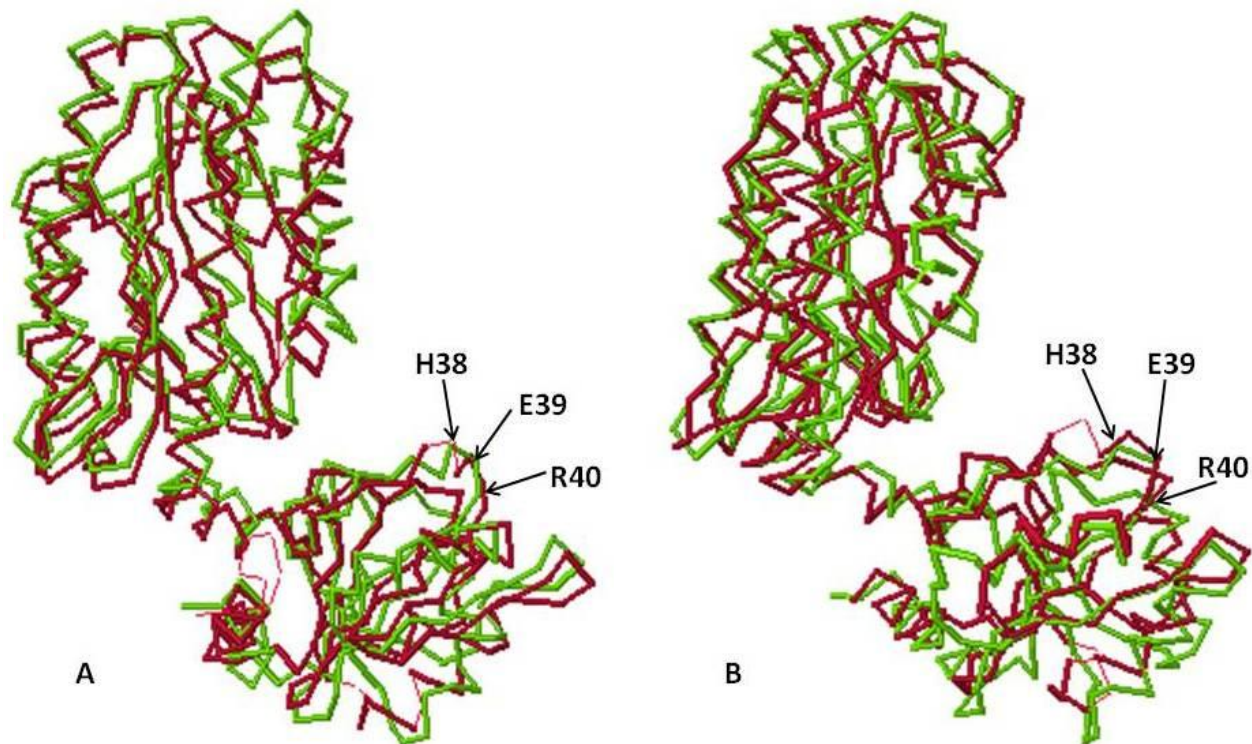
Figure 6.2 Superposition of *L. lactis* prolidase with A: *T. sibricus* prolidase (4fkc) and B: putative dipeptidase from *P. horikoshii* (2how).

L. lactis prolidase is coloured green while *T. sibricus* prolidase and *P. horikoshii* putative dipeptidase structures are coloured red. The amino acid numbering is for *L. lactis* prolidase. The residues in *T. sibricus* prolidase positions equivalent to His 38, Glu 39 and Arg 40 of *L. lactis* prolidase are Leu, Glu and Arg. and the residues in *P. horikoshii* putative dipeptidase positions equivalent to His 38, Glu 39 and Arg 40 of *L. lactis* prolidase are Gly, Glu and Arg. Superposition of the structures was done using *Jmol* (Holm & Rosenström, 2010).

Table 6.1 A summary of the comparison of the loop structures of _L. lactis_ prolidase and related proteins.

Structure	Residue number* and identification											
	32	33	34	35	36	37	38	39	40	41	42	43
L. lactis prolidase	G	L	A	I	D	P	H	E	R	I	A	G
P. furiosus prolidase	G	T	S	P	L	G	-	-	-	G	G	Y
P. horikoshii prolidase	G	A	S	P	L	A	-	-	-	G	G	Y
T. sibricus prolidase	G	F	N	P	L	T	L	E	R	L	F	V
P. horikoshii dipeptidase	G	L	R	L	H	V	G	E	R	L	A	I

*The numbering is for _L. lactis_ prolidase.

"-" indicates that there is a gap (no amino acid residue) in the equivalent position of a homologous protein.

In addition to Asp 36 and His 38 not being conserved among these prolidases, Arg 293, mutation of which does not show allosteric behaviour (Zhang et al., 2009), is not conserved in prolidases from _P. furiosus_ and _P. horikoshii_. The residue in position equivalent to Arg 293 in these two structures is serine. Therefore, not only do these homologous structures lack the charged residues in their loop structures, but they also lack the charged arginine residue proximal to the active site of _L. lactis_ prolidase. Comparison of the metal centers of these related enzymes revealed that their metal-coordinating amino acid residues are not only conserved, but also have almost identical coordination relative to their metal cations (Figure 6.3). Therefore, these residues are not likely to be responsible for the unique catalytic features of _L. lactis_ prolidase. It should be noted that of the four related proteins that were compared with _L. lactis_ prolidase, two are illustrated in Figure 6.3. These were judiciously chosen to represent both categories of the loop structure size, shorter loop structure and loop structure of the same length as that of _L. lactis_ prolidase. The metal centers and metal coordination of the other structures are similar to the ones illustrated in Figure 6.3.
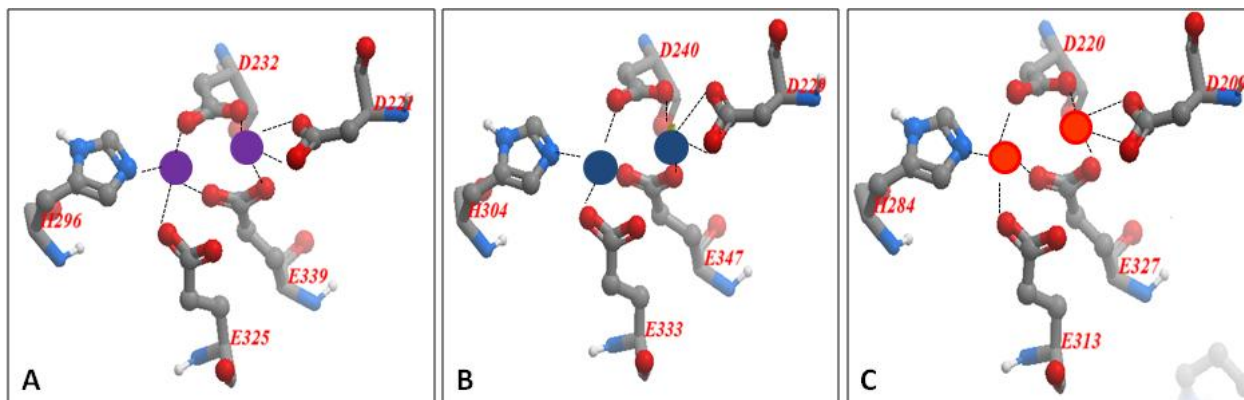
Figure 6.3 Illustration of the metal-coordinating residues of *L. lactis* prolidase and homologous structures. A: *L. lactis* prolidase, B: *T. sibricus* prolidase and C: *P. furiosus* prolidase.

Manganese, cadmium and zinc found in the metal centers *of L. lactis* prolidase, *T. sibricus* prolidase and *P. furiosus* prolidase structures are coloured purple, blue and orange, respectively.

The loop structure is more flexible than other secondary structures found in proteins, such as β sheets and α helices. In addition to its flexibility, located at both ends of the loop structure of *L. lactis* prolidase are glycine residues (Figure 5.14). Due to its size, it exhibits the least steric hindrance among the 20 standard amino acids and gives the structures it is found in flexibility. Therefore, the two glycine residues found at both ends of the loop structure of *L. lactis* prolidase may act as hinges that allow the movement of the loop. We propose that upon substrate binding, the two subunits of *L. lactis* prolidase move closer to each other (Figure 6.4) and the loop residues (including Asp 36 and His 38) and the residues proximal to the active site (e.g. Arg 293) bind. These intersubunit interactions affect the binding of further substrate molecules and leads to demonstration of allostery. Substrate-induced intersubunit interactions responsible for allosteric behaviour have been reported in other enzymes, such as *Escherichia coli* phoshofructokinase-2 (Cabrera et al., 2008; Caniuguir et al., 2005).
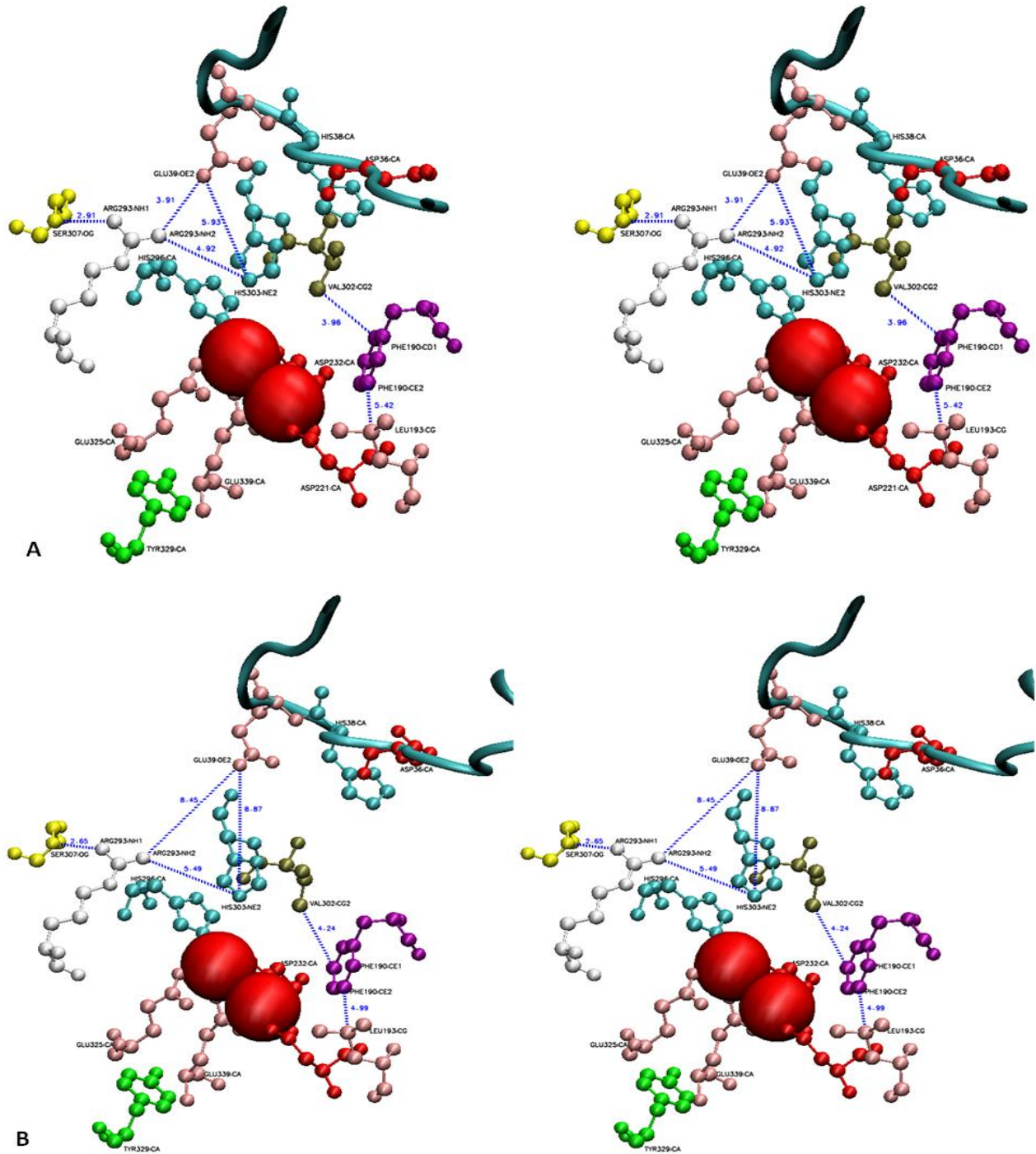
Figure 6.4 Stereodiagrams showing the proximity of the active site and the loop residues of *L. lactis* **prolidase. A: The loop structure is closer to the active site and B: The loop structure is further from the active site.**

The loop structure is shown with a cyan ribbon and manganese atoms are shown in Van der Waals model (red).

6.4 **Proposed mechanism of *L. lactis* prolidase catalysis**

It has been shown that a mutation of His 303 does not show enzyme activity (Zhang et al., 2009). Structural comparison in this current study shows that this amino acid residue is conserved among prolidases. This residue is located near the metal cluster, but is not involved in metal coordination (Figure 5.10). These findings suggest that His 303 may be involved in this enzyme's function. The mechanism of prolidase catalysis has been been previously proposed (Alberto et al., 2011). The proposed mechanism involves the transfer of a proton from a hydroxide ion to the nitrogen of proline found in the proline dipeptide (substrate) by one of the two glutamic acids coordinating one of the two metal atoms. This leads to the liberation of proline and the other amino acid from the dipeptide (Alberto et al., 2011). In this study, we propose that His 303 is involved in the initial steps of peptide hydrolysis by *L. lactis* prolidase. Prolidase from *L. lactis* and other microorganisms demonstrate optimum activity at pH 7.0 or higher (Ghosh et al., 1998; Theriot et al., 2010; Wang et al., 2005; Yang & Tanaka, 2008). This pH is higher than the pK_a value of approximately 6.0 for the side chain of histidine. Therefore, its imidazole ring is unprotonated and nucleophilic at prolidase optimum pH. We propose that the nucleophilic imidazole nitrogen of His 303 abstracts a proton from a surrounding water molecule leading to the production of a nucleophilic hydroxide ion. The hydroxide ion then attacks the carbonyl carbon of the peptide bond and the rest of the reaction proceeds as previously proposed (Alberto et al., 2011). The proposed mechanism of catalysis of *L. lactis* prolidase is illustrated in Figure 6.5. Glutamic acid responsible for proton transfer in the proposed mechanism of catalysis of *L. lactis* prolidase is Glu 325 using its carboxylic oxygen, $O^{\varepsilon 1}$. This is the only oxygen atom free from metal coordination among the oxygen atoms of the two glutamates and the two aspartates coordinating the two manganese atoms (Figure 6.3).
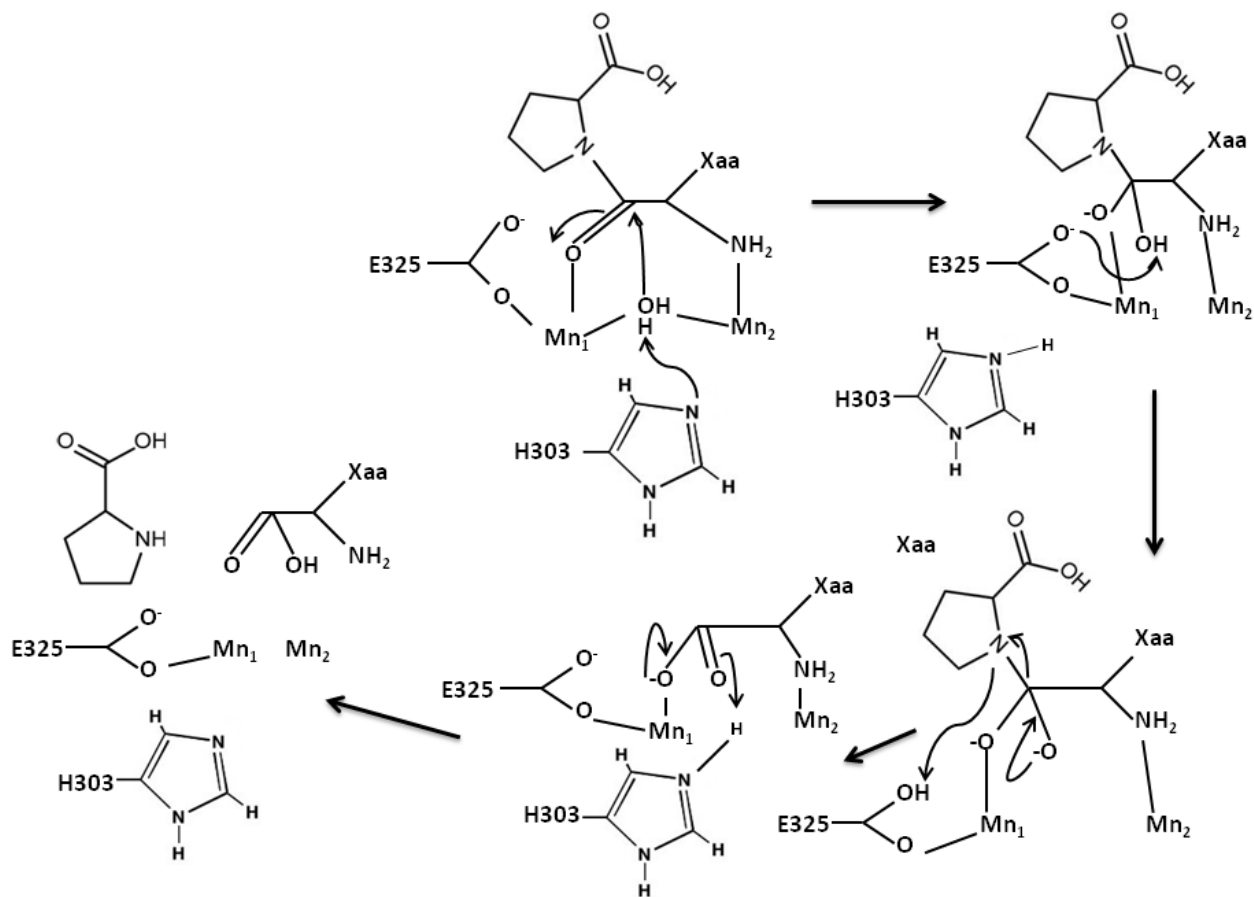
Figure 6.5 The proposed mechanism of dipeptide hydrolysis by *L. lactis* prolidase.
His 303 imidazole nitrogen abstracts a proton from a water molecule making it nucleophilic. The resulting hydroxide ion then attacks the carbonyl carbon of a proline dipeptide bond. Glu 325 then abstracts a hydrogen atom from the hydroxyl group bonded to the carbonyl carbon of the dipeptide and transfers it to proline nitrogen. This leads to the liberation of free proline and the other amino acid (Xaa) of the dipeptide.

Prolidases from *P. furiosus* and *P. horikoshii* prefer cobalt over manganese for catalytic activity (Maher et al., 2004; Theriot et al., 2010); whereas *L. lactis* prolidase shows activities with zinc and manganese. Interestingly, *L. lactis* prolidase shows the highest activity with zinc when the subtrate is Leu - Pro, but when the substrate is Arg - Pro the highest catalytic rate is shown with manganese (Yang & Tanaka , 2008). Altogether, these findings show that not only is the presence of metal atoms in the enzyme active site important for its activity, but also is the identity of the metal involved. Mutations targeted at amino acid residues binding one or both of

the metals in the structure of *P. furious* prolidase led to reduced or lost enzyme activity (Du et al., 2005). This further supports the significance of metals in prolidase activity, but their direct contribution has never been elucidated. In the proposed mechanism of catalysis of prolidase, one of the residues coordinating the metal center (Glu 325 of *L. lactis* prolidase) is also directly involved in enzyme catalysis. The role of metal atoms in prolidase catalysis could, therefore, be the positioning of the active site residues and the substrate so that they can effectively transfer protons/ electrons between them for hydrolysis. In this study, metal-dependent substrate specificity was not clearly explained. The metal-dependent substrate specificity of *L. lactis* prolidase could be due to the fact that different metal atoms have different sizes, therefore, when present in the active site would position the active site residues differently leading to different binding affinities of subtrates. This would lead to different catalytic properties. It would possibly require comparison of the current structure with a structure complex with zinc in the active site to reveal what structural differences exist in the presence of different metal atoms in the metal cluster.

7   SUMMARY AND CONCLUSIONS

The structure of proline is unique among the standard amino acids. Due to this uniqueness, proline-containing peptides are less susceptible to hydrolysis by general peptidases than other peptides. Proline-specific peptidases play a critical role in liberating proline and other amino acids in proline peptides for various functions. These peptidases are involved in hydrolysis of milk caseins by LAB, which rely on the proteolytic system for their amino acid requirements. Hydrolysis of hydrophobic peptides in fermented dairy products, including cheeses, has been shown to reduce their bitterness. Collagen, which is the most abundant protein in humans, is rich in proline. Therefore, proline-specific peptidases are involved in its catabolism for proline recycling and protein synthesis. Two proline-specific dipeptidases (prolinase and prolidase) are involved in the final breakdown of proline-rich peptides. They hydrolyze dipeptides with proline in the N- and C-terminal ends of the peptides, respectively. Lack of prolidase activity has been associated with a hereditary disorder known as prolidase deficiency. Prolidase has been also shown to have structural and functional similarities with organophosphorus acid anhydrolase (OPAA), including shared substrates among the two groups of enzymes. These facts suggest that *L. lactis* prolidase could potentially be used in debittering of fermented dairy products, in treating prolidase deficiency and in toxic organophosphorus compounds detoxification.

L. lactis prolidase has been previously characterized and its catalytic properties elucidated. Unlike other prolidases, it demonstrates allosteric behaviour, metal-dependent substrate specificity and substrate inhibition. The current study focused on the three-dimensional structure determination of *L. lactis* prolidase by X-ray crystallography. Hexagonal plate-like crystals were grown to about 50 μm in their longest dimension using the hanging drop vapour diffusion method. The crystals yielded medium resolution data and successful structure determination was done using molecular replacement method. Three molecules were located in the asymmetric unit of the crystal and the structure was refined against 2.25 Å resolution data. Molecule A and molecule B form a dimer with each other, while molecule C forms a dimer with another molecule in the adjacent crystal asymmetric unit. Molecule C is disordered and incomplete, while molecules A and B are well defined. Although this compromises the quality of the refined model, it does not compromise its structural interpretation since *L. lactis* exits as a dimer biologically and the dimer-forming subunits in the asymmetric unit are well defined.

67

Each subunit of *L. lactis* prolidase has a C- and N-terminal domains linked by a helical linker. The enzyme active site is located in the C-terminal domain and comprises two manganese atoms coordinated by five amino acid residues: two aspartates, two glutamates and histidine. The crystal structure of *L. lactis* has a loop structure from one subunit over the active site of the other subunit. Comparison with prolidases from *P. horikoshii* (1wy2) and *P. furiosus* (1pv9) reveals that *L. lactis* prolidase loop is longer by three amino acid residues: His 38, Glu 39 and Arg 40. On the other hand, the loop is the same length as the loops in other two homologous structures, *P. horikoshii* putative dipeptidase (2how) and *T. sibricus* prolidase (4fkc). Glu 39 and Arg 40 are conserved among the structures of the same length while His 38 is not. Also, Asp 36 on the loop is unique to *L. lactis* prolidase. Previously, site-directed mutagenesis studies have suggested that it is the charge-charge interaction between Asp 36 of one subunit and Arg 293 of the other subunit that is responsible for the allosteric behaviour of this enzyme. His 38 was suggested to be involved in substrate inhibition. The fact that the crystal structure reveals that these two loop amino acids (Asp 36 and His 38) are unique to *L. lactis* further supports their previously proposed involvement in these unique catalytic properties of this prolidase. His 303, of which mutation does not show enzymatic activity, is conserved among the prolidases investigated. The crystal structure shows this amino acid residue is located near the enzyme active site, but it is not involved in metal coordination. We propose that this amino acid acts as a nucleophile to initiate the hydrolysis of peptide substrates by *L. lactis* prolidase. The role of metals in the active site of prolidases, including *L. lactis* prolidase, could be the effective positioning of active site residues for substrate hydrolysis.

Through the crystal structure analysis combined with previously reported kinetic information, this research successfully indicated that the putative loop structure exists as predicted. The location of the loop and the identity of the residues on it support its involvement in the unique catalytic properties of *L. lactis* prolidase including allosteric behaviour and substrate inhibition. Metal dependent substrate specificity, on the other hand, could not be explained with the current data. Further crystallographic studies are required to help explain this unique property of *L. lactis* prolidase.

8 RECOMMENDATIONS FOR FUTURE WORK

Future studies should include X-ray crystallography of various mutants of *L. lactis* prolidase that have been previously characterized. Comparison of the structures of these mutants with that of the wild-type will reveal the structural changes that may be responsible for their different kinetic properties. Co-crystallization experiments should also be conducted. The co-crystallants should include substrate analogues and different metal ions. The structure with the substrate analogues bound to its active site will reveal the interactions of the substrate and the active site residues (local interaction) as well as any global conformations that may result from substrate binding. As stated earlier, one of the unique properties of *L. lactis* prolidase is its metal dependent-substrate specificity. Therefore, crystal structures with different metal ions should help elucidate the contribution of these metal ions in the enzyme catalysis. All this information shall be valuable in the potential application of *L. lactis* prolidase in cheese debittering, treatment of prolidase deficiency and detoxification of organophosphorus compounds.

9 REFERENCES

Adams, P. D., Afonine, P. V., Bunkóczi, G., Chen, V. B., Davis, I. W., Echols, N., Headd, J. J., Hung, L., Kapral, G. J., Grosse-Kunstleve, R. W., McCoy, A. J., Moriarty, N. W., Oeffner, R., Read, R. J., Richardson, D. C., Richardson, J. S., Terwilliger, T. C., & Zwart, P. H. (2010). *PHENIX*: A comprehensive python-based system for macromolecular structure solution. *Acta Crystallographica Section D, Biological Crystallography, 66*, 213-221.

Alberto, M. E., Leopoldini, M., & Russo, N. (2011). Can human prolidase enzyme use different metals for full catalytic activity?. *Inorganic Chemistry, 50*(8), 3394-3403.

Aldridge, W. N. (1950). Some properties of specific cholinesterase with particular reference to the mechanism of inhibition by diethyl *p*-nitrophenyl thiophosphate (E 605) and analogues. *The Biochemical Journal, 46*(4), 451-460.

Altschul, S. F., Madden, T. L., Schaffer, A. A., Zhang, J., Zhang, Z., Miller, W., & Lipman, D. J. (1997). Gapped BLAST and PSI-BLAST: A new generation of protein database search programs. *Nucleic Acids Research, 25*(17), 3389-3402.

Antonijevic, B., & Stojiljkovic, M. P. (2007). Unequal efficacy of pyridinium oximes in acute organophosphate poisoning. *Clinical Medicine & Research, 5*(1), 71-82.

Bard, J., Ercolani, K., Svenson, K., Olland, A., & Somers, W. (2004). Automated systems for protein crystallization. *Methods, 34*(3), 329-347.

Bergfors, T. (2003). Seeds to crystals. *Journal of Structural Biology, 142*(1), 66-76.

Besio, R., Alleva, S., Forlino, A., Lupi, A., Meneghini, C., Minicozzi, V., Profumo, A., Stellato, F., Tenni, R., & Morante, S. (2010). Identifying the structure of the active sites of human recombinant prolidase. *European Biophysics Journal, 39*(6), 935-945.

Beteva, A., Cipriani, S. C., Delageniere, S., Gabadinho, J., Gordon, E. J., Guijarro, M., Hall, D., Larsen, S., Launer, L., Lavault, C. B., Leonard, G. A., Mairs, T., McCarthy, J., Meyer, J.,

Mitchell, E., Monaco, S., Nurizzo, D., Pernot, P., Pieritz, R., Ravelli, R. G. B., Rey, V., Shepard, W., Spruce, D., Stuart, D. I., Svensson, O., Theveneau, P., Thibault, X., Turkenburg, J., Walsh, M., & McSweeney, S. M. (2006). High- throughput sample handling and data collection at synchrotrons: Embedding the ESRF into the high-throughput gene-to- structure pipeline. *Acta Crystallographica Section D, 62*(10), 1162-1169.

Blundell, T. L., Jhoti, H., & Abell, C. (2002). High- throughput crystallography for lead discovery in drug design. *Nature Reviews Drug Discovery, 1*(1), 45-54.

Bockelmann, W. (1995). The proteolytic system of starter and non-starter bacteria: Components and their importance for cheese ripening. *International Dairy Journal, 5*(8), 977-994.

Bruckner, P., & Prockop, D. J. (1981). Proteolytic enzymes as probes for the triple-helical conformation of procollagen. *Analytical Biochemistry, 110*(2), 360-368.

Brunger, A. T. (1992). Free *R* value: a novel statistical quantity for assessing the accuracy of crystal structures. *Nature, 335*, 472-475.

Brzozowski, A. M., & Walton, J. (2001). Clear strategy screens for macromolecular crystallization. *Journal of Applied Crystallography, 34*(2), 97-101.

Burmeister, W. P. (2000). Structural changes in a cryo-cooled protein crystal owing to radiation damage. *Acta Crystallographica Section D, Biological Crystallography, 56*(3), 328-341.

Cabrera, R., Ambrosio, A. L. B., Garratt, R. C., Guixé, V., & Babul, J. (2008). Crystallographic structure of phosphofructokinase-2 from *Escherichia coli* in complex with two ATP molecules. Implications for substrate inhibition. *Journal of Molecular Biology, 383*(3), 588-602.

Caniuguir, A., Cabrera, R., Báez, M., Vásquez, C. C., Babul, J., & Guixé, V. (2005). Role of cys-295 on subunit interactions and allosteric regulation of phosphofructokinase-2 from *Escherichia coli*. *FEBS Letters, 579*(11), 2313-2318.

Chauhan, S., Chauhan, S., D'Cruz, R., Faruqi, S., Singh, K. K., Varma, S., Singh, M., Karthik, V. (2008). Chemical warfare agents. *Environmental Toxicology and Pharmacology, 26,* 113 - 122.

Chayen, N. E. (1998). Comparative studies of protein crystallization by vapour-diffusion and microbatch techniques. *Acta Crystallographica Section D, Biological Crystallography, 54*, 8-15.

Chayen, N. E. (1997). A novel technique to control the rate of vapour diffusion, giving larger protein crystals. *Journal of Applied Crystallography, 30*(2), 198-202.

Chayen, N. E. (2004). Turning protein crystallisation from an art into a science. *Current Opinion in Structural Biology, 14*(5), 577-583.

Chayen, N. E. (2005). Methods for separating nucleation and growth in protein crystallisation. *Progress in Biophysics and Molecular Biology, 88*(3), 329-337.

Chayen, N. E., & Saridakis, E. (2008). Protein crystallization: From purified protein to diffraction- quality crystal. *Nature Methods, 5*(2), 147-153.

Chen, J. A., & Tanaka, T. (2011). Charged residues on a flap-loop structure of *Lactococcus lactis* prolidase play critical roles in allosteric behavior and substrate inhibition. *BBA - Proteins and Proteomics, 1814*(12), 1677-1685.

Chen, V. B., Arendall, W. B., Headd, J. J., Keedy, D. A., Immormino, R. M., Kapral, G. J., Murray, L. W., Richardson, J. S., & Richardson, D. C. (2010). *MolProbity*: All- atom structure validation for macromolecular crystallography. *Acta Crystallographica Section D, Biological Crystallography, 66*(1), 12-21.

Cheng, T., & Calomiris, J. J. (1996). A cloned bacterial enzyme for nerve agent decontamination. *Enzyme and Microbial Technology, 18*(8), 597-601.

Cheng, T., Harvey, S. P., & Stroup, A. N. (1993). Purification and properties of a highly active organophosphorus acid anhydrolase from *Alteromonas undina*. *Applied and Environmental Microbiology, 59*(9), 3138-3140.

Cipriani, F., Felisaz, F., Launer, L., Aksoy, J. S., Caserotto, H., Cusack, S., Dallery, M., diChiaro, F., Guijarro, M., Huet, J., Larsen, S., Lentini, M., McCarthy, J., McSweeney, S., Ravelli, R., Renier, M., Taffut, C., Thompson, A., Leonard, G. A., & Walsh, M. A. (2006). Automation of sample mounting for macromolecular crystallography. *Acta Crystallographica Section D, Biological Crystallography, 62*(10), 1251-1259.

Cowtan, K. (2001). *Phase problem in X-ray crystallography, and its solution*. *Encyclopedia of Life Sciences.* Hoboken, NY: John Wiley & Sons, Ltd.

Cunningham, D. F., & O'Connor, B. (1997). Proline specific peptidases. *Biochimica et Biophysica Acta, 1343*(2), 160-186.

Dale, G. E., Oefner, C., & D'Arcy, A. (2003). The protein as a variable in protein crystallization. *Journal of Structural Biology, 142*(1), 88-97.

Dalton, C. H., Hattersley, I. J., Rutter, S. J., & Chilcott, R. P. (2006). Absorption of the nerve agent VX (*O*- ethyl- S- [2(di-isopropylamino) ethyl] methyl phosphonothioate) through pig, human and guinea pig skin *in vitro*. *Toxicology in Vitro : An International Journal Published in Association with BIBRA, 20*(8), 1532-1536.

D'Arcy, A., Villard, F., & Marsh, M. (2007). An automated microseed matrix- screening method for protein crystallization. *Acta Crystallographica Section D, 63*(4), 550-554.

Dauter, Z. (1999). Data-collection strategies. *Acta Crystallographica Section D, Biological Crystallography, 55*, 1703-1717.

Dauter, Z. (1996). Application of synchrotron radiation in X-ray diffraction studies of crystal structures. *Journal of Molecular Structure: THEOCHEM, 374*(1), 29-35.

DeFrank, J. J., & Cheng, T. C. (1991). Purification and properties of an organophosphorus acid anhydrase from a halophilic bacterial isolate. *The Journal of Bacteriology, 173*(6), 1938-1943.

Delagenière, S., Brenchereau, P., Launer, L., Ashton, A. W., Leal, R., Veyrier, S., Gabadinho, J., Gordon, E. J., Jones, S. D., Levik, K. E., McSweeney, S. M., Monaco, S., Nanao, M., Spruce, D., Svensson, O., Walsh, M. A., & Leonard, G. A. (2011). ISPyB: An information management system for synchrotron macromolecular crystallography. *Bioinformatics, 27*(22), 3186-3192.

DeLucas, L. J., Bray, T. L., Nagy, L., McCombs, D., Chernov, N., Hamrick, D., Cosenza., L., Belgovskiy, A., Stoops, B., & Chait, A. (2003). Efficient protein crystallization. *Journal of Structural Biology, 142*(1), 188-206.

DeLucas, L. J., Hamrick, D., Cosenza, L., Nagy, L., McCombs, D., Bray, T., Chait, A., Stoops, B., Belgovskiy, A., Wilson., W. W., Parham, M., & Chernov, N. (2005). Protein crystallization: Virtual screening and optimization. *Progress in Biophysics and Molecular Biology, 88*(3), 285-309.

Drenth, J. (2007). In MyiLibrary L. (Ed.), *Principles of protein X-ray crystallography* (3rd ed). New York: New York: Springer.

Du, X., Tove, S., Kast-Hutcheson, K., & Grunden, A. M. (2005). Characterization of the dinuclear metal center of *Pyrococcus furiosus* prolidase by analysis of targeted mutants. *FEBS Letters, 579*(27), 6140-6146.

Emsley, P., Lohkamp, B., Scott, W. G., & Cowtan, K. (2010). Features and development of *Coot*. *Acta Crystallographica Section D, Biological Crystallography, 66*, 486-501.

Engelhard, N., Prchal, K., & Nenner, M. (1967). Acetylcholinesterase. *Angewandte Chemie International Edition, 6*(7), 615-626.

Exarchos, K., Exarchos, T., Papaloukas, C., Troganis, A., & Fotiadis, D. (2009). Detection of discriminative sequence patterns in the neighborhood of proline *cis* peptide bonds and their functional annotation. *BMC Bioinformatics, 10*(1), 113-126.

Eyer, P., Szinicz, L., Thiermann, H., Worek, F., & Zilker, T. (2007). Testing of antidotes for organophosphorus compounds: Experimental procedures and clinical reality. *Toxicology, 233*(1), 108-119.

Fallico, V., McSweeney, P. L. H., Horne, J., Pediliggieri, C., Hannon, J. A., Carpino, S., & Licitra, G. (2005). Evaluation of bitterness in ragusano cheese. *Journal of Dairy Science, 88*(4), 1288-1300.

Fermani, S., Falini, G., Minnucci, M., & Ripamonti, A. (2001). Protein crystallization on polymeric film surfaces. *Journal of Crystal Growth, 224*(3), 327-334.

Fernandez-Espla, M., Martin-Hernandez, M., & Fox, P. F. (1997). Purification and characterization of a prolidase from *Lactobacillus casei* subsp. *casei* IFPL 731. *Applied and Environmental Microbiology, 63*(1), 314-316.

Fodje, M., Janzen, K., Berg, R., Black, G., Labiuk, S., Gorin, J., & Grochulski, P. (2012). *MxDC* and *MxLIVE*: Software for data acquisition, information management and remote access to macromolecular crystallography beamlines. *Journal of Synchrotron Radiation, 19*, 274-280.

Gabadinho, J., Beteva, A., Guijarro, M., Rey-Bakaikoa, V., Spruce, D., Bowler, M. W., Brokhauser, S., Flot, D., Gordon, E. J., Hall, D. R., Lavault, B., McCarthy, A. A., McCarthy, J., Mitchell, E., Monaco, S., Mueller-Dieckmann, C., Nurizzo, D., Ravelli, R. B. G., Thibault, X., Walsh, M. A., Leonard, G. A., & McSweeney, S. M. (2010). *MxCuBE*: A synchrotron beamline control environment customized for macromolecular crystallography experiments. *Journal of Synchrotron Radiation, 17*(5), 700-707.

Garman, E. (1999). Cool data: Quantity and quality. *Acta Crystallographica Section D, Biological Crystallography, 55*, 1641-1653.

Garman, E. F., & Schneider, T. R. (1997). Macromolecular cryocrystallography. *Journal of Applied Crystallography, 30*(3), 211-237.

Gavira, J. A., Hernandez-Hernandez, M. A., Gonzalez-Ramirez, L. A., Briggs, R. A., Kolek, S. A., & Stewart, P. D. S. (2011). Combining counter- diffusion and microseeding to increase the success rate in protein crystallization. *Crystal Growth & Design, 11*(6), 2122-2126.

Gelse, K., Pöschl, E., & Aigner, T. (2003). Collagens-structure, function, and biosynthesis. *Advanced Drug Delivery Reviews, 55*(12), 1531-1546.

Ghosh, M., Grunden, A. M., Dunn, D. M., Weiss, R., & Adams, M. W. W. (1998). Characterization of native and recombinant forms of an unusual cobalt-dependent proline dipeptidase (prolidase) from the hyperthermophilic archaeon *Pyrococcus furiosus*. *The Journal of Bacteriology, 180*(18), 4781-4789.

Glynn, P. (1999). Neuropathy target esterase. *The Biochemical Journal, 344*, 625-631.

Grochulski, P., Fodje, M. N., Gorin, J., Labiuk, S. L., & Berg, R. (2011). Beamline 08ID- 1, the prime beamline of the Canadian Macromolecular Crystallography Facility. *Journal of Synchrotron Radiation, 18*(4), 681-684.

Grochulski, P., Fodje, M., Labiuk, S., Gorin, J., Janzen, K., & Berg, R. (2012). Canadian Macromolecular Crystallography Facility: A suite of fully automated beamlines. *Journal of Structural and Functional Genomics, 13*(2), 49-55.

Gruner, S. M., & Ealick, S. E. (1995). Charge coupled device X- ray detectors for macromolecular crystallography. *Structure, 3*(1), 13-15.

Holm, L., & Rosenström, P. (2010). Dali server: Conservation mapping in 3D. *Nucleic Acids Research, 38*, 545-549.

Ishibashi, N., Kouge, K., Shinoda, I., Kanehisa, H., & Okai, H. (1988). A mechanism for bitter taste sensibility in peptides. *Agricultural and Biological Chemistry, 52*(3), 819-827.

Jamrog, D. C., Phillips Jr., G. N., Tapia, R. A., & Zhang, Y. (2005). A global optimization method for the molecular replacement problem in X- ray crystallography. *Mathematical Programming, 103*(2), 399-426.

Jancarik, J., & Kim, S. H. (1991). Sparse matrix sampling: A screening method for crystallization of proteins. *Journal of Applied Crystallography, 24*(4), 409-411.

Jeyakanthan, J., Takada, K., Sawano, M., Ogasahara, K., Mizutani, H., Kunishima, N., Yokoyama, S., & Yutani, K. (2009). Crystal structural and functional analysis of the putative dipeptidase from *Pyrococcus horikoshii* OT3. *Journal of Biophysics,* 1-11.

Jokanović, M. (2009). Current understanding of the mechanisms involved in metabolic detoxification of warfare nerve agents. *Toxicology Letters, 188*(1), 1-10.

Kabsch, W. (2010). Integration, scaling, space- group assignment and post- refinement. *Acta Crystallographica Section D, Biological Crystallography, 66*(2), 133-144.

Kikuchi, S., Tanoue, A., Endo, F., Wakasugi, S., Matsuo, N., & Tsujimoto, G. (2000). A novel nonsense mutation of the PEPD gene in a Japanese patient with prolidase deficiency. *Journal of Human Genetics, 45*(2), 102-104.

Kim, S. C., & Lee, N. M. (2001). Detoxification of sarin , an acetylcholinesterase inhibitor, by recombinant organophosphorus acid anhydrolase. *Journal of Biochemistry and Molecular Biology, 34 (5),* 440 - 445.

Klar, A., Navon-Elkan, P., Rubinow, A., Branski, D., Hurvitz, H., Christensen, E., Khayat, M. & Falik-Zaccai, T. (2010). Prolidase deficiency: It looks like systemic lupus erythematosus but it is not. *European Journal of Pediatrics, 169*(6), 727-732.

Kriminski, S., Caylor, C. L., Nonato, M. C., Finkelstein, K. D., & Thorne, R. E. (2002). Flash-cooling and annealing of protein crystals. *Acta Crystallographica Section D, Biological Crystallography, 58*(3), 459-471.

Kuhn, P., Wilson, K., Patch, M. G., & Stevens, R. C. (2002). The genesis of high- throughput structure- based drug discovery using protein crystallography. *Current Opinion in Chemical Biology, 6*(5), 704-710.

Kunji, E., Mierau, I., Hagting, A., Poolman, B., & Konings, W. (1996). The proteotytic systems of lactic acid bacteria. *Antonie Van Leeuwenhoek, 70*(2), 187-221.

Kurien, B. T., Patel, N. C., Porter, A. C., D'Souza, A., Miller, D., Matsumoto, H., Wang, H., & Scofield, R. H. (2006). Prolidase deficiency and the biochemical assays used in its diagnosis. *Analytical Biochemistry, 349*(2), 165-175.

Laskowski, R. A., MacArthur, M. W., Moss, D. S., & Thornton, J. M. (1993). *PROCHECK*: A program to check the stereochemical quality of protein structures. *Journal of Applied Crystallography, 26*(2), 283-291.

Lebedev, A. A., Vagin, A. A., & Murshudov, G. N. (2008). Model preparation in *MOLREP* and examples of model improvement using X- ray data. *Acta Crystallographica Section D, Biological Crystallography, 64*, 33-39.

Leif Hanson, B., Schall, C. A., & Bunick, G. J. (2003). New techniques in macromolecular cryocrystallography: Macromolecular crystal annealing and cryogenic helium. *Journal of Structural Biology, 142*(1), 77-87.

Liu, M., Bayjanov, J., Renckens, B., Nauta, A., & Siezen, R. (2010). The proteolytic system of lactic acid bacteria revisited: A genomic comparison. *BMC Genomics, 11*(1), 36-50.

Lowther, W. T., & Matthews, B. W. (2002). Metalloaminopeptidases: Common functional themes in disparate structural surroundings. *Chemical Reviews, 102*(12), 4581-4607.

Luft, J. R., Collins, R. J., Fehrman, N. A., Lauricella, A. M., Veatch, C. K., & DeTitta, G. T. (2003). A deliberate approach to screening for initial crystallization conditions of biological macromolecules. *Journal of Structural Biology, 142*(1), 170-179.

Lupi, A., Casado, B., Soli, M., Bertazzoni, M., Annovazzi, L., Viglio, S., Cetta, G., & Iadarola, P. (2002). Therapeutic apheresis exchange in two patients with prolidase deficiency. *The British Journal of Dermatology, 147*(6), 1237-1240.

Lupi, A., Perugini, P., Genta, I., Modena, T., Conti, B., Casado, B., Cetta, G., Pavanetto, F., & Iadarola, P. (2004). Biodegradable microspheres for prolidase delivery to human cultured fibroblasts. *The Journal of Pharmacy and Pharmacology, 56*(5), 597-603.

Lupi, A., Rossi, A., Campari, E., Pecora, F., Lund, A. M., Elcioglu, N. H., Gultepe, M., Rocco, M. D., & Forlino, A. (2006). Molecular characterisation of six patients with prolidase deficiency: Identification of the first small duplication in the prolidase gene and of a mutation generating symptomatic and asymptomatic outcomes within the same family. *Journal of Medical Genetics, 43*(12), E58-64.

Lupi, A., Tenni, R., Rossi, A., Cetta, G., & Forlino, A. (2008). Human prolidase and prolidase deficiency: An overview on the characterization of the enzyme involved in proline recycling and on the effects of its mutations. *Amino Acids, 35*(4), 739-752.

Macilwain, C. (1993). Study proves Iraq used nerve gas. *Nature, 363*(6424), 3.

Maher, M. J., Ghosh, M., Grunden, A. M., Menon, A. L., Adams, M. W. W., Freeman, H. C., & Guss, J. M. (2004). Structure of the prolidase from *Pyrococcus furiosus*. *Biochemistry, 43*(10), 2771-2783.

Manco, G. (2008). Enzymes with phosphotriesterase and lactonase activities in archaea. *Current Chemical Biology, 2*(3), 237-248.

McCoy, A. J., Grosse-Kunstleve, R., Adams, P. D., Winn, M. D., Storoni, L. C., & Read, R. J. (2007). *Phaser* crystallographic software. *Journal of Applied Crystallography, 40,* 658-674.

McPherson, A. (2004). Introduction to protein crystallization. *Methods, 34*(3), 254-265.

McPherson, A., & Gavira, J. A. (2014). Introduction to protein crystallization. *Acta Crystallographica Section F, 70*(1), 2-20.

Minor, W., & Otwinowski, Z. (1997). *HKL2000* (denzo-SMN) software package. processing of X-ray diffraction data collected in oscillation mode. *Methods in Enzymology, Macromolecular Crystallography, Academic Press, New York.*

Minor, D. L. (2007). The neurobiologist's guide to structural biology: A primer on why macromolecular structure matters and how to evaluate structural data. *Neuron, 54*(4), 511-533.

Moriarty, N. W., Grosse-Kunstleve, R., & Adams, P. D. (2009). *electronic Ligand Builder and Optimization Workbench* (*eLBOW*): A tool for ligand coordinate and restraint generation. *Acta Crystallographic Section D, Biological Crystallography, 65*(10), 1074-1080

Murshudov, G. N., Vagin, A. A., & Dodson, E. J. (1997). Refinement of macromolecular structures by the maximum- likelihood method. *Acta Crystallographica Section D, Biological Crystallography, 53*(3), 240-255.

Myara, I., Charpentier, C., & Lemonnier, A. (1984). Prolidase and prolidase deficiency. *Life Sciences, 34*(21), 1985-1998.

Navaza, J. (1994). *AMoRe*: An automated package for molecular replacement. *Acta Crystallographica Section A Foundations of Crystallography, 50*(2), 157-163.

Navaza, J. (2001). Implementation of molecular replacement in *AMoRe. Acta Crystallographica Section D, Biological Crystallography, 57*(10), 1367-1372.

Okumura, T., Ninomiya, N., & Ohta, M. (2003). The chemical disaster response system in Japan. *Prehospital and Disaster Medicine, 18*(3), 189-192.

Okumura, T., Takasu, N., Ishimatsu, S., Miyanoki, S., Mitsuhashi, A., Kumada, K., Tanaka, K., & Hinohara, S. (1996). Report on 640 victims of the Tokyo subway sarin attack. *Annals of Emergency Medicine, 28*(2), 129-135.

Park, M., Hill, C. M., Li, Y., Hardy, R. K., Khanna, H., Khang, Y., & Raushel, F. M. (2004). Catalytic properties of the PepQ prolidase from *Escherichia coli*. *Archives of Biochemistry and Biophysics, 429*(2), 224-230.

Paul, M., Nuñez, A., Van Hekken, D., & Renye, J. (2014). Sensory and protein profiles of Mexican chihuahua cheese. *Journal of Food Science and Technology, 51*(11), 3432-3438.

Perugini, P., Hassan, K., Genta, I., Modena, T., Pavanetto, F., Cetta, G., Zanone, C., Iadarola, P., Asti, A., & Conti, B. (2005). Intracellular delivery of liposome-encapsulated prolidase in cultured fibroblasts from prolidase-deficient patients. *Journal of Controlled Release, 102*(1), 181-190.

Pettersen, E. F., Goddard, T. D., Huang, C. C., Couch, G. S., Greenblatt, D. M., Meng, E. C., & Ferrin, T. E. (2004). UCSF Chimera-a visualization system for exploratory research and analysis. *Journal of Computational Chemistry, 25*(13), 1605-1612.

Phang, J. M., Donald, S. P., Pandhare, J., & Liu, Y. (2008). The metabolism of proline, a stress substrate, modulates carcinogenic pathways. *Amino Acids, 35*(4), 681-690.

Pinto, G., Caira, S., Cuollo, M., Lilla, S., Chianese, L., & Addeo, F. (2012). Bioactive casein phosphopeptides in dairy products as nutraceuticals for functional foods. *Milk Protein, InTech,* 1-44.

Popov, A. N., & Bourenkov, G. P. (2003). Choice of data-collection parameters based on statistic modelling. *Acta Crystallographica Section D, Biological Crystallography, 59*(7), 1145-1153.

Pothineni, S. B., Strutz, T., & Lamzin, V. S. (2006). Automated detection and centring of cryocooled protein crystals. *Acta Crystallographica Section D, Biological Crystallography, 62*(11), 1358-1368.

Powell, G. F., Rasco, M. A., & Maniscalco, R. M. (1974). A prolidase deficiency in man with iminopeptiduria. *Metabolism, 23*(6), 505-513.

Ravelli, R. B. G., Cipriani, F., & Lavault, B. (2006). C3D: A program for the automated centring of cryocooled crystals. *Acta Crystallographica Section D, 62*(11), 1348-1357.

Raven, N. D., & Sharp, R. J. (1997). Development of defined and minimal media for the growth of the hyperthermophilic archaeon *Pyrococcus furiosus* Vc1. *FEMS Microbiology Letters, 146*(1), 135-141.

Rong, L., Komatsu, H., & Yoda, S. (2002). Control of heterogeneous nucleation of lysozyme crystals by using poly-L-lysine modified substrate. *Journal of Crystal Growth, 235*(1), 489-493.

Salemme, F. R. (1972). A free interface diffusion technique for the crystallization of proteins for X-ray crystallography. *Archives of Biochemistry and Biophysics, 151*(2), 533-539.

Saridakis, E., & Chayen, N. E. (2009). Towards a 'universal' nucleant for protein crystallization. *Trends in Biotechnology, 27*(2), 99-106.

Scapin, G. (2013). Molecular replacement then and now. *Acta Crystallographica Section D, Biological Crystallography, 69*(11), 2266-2275.

Stucky, K., Robert Klein, J., Schüller, A., Matern, H., Henrich, B., & Plapp, R. (1995). Cloning and DNA sequence analysis of *pepQ* , a prolidase gene from *Lactobacillus delbrueckii* subsp. *lactis* DSM7290 and partial characterization of its product. *Molecular and General Genetics, 247*(4), 494-500.

Suzuki, J., Kohno, T., Tsukagosi, M., Furuhata, T., & Yamazaki, K. (1997). Eighteen cases exposed to sarin in Matsumoto, Japan. *Internal Medicine (Tokyo, Japan), 36*(7), 466-470.

Szinicz, L. (2005). History of chemical and biological warfare agents. *Toxicology, 214*(3), 167-181.

Taylor, G. (2003). The phase problem. *Acta Crystallographica Section D, Biological Crystallography, 59*, 1881-1890.

Theriot, C., Tove, S., & Grunden, A. (2010). Characterization of two proline dipeptidases (prolidases) from the hyperthermophilic archaeon *Pyrococcus horikoshii*. *Applied Microbiology and Biotechnology, 86*(1), 177-188.

Trofimov, A. A., Slutskaya, E. A., Polyakov, K. M., Dorovatovskii, P. V., Gumerov, V. M., & Popov, V. O. (2012). Influence of intermolecular contacts on the structure of recombinant prolidase from *Thermococcus sibiricus*. *Acta Crystallographica Section F, 68*, 1275-1278.

Tsekova, D., Dimitrova, S., & Nanev, C. N. (1999). Heterogeneous nucleation (and adhesion) of lysozyme crystals. *Journal of Crystal Growth, 196*(2), 226-233.

Urzhumtseva, L., Afonine, P. V., Adams, P. D., & Urzhumtsev, A. (2009). Crystallographic model quality at a glance. *Acta Crystallographica.Section D, Biological Crystallography, 65*(3), 297-300.

Vagin, A., & Teplyakov, A. (1997). *MOLREP* : An automated program for molecular replacement. *Journal of Applied Crystallography, 30*(6), 1022-1025.

Vagin, A., & Teplyakov, A. (2010). Molecular replacement with *MOLREP*. *Acta Crystallographica Section D, 66*(1), 22-25.

van Kranenburg, R., Kleerebezem, M., van, H. V., Ursing, B. M., Boekhorst, J., Smit, B. A., Ayad, E. H. E., Smit, G., & Siezen, R. J. (2002). Flavour formation from amino acids by lactic acid bacteria: Predictions from genome sequence analysis. *International Dairy Journal, 12*(2), 111-121.

Walter, R. L., Thiel, D. J., Barna, S. L., Tate, M. W., Wall, M. E., Eikenberry, E. F., Gruner, S. M., & Ealick, S. E. (1995). High- resolution macromolecular structure determination using CCD detectors and synchrotron radiation. *Structure, 3*(8), 835-844.

Walter, T. S., Diprose, J. M., Mayo, C. J., Siebold, C., Pickford, M. G., Carter, L., Sutton, G. C., Berrow, N. S., Brown, J., Berry, I. M., Stewart-Jones, G. B. E., Grimes, J. M., Stammers, D. K., Esnouf, R. M., Jones, E. Y., Owens, R. J., Stuart, D. I., & Harlos, K. (2005). A procedure for setting up high- throughput nanolitre crystallization experiments.

Crystallization workflow for initial screening, automated storage, imaging and optimization. *Acta Crystallographica.Section D, Biological Crystallography, 61*(6), 651-657.

Wang, S., Liu, M., Chi, M., Wang, Q., & Sun, M. (2004). Production of human liver prolidase by *Saccharomyces cerevisiae* as host cells. *Acta Pharmacologica Sinica, 25*(6), 794-800.

Wang, S., Zhi, Q., & Sun, M. (2005). Purification and characterization of recombinant human liver prolidase expressed in *Saccharomyces cerevisiae*. *Archives of Toxicology, 79*(5), 253-259.

Weik, M., Ravelli, R. B., Silman, I., Sussman, J. L., Gros, P., & Kroon, J. (2001). Specific protein dynamics near the solvent glass transition assayed by radiation-induced structural changes. *Protein Science : A Publication of the Protein Society, 10*(10), 1953-1961.

Weik, M., Ravelli, R. B. G., Kryger, G., Mcsweeney, S., Raves, M. L., Harel, M., Gros, P., Silman, I., Kroon, J., & Sussman, J. L. (2000). Specific chemical and structural damage to proteins produced by synchrotron radiation. *Proceedings of the National Academy of Sciences of the United States of America, 97*(2), 623-628.

Wilkinson, M. G., & Kilcawley, K. N. (2005). Mechanisms of incorporation and release of enzymes into cheese during ripening. *International Dairy Journal, 15*(6), 817-830.

Winn, M. D., Ballard, C. C., Cowtan, K. D., Dodson, E. J., Emsley, P., Evans, P. R., Keegan, R. M., Krissinel, E. B., Leslie, A. G. W., McCoy, A., McNicholas, S. J., Murshudov, G. N., Pannu, N. S., Potterton, E. A., Powell, H. R., Read, R. J., Vagin, A., & Wilson, K. S. (2011). Overview of the *CCP4* suite and current developments. *Acta Crystallographica Section D, Biological Crystallography, 67*, 235-242.

Winter, G. (2010). *xia2*: An expert system for macromolecular crystallography data reduction. *Journal of Applied Crystallography, 43*(1), 186-190.

Winter, G., & McAuley, K. E. (2011). Automated data collection for macromolecular crystallography. *Methods, 55*(1), 81-93.

Wlodawer, A., Minor, W., Dauter, Z., & Jaskolski, M. (2008). Protein crystallography for non-crystallographers, or how to get the best (but not more) from published macromolecular structures. *FEBS Journal, 275*(1), 1-21.

Worek, F., Eyer, P., Aurbek, N., Szinicz, L., & Thiermann, H. (2007). Recent advances in evaluation of oxime efficacy in nerve agent poisoning by in vitro analysis. *Toxicology and Applied Pharmacology, 219*(2-3), 226-234.

Worek, F., Thiermann, H., Szinicz, L., & Eyer, P. (2004). Kinetic analysis of interactions between human acetylcholinesterase, structurally different organophosphorus compounds and oximes. *Biochemical Pharmacology, 68*(11), 2237-2248.

Yanagisawa, N., Morita, H., & Nakajima, T. (2006). Sarin experiences in Japan: Acute toxicity and long-term effects. *Journal of the Neurological Sciences, 249*(1), 76-85.

Yanagisawa, N., Morita, H., Nakajima, T., Okudera, H., Shimizu, M., Hirabayashi, H., Okudera, H., Nohara, M., Midorikawa, Y., & Mimura, S. (1995). Sarin poisoning in Matsumoto, Japan. *The Lancet, 346*(8970), 290-293.

Yang, S. I., & Tanaka, T. (2008). Characterization of recombinant prolidase from *Lactococcus lactis*-changes in substrate specificity by metal cations, and allosteric behavior of the peptidase.(author abstract)(report). *FEBS Journal, 275*(2), 271-280.

Yang, Y. (1999). Chemical detoxificatio of nerve agent VX. *Accounts of Chemical Research, 32 (2),* 109 - 115.

Yaron, A., & Naider, F. (1993). Proline-dependent structural and biological properties of peptides and proteins. *Critical Reviews in Biochemistry and Molecular Biology, 28*(1), 31-81.

Zhang, G., Chen, J. A., & Tanaka, T. (2009). Deregulation of allosteric response of *Lactococcus lactis* prolidase and its effects on enzyme activity. *Biochimica et Biophysica Acta, 1794*(6), 968-975.

10 APPENDIX

Table A1. Hampton Research Crystal Screen HR2-110 reagent formulation.

Reagent #	Formulation
1	30 % v/v 2-Methyl-2, 4-pentanedio, 0.1 M Sodium acetate trihydtrate pH 4.6, 0.02 M Calcium chloride dihydrate
2	0.4 M Potassium sodium tartrate tetrahydrate
3	0.4 M Ammonium phosphate monobasic
4	2.0 M Ammonium sulfate, 0.1 M TRIS hydrochloride pH 8.5
5	30 % v/v 2-Methyl-2, 4-pentanediol, 0.1 M HEPES sodium pH 7.5, 0.2 M Sodium citrate tribasic dihydrate
6	30 % w/v Polyethylene glycol 4,000, 0.1 M TRIS hydrochloride pH 8.5, 0.2 M, Magnesium chloride hexahydrate
7	1.4 M Sodium acetate trihydrate, 0.1 M Sodium cacodylate trihydrate pH 6.5
8	30 % v/v 2-Propanol, 0.1 M Sodium cacodylate trihydrate pH 6.5, 0.2 M Sodium citrate tribasic dihydrate
9	30 % w/v Polyethylene glycol 4,000, 0.1 M Sodium citrate tribasic dihydrate pH 5.6, 0.2 M Ammonium acetate
10	30 % w/v Polyethylene glycol 4,000, 0.1 M Sodium acetate trihydrate pH 4.6, 0.2 M Ammonium acetate
11	1.0 M Ammonium phosphate monobasic, 0.1 M Sodium citrate tribasic dihydrate pH 5.6
12	30 % v/v 2-Propanol, 0.1 M HEPES sodium pH 7.5, 0.2 M Magnesium chloride hexahydrate
13	30% v/v Polyethylene glycol 400, 0.1 M TRIS hydrochloride pH 8.5, 0.2 M Sodium citrate tribasic dihydrate
14	28 % v/v Polyethylene glycol 400, 0.1 M HEPES sodium pH 7.5, 0.2 M Calcium chloride dihydrate
15	30 % w/v Polyethylene glycol 8,000, 0.1 M Sodium cacodylate trihydrate pH 6.5, 0.2 M Ammonium sulfate
16	1.5 M Lithium sulfate monohydrate, 0.1 M HEPES sodium pH 7.5
17	30 % w/v Polyethylene glycol 4,000, 0.1 M TRIS hydrochloride pH 8.5, 0.2 M Lithium sulfate monohydrate
18	20 % w/v Polyethylene glycol 8,000, 0.1 M Sodium cacodylate trihydrate pH 6.5, 0.2 M Magnesium acetate tetrahydrate
19	30 % v/v 2-Propanol, 0.1 M TRIS hydrochloride pH 8.5, 0.2 M Ammonium acetate
20	25 % w/v Polyethylene glycol 4,000, 0.1 M Sodium acetate trihydrate pH 4.6, 0.2 M Ammonium sulfate
21	30 % v/v (+/-)-2-Methyl-2, 4-pentanediol, 0.1 M Sodium cacodylate trihydrate pH 6.5
22	30 % w/v Polyethylene glycol 4,000, 0.1 M TRIS hydrochloride pH 8.5, 0.2 M Sodium acetate trihydrate
23	30 % v/v Polyethylene glycol 400, 0.1 M HEPES sodium pH 7.5, 0.2 M Magnesium chloride hexahydrate
24	20 % v/v 2-Propanol, 0.1 M Sodium acetate trihydrate pH 4.6, 0.2 M Calcium

	chloride dihydrate
25#	1.0 M Sodium acetate trihydrate, 0.1 M Imidazole pH 6.5
26	30 % v/v (+/-)-2-Methyl-2, 4-pentanediol, 0.1 M Sodium citrate tribasic dihydrate pH 5.6, 0.2 M Ammonium acetate
27#	20% v/v 2-Propanol, 0.1 M HEPES sodium pH 7.5, 0.2 M Sodium citrate tribasic dihydrate
28	30 % w/v Polyethylene glycol 8,000, 0.1 M Sodium cacodylate trihydrate pH 6.5, 0.2 M Sodium acetate trihydrate
29	0.8 M Potassium sodium tartrate tetrahydrate, 0.1 M HEPES sodium pH 7.5
30	30 % w/v Polyethylene glycol 8,000, 0.2 M Ammonium sulfate
31	30 % w/v Polyethylene glycol 4,000, 0.2 M Ammonium sulfate
32	2.0 M Ammonium sulfate
33	4.0 M Sodium formate
34	2.0 M Sodium formate, 0.1 M Sodium acetate trihydrate pH 4.6
35	0.8 M Sodium phosphate monobasic monohydrate, 0.8 M Potassium phosphate monobasic, 0.1 M HEPES sodium pH 7.5
36	8 % w/v Polyethylene glycol 8,000, 0.1 M TRIS hydrochloride pH 8.5
37	8 % w/v Polyethylene glycol 4,000, 0.1 M Sodium acetate trihydrate pH 4.6
38	1.4 M Sodium citrate tribasic dihydrate, 0.1 M HEPES sodium pH 7.5
39	2 % v/v Polyethylene glycol 400, 2.0 M Ammonium sulfate, 0.1 M HEPES sodium pH 7.5
40	20 % v/v 2-Propanol, 20 % w/v Polyethylene glycol 4,000, 0.1 M Sodium citrate tribasic dihydrate pH 5.6
41	10 % v/v 2-Propanol, 20 % w/v Polyethylene glycol 4,000, 0.1 M HEPES sodium pH 7.5
42	20 % w/v Polyethylene glycol 8,000, 0.05 M Potassium phosphate monobasic
43	30 % w/v Polyethylene glycol 1,500
44	0.2 M Magnesium formate dihydrate
45	18 % w/v Polyethylene glycol 8,000, 0.1 M Sodium cacodylate trihydrate pH 6.5, 0.2 M Zinc acetate dihydrate
46	18 % w/v Polyethylene glycol 8,000, 0.1 M Sodium cacodylate trihydrate pH 6.5, 0.2 M Calcium acetate hydrate
47	2.0 M Ammonium sulfate, 0.1 M Sodium acetate trihydrate pH 4.6
48	2.0 M Ammonium phosphate monobasic, 0.1 M TRIS hydrochloride pH 8.5
49	2 % w/v Polyethylene glycol 8,000, 1.0 M Lithium sulfate monohydrate
50	15 % w/v Polyethylene glycol 8,000, 0.5 M Lithium sulfate monohydrate

#Did not use this reagent for screening based on its poor record of producing crystals (Rowlett 2005)

Table A2.   Hampton Research Crystal Screen 2 HR2-112 reagent formulation.

Reagent #	Formulation
1	10 % w/v Polyethylene glycol 6,000, 2.0 M Sodium chloride
2	0.01 M Hexadecyltrimethylammonium bromide, 0.5 M Sodium chloride, 0.01 M Magnesium chloride hexahydrate

3	25 % v/v Ethylene glycol
4	35 % v/v 1,4-Dioxane
5	5 % v/v 2-Propanol, 2.0 M Ammonium sulfate
6	1.0 M Imidazole pH 7.0
7	10 % w/v Polyethylene glycol 1,000, 10 % w/v Polyethylene glycol 8,000
8	10 % v/v Ethanol, 1.5 M Sodium chloride
9	2.0 M Sodium chloride, 0.1 M Sodium acetate trihydrate pH 4.6
10	30 % v/v (+/-)-2-Methyl-2, 4-pentanediol, 0.1 M Sodium acetate trihydrate pH 4.6, 0.2 M Sodium chloride
11	1.0 M 1,6-Hexanediol, 0.1 M Sodium acetate trihydrate pH 4.6, 0.01 M Cobalt (II) chloride hexahydrate
12	30 % v/v Polyethylene glycol 400, 0.1 M Sodium acetate trihydrate pH 4.6, 0.1 M Cadmium chloride hydrate
13	30 % w/v Polyethylene glycol monomethyl ether 2,000, 0.1 M Sodium acetate trihydrate pH 4.6, 0.2 M Ammonium sulfate
14	2.0 M Ammonium sulfate, 0.1 M Sodium citrate tribasic dihydrate pH 5.6, 0.2 M Potassium sodium tartrate tetrahydrate
15	1.0 M Lithium sulfate monohydrate, 0.1 M Sodium citrate tribasic dihydrate pH 5.6, 0.5 M Ammonium sulfate
16	2 % v/v Ethylene imine polymer, 0.1 M Sodium citrate tribasic dihydrate pH 5.6, 0.5 M Sodium chloride
17	35 % v/v tert-Butanol, 0.1 M Sodium citrate tribasic dihydrate pH 5.6
18	10 % v/v Jeffamine M-600, 0.1 M Sodium citrate tribasic dihydrate pH 5.6, 0.01 M Iron (III) chloride hexahydrate
19	2.5 M 1,6-Hexanediol, 0.1 M Sodium citrate tribasic dihydrate pH 5.6
20	1.6 M Magnesium sulfate heptahydrate, 0.1 M MES monohydrate pH 6.5
21	2.0 M Sodium chloride, 0.1 M MES monohydrate pH 6.5, 0.1 M Sodium phosphate monobasic monohydrate, 0.1 M Potassium phosphate monobasic
22	12 % w/v Polyethylene glycol 20,000, 0.1 M MES monohydrate pH 6.5
23	10 % v/v 1,4-Dioxane, 0.1 M MES monohydrate pH 6.5, 1.6 M Ammonium sulfate
24	30 % v/v Jeffamine M-600 ®, 0.1 M MES monohydrate pH 6.5, 0.05 M Cesium chloride
25	1.8 M Ammonium sulfate, 0.1 M MES monohydrate pH 6.5, 0.01 M Cobalt (II) chloride hexahydrate
26	30 % w/v Polyethylene glycol monomethyl ether 5,000, 0.1 M MES monohydrate pH 6.5, 0.2 M Ammonium sulfate
27	25% v/v Polyethylene glycol monomethyl ether 550, 0.1 M MES monohydrate pH 6.5, 0.01 M Zinc sulfate heptahydrate
28	1.6 M Sodium citrate tribasic dihydrate pH 6.5
29	30 % v/v (+/-)-2-Methyl-2, 4-pentanediol, 0.1 M HEPES pH 7.5, 0.5 M Ammonium sulfate
30	10 % w/v Polyethylene glycol 6,000, 5 % v/v (+/-)-2-Methyl-2, 4-pentanediol, 0.1 M HEPES pH 7.5
31	20% v/v Jeffamine M-600 ®, 0.1 M HEPES pH 7.5,
32	1.6 M Ammonium sulfate, 0.1 M HEPES pH 7.5, 0.1 M Sodium chloride

33	2.0 M Ammonium formate, 0.1 M HEPES pH 7.5
34	1.0 M Sodium acetate trihydrate, 0.1 M HEPES pH 7.5, 0.05 M Cadmium sulfate hydrate
35	70 % v/v (+/-)-2-Methyl-2, 4-pentanediol, 0.1 M HEPES pH 7.5
36	4.3 M Sodium chloride, 0.1 M HEPES pH 7.5
37	10 % w/v Polyethylene glycol 8,000, 8 % v/v Ethylene glycol, 0.1 M HEPES pH 7.5
38	20 % w/v Polyethylene glycol 10,000, 0.1 M HEPES pH 7.5
39	3.4 M 1,6-Hexanediol, 0.1 M Tris pH 8.5, 0.2 M Magnesium chloride hexahydrate
40	25 % v/v tert-Butanol, 0.1 M Tris pH 8.5
41	1.0 M Lithium sulfate monohydrate, 0.1 M Tris pH 8.5, 0.01 M Nickel (II) chloride hexahydrate
42	12 % v/v Glycerol, 0.1 M Tris pH 8.5, 1.5 M Ammonium sulfate
43	50 % v/v (+/-)-2-Methyl-2, 4-pentanediol, 0.1 M Tris pH 8.5, 0.2 M Ammonium phosphate monobasic
44	20 % v/v Ethanol, 0.1 M Tris pH 8.5
45	20 % w/v Polyethylene glycol monomethyl ether 2,000, 0.1 M Tris pH 8.5, 0.01 M Nickel (II) chloride hexahydrate
46	20 % v/v Polyethylene glycol monomethyl ether 550, 0.1 M BICINE pH 9.0, 0.1 M Sodium chloride
47	2.0 M Magnesium chloride hexahydrate, 0.1 M BICINE pH 9.0
48	2 % v/v 1,4-Dioxane, 10% w/v Polyethylene glycol 20,000, 0.1 M BICINE pH 9.0

Table A3.   Self-made crystallization reagent formulations: Optimization of Hampton Research lead conditions.

Reagent #	Formulation
1	10 % PEG 8000, 0.1 M Na Cacodylate (pH 6.0), 0.1 M Mg Acetate
2	10 % PEG 8000, 0.1 M Na Cacodylate (pH 6.0), 0.1 M Ca Acetate
3	10 % PEG 8000, 0.1 M Na Cacodylate (pH 6.0), 0.1 M ZnCl2
4	10 % PEG 8000, 0.1 M Na Cacodylate (pH 6.0), 0.1 M MnCl2
5	12 % PEG 8000, 0.1 M Na Cacodylate (pH 6.0), 0.1 M Mg Acetate
6	12 % PEG 8000, 0.1 M Na Cacodylate (pH 6.0), 0.1 M Ca Acetate
7	12 % PEG 8000, 0.1 M Na Cacodylate (pH 6.0), 0.1 M ZnCl2
8	12 % PEG 8000, 0.1 M Na Cacodylate (pH 6.0), 0.1 M MnCl2
9	14 % PEG 8000, 0.1 M Na Cacodylate (pH 6.0), 0.1 M Mg Acetate
10	14 % PEG 8000, 0.1 M Na Cacodylate (pH 6.0), 0.1 M Ca Acetate
11	14 % PEG 8000, 0.1 M Na Cacodylate (pH 6.0), 0.1 M ZnCl2
12	14 % PEG 8000, 0.1 M Na Cacodylate (pH 6.0), 0.1 M MnCl2
13	16 % PEG 8000, 0.1 M Na Cacodylate (pH 6.0), 0.1 M Mg Acetate
14	16 % PEG 8000, 0.1 M Na Cacodylate (pH 6.0), 0.1 M Ca Acetate
15	16 % PEG 8000, 0.1 M Na Cacodylate (pH 6.0), 0.1 M ZnCl2
16	16 % PEG 8000, 0.1 M Na Cacodylate (pH 6.0), 0.1 M MnCl2
17	18 % PEG 8000, 0.1 M Na Cacodylate (pH 6.0), 0.1 M Mg Acetate
18	18 % PEG 8000, 0.1 M Na Cacodylate (pH 6.0), 0.1 M Ca Acetate
19	18 % PEG 8000, 0.1 M Na Cacodylate (pH 6.0), 0.1 M ZnCl2
20	18 % PEG 8000, 0.1 M Na Cacodylate (pH 6.0), 0.1 M MnCl2

21	20 % PEG 8000, 0.1 M Na Cacodylate (pH 6.0), 0.1 M Mg Acetate
22	20 % PEG 8000, 0.1 M Na Cacodylate (pH 6.0), 0.1 M Ca Acetate
23	20 % PEG 8000, 0.1 M Na Cacodylate (pH 6.0), 0.1 M ZnCl2
24	20 % PEG 8000, 0.1 M Na Cacodylate (pH 6.0), 0.1 M MnCl2
25	10 % PEG 8000, 0.1 M Na Cacodylate (pH 6.5), 0.1 M Mg Acetate
26	10 % PEG 8000, 0.1 M Na Cacodylate (pH 6.5), 0.1 M Ca Acetate
27	10 % PEG 8000, 0.1 M Na Cacodylate (pH 6.5), 0.1 M ZnCl2
28	10 % PEG 8000, 0.1 M Na Cacodylate (pH 6.5), 0.1 M MnCl2
29	12 % PEG 8000, 0.1 M Na Cacodylate (pH 6.5), 0.1 M Mg Acetate
30	12 % PEG 8000, 0.1 M Na Cacodylate (pH 6.5), 0.1 M Ca Acetate
31	12 % PEG 8000, 0.1 M Na Cacodylate (pH 6.5), 0.1 M ZnCl2
32	12 % PEG 8000, 0.1 M Na Cacodylate (pH 6.5), 0.1 M MnCl2
33	14 % PEG 8000, 0.1 M Na Cacodylate (pH 6.5), 0.1 M Mg Acetate
34	14 % PEG 8000, 0.1 M Na Cacodylate (pH 6.5), 0.1 M Ca Acetate
35	14 % PEG 8000, 0.1 M Na Cacodylate (pH 6.5), 0.1 M ZnCl2
36	14 % PEG 8000, 0.1 M Na Cacodylate (pH 6.5), 0.1 M MnCl2
37	16 % PEG 8000, 0.1 M Na Cacodylate (pH 6.5), 0.1 M Mg Acetate
38	16 % PEG 8000, 0.1 M Na Cacodylate (pH 6.5), 0.1 M Ca Acetate
39	16 % PEG 8000, 0.1 M Na Cacodylate (pH 6.5), 0.1 M ZnCl2
40	16 % PEG 8000, 0.1 M Na Cacodylate (pH 6.5), 0.1 M MnCl2
41	18 % PEG 8000, 0.1 M Na Cacodylate (pH 6.5), 0.1 M Mg Acetate
42	18 % PEG 8000, 0.1 M Na Cacodylate (pH 6.5), 0.1 M Ca Acetate
43	18 % PEG 8000, 0.1 M Na Cacodylate (pH 6.5), 0.1 M ZnCl2
44	18 % PEG 8000, 0.1 M Na Cacodylate (pH 6.5), 0.1 M MnCl2
45	20 % PEG 8000, 0.1 M Na Cacodylate (pH 6.5), 0.1 M Mg Acetate
46	20 % PEG 8000, 0.1 M Na Cacodylate (pH 6.5), 0.1 M Ca Acetate
47	20 % PEG 8000, 0.1 M Na Cacodylate (pH 6.5), 0.1 M ZnCl2
48	20 % PEG 8000, 0.1 M Na Cacodylate (pH 6.5), 0.1 M MnCl2
49	10 % PEG 8000, 0.1 M Na Cacodylate (pH 7.0), 0.1 M Mg Acetate
50	10 % PEG 8000, 0.1 M Na Cacodylate (pH 7.0), 0.1 M Ca Acetate
51	10 % PEG 8000, 0.1 M Na Cacodylate (pH 7.0), 0.1 M ZnCl2
51	10 % PEG 8000, 0.1 M Na Cacodylate (pH 7.0), 0.1 M MnCl2
53	12 % PEG 8000, 0.1 M Na Cacodylate (pH 7.0), 0.1 M Mg Acetate
54	12 % PEG 8000, 0.1 M Na Cacodylate (pH 7.0), 0.1 M Ca Acetate
55	12 % PEG 8000, 0.1 M Na Cacodylate (pH 7.0), 0.1 M ZnCl2
56	12 % PEG 8000, 0.1 M Na Cacodylate (pH 7.0), 0.1 M MnCl2
57	14 % PEG 8000, 0.1 M Na Cacodylate (pH 7.0), 0.1 M Mg Acetate
58	14 % PEG 8000, 0.1 M Na Cacodylate (pH 7.0), 0.1 M Ca Acetate
59	14 % PEG 8000, 0.1 M Na Cacodylate (pH 7.0), 0.1 M ZnCl2
60	14 % PEG 8000, 0.1 M Na Cacodylate (pH 7.0), 0.1 M MnCl2
61	16 % PEG 8000, 0.1 M Na Cacodylate (pH 7.0), 0.1 M Mg Acetate
62	16 % PEG 8000, 0.1 M Na Cacodylate (pH 7.0), 0.1 M Ca Acetate
63	16 % PEG 8000, 0.1 M Na Cacodylate (pH 7.0), 0.1 M ZnCl2
64	16 % PEG 8000, 0.1 M Na Cacodylate (pH 7.0), 0.1 M MnCl2

65	18 % PEG 8000, 0.1 M Na Cacodylate (pH 7.0), 0.1 M Mg Acetate
66	18 % PEG 8000, 0.1 M Na Cacodylate (pH 7.0), 0.1 M Ca Acetate
67	18 % PEG 8000, 0.1 M Na Cacodylate (pH 7.0), 0.1 M ZnCl2
68	18 % PEG 8000, 0.1 M Na Cacodylate (pH 7.0), 0.1 M MnCl2
69	20 % PEG 8000, 0.1 M Na Cacodylate (pH 7.0), 0.1 M Mg Acetate
70	20 % PEG 8000, 0.1 M Na Cacodylate (pH 7.0), 0.1 M Ca Acetate
71	20 % PEG 8000, 0.1 M Na Cacodylate (pH 7.0), 0.1 M ZnCl2
72	20 % PEG 8000, 0.1 M Na Cacodylate (pH 7.0), 0.1 M MnCl2
73	11 % PEG 8000, 0.1 M Na Cacodylate (pH 6.5), 0.1 M MnCl2
74	12 % PEG 8000, 0.1 M Na Cacodylate (pH 6.5), 0.1 M MnCl2
75	13 % PEG 8000, 0.1 M Na Cacodylate (pH 6.5), 0.1 M MnCl2
76	14 % PEG 8000, 0.1 M Na Cacodylate (pH 6.5), 0.1 M MnCl2
77	15 % PEG 8000, 0.1 M Na Cacodylate (pH 6.5), 0.1 M MnCl2
78	16 % PEG 8000, 0.1 M Na Cacodylate (pH 6.5), 0.1 M MnCl2
79	11 % PEG 8000, 0.1 M Na Cacodylate (pH 6.5), 0.1 M MnCl2, 10 mM Leu-Pro
80	12 % PEG 8000, 0.1 M Na Cacodylate (pH 6.5), 0.1 M MnCl2, 10 mM Leu-Pro
81	13 % PEG 8000, 0.1 M Na Cacodylate (pH 6.5), 0.1 M MnCl2, 10 mM Leu-Pro
82	14 % PEG 8000, 0.1 M Na Cacodylate (pH 6.5), 0.1 M MnCl2, 10 mM Leu-Pro
83	15 % PEG 8000, 0.1 M Na Cacodylate (pH 6.5), 0.1 M MnCl2, 10 mM Leu-Pro
84	16 % PEG 8000, 0.1 M Na Cacodylate (pH 6.5), 0.1 M MnCl2, 10 mM Leu-Pro
85	14 % PEG 8000, 0.1 M Na Cacodylate (pH 6.5), 0.1 M MnCl2, 5 mM Leu
86	15 % PEG 8000, 0.1 M Na Cacodylate (pH 6.5), 0.1 M MnCl2, 5 mM Leu
87	16 % PEG 8000, 0.1 M Na Cacodylate (6.5), 0.1 M MnCl2, 5 mM Leu
88	14 % PEG 8000, 0.1 M Na Cacodylate (pH 6.5), 0.1 M MnCl2, 10 mM Leu
89	15 % PEG 8000, 0.1 M Na Cacodylate (pH 6.5), 0.1 M MnCl2, 10 mM Leu
90	16 % PEG 8000, 0.1 M Na Cacodylate (pH 6.5), 0.1 M MnCl2, 10 mM Leu
91	15 % PEG 8000, 0.1 M Na Cacodylate (pH 6.5), 0.1 M Ca Acetate, 5 mM Leu-Pro
92	16 % PEG 8000, 0.1 M Na Cacodylate (pH 6.5), 0.1 M Ca Acetate, 5 mM Leu-Pro
93	17 % PEG 8000, 0.1 M Na Cacodylate (pH 6.5), 0.1 M Ca Acetate, 5 mM Leu-Pro
94	15 % PEG 8000, 0.1 M Na Cacodylate (pH 6.5), 0.1 M Ca Acetate, 10 mM Leu-Pro
95	16 % PEG 8000, 0.1 M Na Cacodylate (pH 6.5), 0.1 M Ca Acetate, 10 mM Leu-Pro
96	17 % PEG 8000, 0.1 M Na Cacodylate (pH 6.5), 0.1 M Ca Acetate, 10 mM Leu-Pro
97	11 % PEG 8000, 0.1 M Na Cacodylate (pH 6.5), 0.2 M MnCl2
98	12 % PEG 8000, 0.1 M Na Cacodylate (pH 6.5), 0.2 M MnCl2
99	13 % PEG 8000, 0.1 M Na Cacodylate (pH 6.5), 0.2 M MnCl2
100	14 % PEG 8000, 0.1 M Na Cacodylate (pH 6.5), 0.2 M MnCl2
101	15 % PEG 8000, 0.1 M Na Cacodylate (pH 6.5), 0.2 M MnCl2
102	16 % PEG 8000, 0.1 M Na Cacodylate (pH 6.5), 0.2 M MnCl2
103	11 % PEG 8000, 0.1 M Na Cacodylate (pH 6.5), 0.1 M Ca Acetate
104	12 % PEG 8000, 0.1 M Na Cacodylate (pH 6.5), 0.1 M Ca Acetate
105	13 % PEG 8000, 0.1 M Na Cacodylate (pH 6.5), 0.1 M Ca Acetate
106	14 % PEG 8000, 0.1 M Na Cacodylate (pH 6.5), 0.1 M Ca Acetate
107	15 % PEG 8000, 0.1 M Na Cacodylate (pH 6.5), 0.1 M Ca Acetate
108	16 % PEG 8000, 0.1 M Na Cacodylate (pH 6.5), 0.1 M Ca Acetate

109	17 % PEG 8000, 0.1 M Na Cacodylate (pH 6.5), 0.1 M Ca Acetate
109	11 % PEG 8000, 0.1 M Na Cacodylate (pH 6.5), 0.1 M Mg Acetate
110	12 % PEG 8000, 0.1 M Na Cacodylate (pH 6.5), 0.1 M Mg Acetate
111	13 % PEG 8000, 0.1 M Na Cacodylate (pH 6.5), 0.1 M Mg Acetate
112	14 % PEG 8000, 0.1 M Na Cacodylate (6.5), 0.1 M Mg Acetate
113	15 % PEG 8000, 0.1 M Na Cacodylate (pH 6.5), 0.1 M Mg Acetate
114	16 % PEG 8000, 0.1 M Na Cacodylate (pH 6.5), 0.1 M Mg Acetate
115	11 % PEG 8000, 0.1 M Na Cacodylate (pH 6.5), 0.1 M Co (II) Nitrate
116	12 % PEG 8000, 0.1 M Na Cacodylate (pH 6.5), 0.1 M Co (II) Nitrate
117	13 % PEG 8000, 0.1 M Na Cacodylate (pH 6.5), 0.1 M Co (II) Nitrate
118	14 % PEG 8000, 0.1 M Na Cacodylate (pH 6.5), 0.1 M Co (II) Nitrate
119	15 % PEG 8000, 0.1 M Na Cacodylate (pH 6.5), 0.1 M Co (II) Nitrate
120	16 % PEG 8000, 0.1 M Na Cacodylate (pH 6.5), 0.1 M Co (II) Nitrate
121	11 % PEG 6000, 0.1 M Na Cacodylate (pH 6.5), 0.1 M MnCl2
122	12 % PEG 6000, 0.1 M Na Cacodylate (pH 6.5), 0.1 M MnCl2
123	13 % PEG 6000, 0.1 M Na Cacodylate (pH 6.5), 0.1 M MnCl2
124	14 % PEG 6000, 0.1 M Na Cacodylate (pH 6.5), 0.1 M MnCl2
125	15 % PEG 6000, 0.1 M Na Cacodylate (pH 6.5), 0.1 M MnCl2
126	16 % PEG 6000, 0.1 M Na Cacodylate (pH 6.5), 0.1 M MnCl2
127	17 % PEG 6000, 0.1 M Na Cacodylate (pH 6.5), 0.1 M MnCl2
128	18 % PEG 6000, 0.1 M Na Cacodylate (pH 6.5), 0.1 M MnCl2
129	19 % PEG 6000, 0.1 M Na Cacodylate (pH 6.5), 0.1 M MnCl2
130	20 % PEG 6000, 0.1 M Na Cacodylate (pH 6.5), 0.1 M MnCl2
131	21 % PEG 6000, 0.1 M Na Cacodylate (pH 6.5), 0.1 M MnCl2
132	22 % PEG 6000, 0.1 M Na Cacodylate (pH 6.5), 0.1 M MnCl2
133	11 % PEG 8000, 0.1 M Na Cacodylate (pH 6.5), 0.2 M MnCl2
134	12 % PEG 8000, 0.1 M Na Cacodylate (pH 6.5), 0.2 M MnCl2
135	13 % PEG 8000, 0.1 M Na Cacodylate (pH 6.5), 0.2 M MnCl2
136	14 % PEG 8000, 0.1 M Na Cacodylate (pH 6.5), 0.2 M MnCl2
137	15 % PEG 8000, 0.1 M Na Cacodylate (pH 6.5), 0.2 M MnCl2
138	16 % PEG 8000, 0.1 M Na Cacodylate (pH 6.5), 0.2 M MnCl2

Table A4.　　Self-made crystallization reagent formulations: Optimization of Hauptman Woodward Research Institute lead conditions

1	0.16 M Calcium acetate hydrate, 0.08 M Sodium cacodylate trihydrate (pH 6.5), 11 % (w/v) PEG 8000, 20 % (v/v) glycerol
2	0.16 M Calcium acetate hydrate, 0.08 M Sodium cacodylate trihydrate (pH 6.5), 12 % (w/v) PEG 8000, 20 % (v/v) glycerol
3	0.16 M Calcium acetate hydrate, 0.08 M Sodium cacodylate trihydrate (pH 6.5), 13 % (w/v) PEG 8000, 20 % (v/v) glycerol
4	0.16 M Calcium acetate hydrate, 0.08 M Sodium cacodylate trihydrate (pH 6.5), 14 % (w/v) PEG 8000, 20 % (v/v) glycerol
5	0.16 M Calcium acetate hydrate, 0.08 M Sodium cacodylate trihydrate (pH 6.5), 15 % (w/v) PEG 8000, 20 % (v/v) glycerol
6	0.16 M Calcium acetate hydrate, 0.08 M Sodium cacodylate trihydrate (pH 6.5), 16

	% (w/v) PEG 8000, 20 % (v/v) glycerol
7	0.16 M Calcium acetate hydrate, 0.08 M Sodium cacodylate trihydrate (pH 6.5), 14 % (w/v) PEG 8000, 17 % (v/v) glycerol
8	0.16 M Calcium acetate hydrate, 0.08 M Sodium cacodylate trihydrate (pH 6.5), 14 % (w/v) PEG 8000, 18 % (v/v) glycerol
9	0.16 M Calcium acetate hydrate, 0.08 M Sodium cacodylate trihydrate (pH 6.5), 14 % (w/v) PEG 8000, 19 % (v/v) glycerol
10	0.16 M Calcium acetate hydrate, 0.08 M Sodium cacodylate trihydrate (pH 6.5), 14 % (w/v) PEG 8000, 20 % (v/v) glycerol
11	0.16 M Calcium acetate hydrate, 0.08 M Sodium cacodylate trihydrate (pH 6.5), 14 % (w/v) PEG 8000, 21 % (v/v) glycerol
12	0.16 M Calcium acetate hydrate, 0.08 M Sodium cacodylate trihydrate (pH 6.5), 14 % (w/v) PEG 8000, 22 % (v/v) glycerol
13	0.2 M Calcium chloride (pH 6.5), 18 % (w/v) PEG 3350
14	0.2 M Calcium chloride (pH 6.5), 19 % (w/v) PEG 3350
15	0.2 M Calcium chloride (pH 6.5), 20 % (w/v) PEG 3350
16	0.2 M Calcium chloride (pH 6.5), 21 % (w/v) PEG 3350
17	0.2 M Calcium chloride (pH 6.5), 22 % (w/v) PEG 3350
18	0.2 M Calcium chloride (pH 6.5), 23 % (w/v) PEG 3350
19	0.2 M Calcium acetate hydrate (pH 7.5), 18 % (w/v) PEG 3350
20	0.2 M Calcium acetate hydrate (pH 7.5), 19 % (w/v) PEG 3350
21	0.2 M Calcium acetate hydrate (pH 7.5), 20 % (w/v) PEG 3350
22	0.2 M Calcium acetate hydrate (pH 7.5), 21 % (w/v) PEG 3350
23	0.2 M Calcium acetate hydrate (pH 7.5), 22 % (w/v) PEG 3350
24	0.2 M Calcium acetate hydrate (pH 7.5), 23 % (w/v) PEG 3350
25	0.1 M Lithium chloride, 0.1 M Tris (pH 8.0), 17 % PEG 8000
26	0.1 M Lithium chloride, 0.1 M Tris (pH 8.0), 18 % PEG 8000
27	0.1 M Lithium chloride, 0.1 M Tris (pH 8.0), 19 % PEG 8000
28	0.1 M Lithium chloride, 0.1 M Tris (pH 8.0), 20 % PEG 8000
29	0.1 M Lithium chloride, 0.1 M Tris (pH 8.0), 21 % PEG 8000
30	0.1 M Lithium chloride, 0.1 M Tris (pH 8.0), 22 % PEG 8000
31	0.1 M Ammonium thiocyanate, 0.1 M Tris (pH 8.0), 17 % PEG 8000
32	0.1 M Ammonium thiocyanate, 0.1 M Tris (pH 8.0), 18 % PEG 8000
33	0.1 M Ammonium thiocyanate, 0.1 M Tris (pH 8.0), 19 % PEG 8000
34	0.1 M Ammonium thiocyanate, 0.1 M Tris (pH 8.0), 20 % PEG 8000
35	0.1 M Ammonium thiocyanate, 0.1 M Tris (pH 8.0), 21 % PEG 8000
36	0.1 M Ammonium thiocyanate, 0.1 M Tris (pH 8.0), 22 % PEG 8000
37	0.72 M Lithium sulphate monohydrate, 0.1 M Bis-Tris Propane (pH 7.0)
38	0.76 M Lithium sulphate monohydrate, 0.1 M Bis-Tris Propane (pH 7.0)
39	0.80 M Lithium sulphate monohydrate, 0.1 M Bis-Tris Propane (pH 7.0)
40	0.84 M Lithium sulphate monohydrate, 0.1 M Bis-Tris Propane (pH 7.0)
41	0.88 M Lithium sulphate monohydrate, 0.1 M Bis-Tris Propane (pH 7.0)
42	0.92 M Lithium sulfate monohydrate, 0.1 M Bis-Tris Propane (pH 7.0)
43	1.2 M Lithium sulfate monohydrate, 0.1 M Tris (pH 8.5)
44	1.3 M Lithium sulfate monohydrate, 0.1 M Tris (pH 8.5)

45	1.4 M Lithium sulfate monohydrate, 0.1 M Tris (pH 8.5)
46	1.5 M Lithium sulfate monohydrate, 0.1 M Tris (pH 8.5)
47	1.6 M Lithium sulfate monohydrate, 0.1 M Tris (pH 8.5)
48	1.7 M Lithium sulfate monohydrate, 0.1 M Tris (pH 8.5)
49	0.08 M Lithium chloride, 0.1 M Tris (pH 8.0), 20 % PEG 8000
50	0.09 M Lithium chloride, 0.1 M Tris (pH 8.0), 20 % PEG 8000
51	0.1 M Lithium chloride, 0.1 M Tris (pH 8.0), 20 % PEG 8000
52	0.11 M Lithium chloride, 0.1 M Tris (pH 8.0), 20 % PEG 8000
53	0.12 M Lithium chloride, 0.1 M Tris (pH 8.0), 20 % PEG 8000
54	0.13 M Lithium chloride, 0.1 M Tris (pH 8.0), 20 % PEG 8000
55	0.08 M Ammonium thiocyanate, 0.1 M Tris (pH 8.0), 20 % PEG 8000
56	0.09 M Ammonium thiocyanate, 0.1 M Tris (pH 8.0), 20 % PEG 8000
57	0.10 M Ammonium thiocyanate, 0.1 M Tris (pH 8.0), 20 % PEG 8000
58	0.11 M Ammonium thiocyanate, 0.1 M Tris (pH 8.0), 20 % PEG 8000
59	0.12 M Ammonium thiocyanate, 0.1 M Tris (pH 8.0), 20 % PEG 8000
60	0.13 M Ammonium thiocyanate, 0.1 M Tris (pH 8.0), 20 % PEG 8000
61	0.1 M Calcium acetate, 0.1 M Bis-Tris Propane (pH 7.0), 17 % (w/v) PEG 4000
62	0.1 M Calcium acetate, 0.1 M Bis-Tris Propane (pH 7.0), 18 % (w/v) PEG 4000
63	0.1 M Calcium acetate, 0.1 M Bis-Tris Propane (pH 7.0), 19 % (w/v) PEG 4000
64	0.1 M Calcium acetate, 0.1 M Bis-Tris Propane (pH 7.0), 20 % (w/v) PEG 4000
65	0.1 M Calcium acetate, 0.1 M Bis-Tris Propane (pH 7.0), 21 % (w/v) PEG 4000
66	0.1 M Calcium acetate, 0.1 M Bis-Tris Propane (pH 7.0), 22 % (w/v) PEG 4000
67	0.08 M Calcium acetate, 0.1 M Bis-Tris Propane (pH 7.0), 20 % (w/v) PEG 4000
68	0.09 M Calcium acetate, 0.1 M Bis-Tris Propane (pH 7.0), 20 % (w/v) PEG 4000
69	0.10 M Calcium acetate, 0.1 M Bis-Tris Propane (pH 7.0), 20 % (w/v) PEG 4000
70	0.11 M Calcium acetate, 0.1 M Bis-Tris Propane (pH 7.0), 20 % (w/v) PEG 4000
71	0.12 M Calcium acetate, 0.1 M Bis-Tris Propane (pH 7.0), 20 % (w/v) PEG 4000
72	0.13 M Calcium acetate, 0.1 M Bis-Tris Propane (pH 7.0), 20 % (w/v) PEG 4000
73	0.16 M Manganese chloride, 0.08 M Sodium cacodylate trihydrate (pH 6.5), 11 % (w/v) PEG 8000, 20 % (v/v) glycerol
74	0.16 M Manganese chloride, 0.08 M Sodium cacodylate trihydrate (pH 6.5), 12 % (w/v) PEG 8000, 20 % (v/v) glycerol
75	0.16 M Manganese chloride, 0.08 M Sodium cacodylate trihydrate (pH 6.5), 13 % (w/v) PEG 8000, 20 % (v/v) glycerol
76	0.16 M Manganese chloride, 0.08 M Sodium cacodylate trihydrate (pH 6.5), 14 % (w/v) PEG 8000, 20 % (v/v) glycerol
77	0.16 M Calcium acetate hydrate, 0.08 M Sodium cacodylate trihydrate (pH 6.5), 15 % (w/v) PEG 8000, 20 % (v/v) glycerol
78	0.16 M Manganese chloride, 0.08 M Sodium cacodylate trihydrate (pH 6.5), 16 % (w/v) PEG 8000, 20 % (v/v) glycerol
79	0.16 M Manganese chloride, 0.08 M Sodium cacodylate trihydrate (pH 6.5), 14 % (w/v) PEG 8000, 17 % (v/v) glycerol
80	0.16 M Manganese chloride, 0.08 M Sodium cacodylate trihydrate (pH 6.5), 14 % (w/v) PEG 8000, 18 % (v/v) glycerol
81	0.16 M Manganese chloride, 0.08 M Sodium cacodylate trihydrate (pH 6.5), 14 %

	(w/v) PEG 8000, 19 % (v/v) glycerol
82	0.16 M Manganese chloride, 0.08 M Sodium cacodylate trihydrate (pH 6.5), 14 % (w/v) PEG 8000, 20 % (v/v) glycerol
83	0.16 M Manganese chloride, 0.08 M Sodium cacodylate trihydrate (pH 6.5), 14 % (w/v) PEG 8000, 21 % (v/v) glycerol
84	0.16 M Manganese chloride, 0.08 M Sodium cacodylate trihydrate (pH 6.5), 14 % (w/v) PEG 8000, 22 % (v/v) glycerol
85	0.16 M Calcium acetate hydrate, 0.08 M Sodium cacodylate trihydrate (pH 6.5), 14 % (w/v) PEG 8000, 23 % (v/v) glycerol
86	0.16 M Calcium acetate hydrate, 0.08 M Sodium cacodylate trihydrate (pH 6.5), 14 % (w/v) PEG 8000, 24 % (v/v) glycerol
87	0.16 M Calcium acetate hydrate, 0.08 M Sodium cacodylate trihydrate (pH 6.5), 14 % (w/v) PEG 8000, 25 % (v/v) glycerol
88	0.16 M Calcium acetate hydrate, 0.08 M Sodium cacodylate trihydrate (pH 6.5), 14 % (w/v) PEG 8000, 26 % (v/v) glycerol
89	0.16 M Calcium acetate hydrate, 0.08 M Sodium cacodylate trihydrate (pH 6.5), 14 % (w/v) PEG 8000, 27 % (v/v) glycerol
90	0.16 M Calcium acetate hydrate, 0.08 M Sodium cacodylate trihydrate (pH 6.5), 14 % (w/v) PEG 8000, 28 % (v/v) glycerol
91	0.16 M Manganese chloride, 0.08 M Sodium cacodylate trihydrate (pH 6.5), 14 % (w/v) PEG 8000, 23 % (v/v) glycerol
92	0.16 M Manganese chloride, 0.08 M Sodium cacodylate trihydrate (pH 6.5), 14 % (w/v) PEG 8000, 24 % (v/v) glycerol
93	0.16 M Manganese chloride, 0.08 M Sodium cacodylate trihydrate (pH 6.5), 14 % (w/v) PEG 8000, 25 % (v/v) glycerol
94	0.16 M Manganese chloride, 0.08 M Sodium cacodylate trihydrate (pH 6.5), 14 % (w/v) PEG 8000, 26 % (v/v) glycerol
95	0.16 M Calcium acetate hydrate, 0.08 M Sodium cacodylate trihydrate (pH 6.5), 14 % (w/v) PEG 8000, 27 % (v/v) glycerol
96	0.16 M Manganese chloride, 0.08 M Sodium cacodylate trihydrate (pH 6.5), 14 % (w/v) PEG 8000, 28 % (v/v) glycerol
97	0.16 M Calcium acetate hydrate, 0.08 M Sodium cacodylate trihydrate (pH 6.5), 11 % (w/v) PEG 8000, 20 % (v/v) glycerol, 10 mM Leu-Pro
98	0.16 M Calcium acetate hydrate, 0.08 M Sodium cacodylate trihydrate (pH 6.5), 12 % (w/v) PEG 8000, 20 % (v/v) glycerol, 10 mM Leu-Pro
99	0.16 M Calcium acetate hydrate, 0.08 M Sodium cacodylate trihydrate (pH 6.5), 13 % (w/v) PEG 8000, 20 % (v/v) glycerol, 10 mM Leu-Pro
100	0.16 M Calcium acetate hydrate, 0.08 M Sodium cacodylate trihydrate (pH 6.5), 14 % (w/v) PEG 8000, 20 % (v/v) glycerol, 10 mM Leu-Pro
101	0.16 M Calcium acetate hydrate, 0.08 M Sodium cacodylate trihydrate (pH 6.5), 15 % (w/v) PEG 8000, 20 % (v/v) glycerol, 10 mM Leu-Pro
102	0.16 M Calcium acetate hydrate, 0.08 M Sodium cacodylate trihydrate (pH 6.5), 16 % (w/v) PEG 8000, 20 % (v/v) glycerol, 10 mM Leu-Pro
103	0.16 M Calcium acetate hydrate, 0.08 M Sodium cacodylate trihydrate (pH 6.5), 14 % (w/v) PEG 8000, 17 % (v/v) glycerol, 10 mM Leu-Pro

104	0.16 M Calcium acetate hydrate, 0.08 M Sodium cacodylate trihydrate (pH 6.5), 14 % (w/v) PEG 8000, 18 % (v/v) glycerol, 10 mM Leu-Pro
105	0.16 M Calcium acetate hydrate, 0.08 M Sodium cacodylate trihydrate (pH 6.5), 14 % (w/v) PEG 8000, 19 % (v/v) glycerol, 10 mM Leu-Pro
106	0.16 M Calcium acetate hydrate, 0.08 M Sodium cacodylate trihydrate (pH 6.5), 14 % (w/v) PEG 8000, 20 % (v/v) glycerol, 10 mM Leu-Pro
107	0.16 M Calcium acetate hydrate, 0.08 M Sodium cacodylate trihydrate (pH 6.5), 14 % (w/v) PEG 8000, 21 % (v/v) glycerol, 10 mM Leu-Pro
108	0.16 M Calcium acetate hydrate, 0.08 M Sodium cacodylate trihydrate (pH 6.5), 14 % (w/v) PEG 8000, 22 % (v/v) glycerol, 10 mM Leu-Pro
109	0.16 M Calcium acetate hydrate, 0.08 M Sodium cacodylate trihydrate (pH 6.5), 11 % (w/v) PEG 8000, 20 % (v/v) glycerol, 10 mM Pro
110	0.16 M Calcium acetate hydrate, 0.08 M Sodium cacodylate trihydrate (pH 6.5), 12 % (w/v) PEG 8000, 20 % (v/v) glycerol, 10 mM Pro
111	0.16 M Calcium acetate hydrate, 0.08 M Sodium cacodylate trihydrate (pH 6.5), 13 % (w/v) PEG 8000, 20 % (v/v) glycerol, 10 mM Pro
112	0.16 M Calcium acetate hydrate, 0.08 M Sodium cacodylate trihydrate (pH 6.5), 14 % (w/v) PEG 8000, 20 % (v/v) glycerol, 10 mM Pro
113	0.16 M Calcium acetate hydrate, 0.08 M Sodium cacodylate trihydrate (pH 6.5), 15 % (w/v) PEG 8000, 20 % (v/v) glycerol, 10 mM Pro
114	0.16 M Calcium acetate hydrate, 0.08 M Sodium cacodylate trihydrate (pH 6.5), 16 % (w/v) PEG 8000, 20 % (v/v) glycerol, 10 mM Pro
115	0.16 M Calcium acetate hydrate , 0.08 M Sodium cacodylate trihydrate (pH 6.5), 14 % (w/v) PEG 8000, 17 % (v/v) glycerol, 10 mM Pro
116	0.16 M Calcium acetate hydrate, 0.08 M Sodium cacodylate trihydrate (pH 6.5), 14 % (w/v) PEG 8000, 18 % (v/v) glycerol, 10 mM Pro
117	0.16 M Calcium acetate hydrate, 0.08 M Sodium cacodylate trihydrate (pH 6.5), 14 % (w/v) PEG 8000, 19 % (v/v) glycerol, 10 mM Pro
118	0.16 M Calcium acetate hydrate, 0.08 M Sodium cacodylate trihydrate (pH 6.5), 14 % (w/v) PEG 8000, 20 % (v/v) glycerol, 10 mM Pro
119	0.16 M Calcium acetate hydrate, 0.08 M Sodium cacodylate trihydrate (pH 6.5), 14 % (w/v) PEG 8000, 21 % (v/v) glycerol, 10 mM Pro
120	0.16 M Calcium acetate hydrate, 0.08 M Sodium cacodylate trihydrate (pH 6.5), 14 % (w/v) PEG 8000, 22 % (v/v) glycerol, 10 mM Pro, 10 mM Arg
121	0.16 M Calcium acetate hydrate, 0.08 M Sodium cacodylate trihydrate (pH 6.5), 11 % (w/v) PEG 8000, 20 % (v/v) glycerol, 10 mM Pro, 10 mM Arg
122	0.16 M Calcium acetate hydrate, 0.08 M Sodium cacodylate trihydrate (pH 6.5), 12 % (w/v) PEG 8000, 20 % (v/v) glycerol, 10 mM Pro, 10 mM Arg
123	0.16 M Calcium acetate hydrate, 0.08 M Sodium cacodylate trihydrate (pH 6.5), 13 % (w/v) PEG 8000, 20 % (v/v) glycerol, 10 mM Pro, 10 mM Arg
124	0.16 M Calcium acetate hydrate, 0.08 M Sodium cacodylate trihydrate (pH 6.5), 14 % (w/v) PEG 8000, 20 % (v/v) glycerol, 10 mM Pro, 10 mM Arg
125	0.16 M Calcium acetate hydrate, 0.08 M Sodium cacodylate trihydrate (pH 6.5), 15 % (w/v) PEG 8000, 20 % (v/v) glycerol, 10 mM Pro, 10 mM Arg
126	0.16 M Calcium acetate hydrate, 0.08 M Sodium cacodylate trihydrate (pH 6.5), 16

	% (w/v) PEG 8000, 20 % (v/v) glycerol, 10 mM Pro, 10 mM Arg
127	0.16 M Calcium acetate hydrate , 0.08 M Sodium cacodylate trihydrate (pH 6.5), 14 % (w/v) PEG 8000, 17 % (v/v) glycerol, 10 mM Pro, 10 mM Arg
128	0.16 M Calcium acetate hydrate, 0.08 M Sodium cacodylate trihydrate (pH 6.5), 14 % (w/v) PEG 8000, 18 % (v/v) glycerol, 10 mM Pro, 10 mM Arg
129	0.16 M Calcium acetate hydrate, 0.08 M Sodium cacodylate trihydrate (pH 6.5), 14 % (w/v) PEG 8000, 19 % (v/v) glycerol, 10 mM Pro, 10 mM Arg
130	0.16 M Calcium acetate hydrate, 0.08 M Sodium cacodylate trihydrate (pH 6.5), 14 % (w/v) PEG 8000, 20 % (v/v) glycerol, 10 mM Pro, 10 mM Arg
131	0.16 M Calcium acetate hydrate, 0.08 M Sodium cacodylate trihydrate (pH 6.5), 14 % (w/v) PEG 8000, 21 % (v/v) glycerol, 10 mM Pro, 10 mM Arg
132	0.16 M Calcium acetate hydrate, 0.08 M Sodium cacodylate trihydrate (pH 6.5), 14 % (w/v) PEG 8000, 22 % (v/v) glycerol, 10 mM Pro, 10 mM Arg
133	0.16 M Calcium acetate hydrate, 0.08 M Sodium cacodylate trihydrate (pH 6.5), 11 % (w/v) PEG 8000, 20 % (v/v) glycerol, 10 mM Pro, 10 mM Leu
134	0.16 M Calcium acetate hydrate, 0.08 M Sodium cacodylate trihydrate (pH 6.5), 12 % (w/v) PEG 8000, 20 % (v/v) glycerol, 10 mM Pro, 10 mM Leu
135	0.16 M Calcium acetate hydrate, 0.08 M Sodium cacodylate trihydrate (pH 6.5), 13 % (w/v) PEG 8000, 20 % (v/v) glycerol, 10 mM Pro, 10 mM Leu
136	0.16 M Calcium acetate hydrate, 0.08 M Sodium cacodylate trihydrate (pH 6.5), 14 % (w/v) PEG 8000, 20 % (v/v) glycerol, 10 mM Pro, 10 mM Leu
137	0.16 M Calcium acetate hydrate, 0.08 M Sodium cacodylate trihydrate (pH 6.5), 15 % (w/v) PEG 8000, 20 % (v/v) glycerol, 10 mM Pro, 10 mM Leu
138	0.16 M Calcium acetate hydrate, 0.08 M Sodium cacodylate trihydrate (pH 6.5), 16 % (w/v) PEG 8000, 20 % (v/v) glycerol, 10 mM Pro, 10 mM Leu
139	0.16 M Calcium acetate hydrate , 0.08 M Sodium cacodylate trihydrate (pH 6.5), 14 % (w/v) PEG 8000, 17 % (v/v) glycerol, 10 mM Pro, 10 mM Leu
140	0.16 M Calcium acetate hydrate, 0.08 M Sodium cacodylate trihydrate (pH 6.5), 14 % (w/v) PEG 8000, 18 % (v/v) glycerol, 10 mM Pro, 10 mM Leu
141	0.16 M Calcium acetate hydrate, 0.08 M Sodium cacodylate trihydrate (pH 6.5), 14 % (w/v) PEG 8000, 19 % (v/v) glycerol, 10 mM Pro, 10 mM Leu
142	0.16 M Calcium acetate hydrate, 0.08 M Sodium cacodylate trihydrate (pH 6.5), 14 % (w/v) PEG 8000, 20 % (v/v) glycerol, 10 mM Pro, 10 mM Leu
143	0.16 M Calcium acetate hydrate, 0.08 M Sodium cacodylate trihydrate (pH 6.5), 14 % (w/v) PEG 8000, 21 % (v/v) glycerol, 10 mM Pro, 10 mM Leu
144	0.16 M Calcium acetate hydrate, 0.08 M Sodium cacodylate trihydrate (pH 6.5), 14 % (w/v) PEG 8000, 22 % (v/v) glycerol, 10 mM Pro, 10 mM Leu
145	0.16 M Calcium acetate hydrate, 0.08 M Sodium cacodylate trihydrate (pH 6.5), 11 % (w/v) PEG 8000, 20 % (v/v) glycerol, 10 mM Pro, 10 mM Phe
146	0.16 M Calcium acetate hydrate, 0.08 M Sodium cacodylate trihydrate (pH 6.5), 12 % (w/v) PEG 8000, 20 % (v/v) glycerol, 10 mM Pro, 10 mM Phe
147	0.16 M Calcium acetate hydrate, 0.08 M Sodium cacodylate trihydrate (pH 6.5), 13 % (w/v) PEG 8000, 20 % (v/v) glycerol, 10 mM Pro, 10 mM Phe
148	0.16 M Calcium acetate hydrate, 0.08 M Sodium cacodylate trihydrate (pH 6.5), 14 % (w/v) PEG 8000, 20 % (v/v) glycerol, 10 mM Pro, 10 mM Phe

149	0.16 M Calcium acetate hydrate, 0.08 M Sodium cacodylate trihydrate (pH 6.5), 15 % (w/v) PEG 8000, 20 % (v/v) glycerol, 10 mM Pro, 10 mM Phe
150	0.16 M Calcium acetate hydrate, 0.08 M Sodium cacodylate trihydrate (pH 6.5), 16 % (w/v) PEG 8000, 20 % (v/v) glycerol, 10 mM Pro, 10 mM Phe
151	0.16 M Calcium acetate hydrate , 0.08 M Sodium cacodylate trihydrate (pH 6.5), 14 % (w/v) PEG 8000, 17 % (v/v) glycerol, 10 mM Pro, 10 mM Phe
152	0.16 M Calcium acetate hydrate, 0.08 M Sodium cacodylate trihydrate (pH 6.5), 14 % (w/v) PEG 8000, 18 % (v/v) glycerol, 10 mM Pro, 10 mM Phe
153	0.16 M Calcium acetate hydrate, 0.08 M Sodium cacodylate trihydrate (pH 6.5), 14 % (w/v) PEG 8000, 19 % (v/v) glycerol, 10 mM Pro, 10 mM Phe
154	0.16 M Calcium acetate hydrate, 0.08 M Sodium cacodylate trihydrate (pH 6.5), 14 % (w/v) PEG 8000, 20 % (v/v) glycerol, 10 mM Pro, 10 mM Phe
155	0.16 M Calcium acetate hydrate, 0.08 M Sodium cacodylate trihydrate (pH 6.5), 14 % (w/v) PEG 8000, 21 % (v/v) glycerol, 10 mM Pro, 10 mM Phe
156	0.16 M Calcium acetate hydrate, 0.08 M Sodium cacodylate trihydrate (pH 6.5), 14 % (w/v) PEG 8000, 22 % (v/v) glycerol, 10 mM Pro, 10 mM Phe